

---

# Master Thesis

---

## Experimental Determination of Solubilities of CO<sub>2</sub> in Crude Oil and Water

XIA Jing



Submitted to the Department of Petroleum Engineering at the Mining  
University of Leoben, Austria

**Supervised by:** Dr. Klaus Potsch OMV, Univ.-Prof. Leonhard Ganzer

Department **MINERAL RESOURCES & PETROLEUM ENGINEERING**  
Chair of **Reservoir Engineering**

Head: Univ.Prof. Dipl.Ing. Dr.mont. Leonhard Ganzer

An  
Jing Xia  
Salzlände 14/11/3  
8700 Leoben

Franz-Josef-Straße 18  
8700 Leoben  
Austria

Tel.: +43 (0)3842 402-3000  
Fax: +43 (0)3842 402-8202

e-mail: leonhard.ganzer@mu-leoben.at

Thesis-JingXia.doc

Betr.: **Thesis**

Leoben, am 20. Feb. 2007

Sehr geehrter Herr Xia!

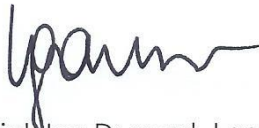
Das von der OMV zur Verfügung gestellte Thema der Thesis mit dem Titel

**EXPERIMENTAL DETERMINATION OF SOLUBILITIES OF CO<sub>2</sub> IN CRUDE OILS AND WATER**

wurde Ihnen zur Ausarbeitung übertragen. Die Arbeiten werden von Ihnen in der OMV unter Betreuung von Dr. Klaus Potsch und am Department für Mineral Resources and Petroleum Engineering unter der Betreuung von Herrn Univ.Prof. Leonhard Ganzer durchgeführt.

Dieses Schreiben wird nach Abschluss der Arbeit mit eingebunden.

Mit freundlichen Grüßen und Glück auf!



Univ.Prof.Dipl.Ing.Dr.mont. Leonhard Ganzer

---

# Affidavit

Herewith I declare in the lieu of oath that this master thesis is entirely of my own work using only literature cited at the end of this volume

---

(XIA Jing)

Vienna, August 2007

# Table of Contents

<b>Kurzfassung</b> .....	<b>9</b>
<b>Abstract</b> .....	<b>10</b>
<b>1. Introduction</b> .....	<b>11</b>
1.1 CO <sub>2</sub> Flooding Modeling.....	11
1.2 Physical Properties of Carbon Dioxide.....	12
1.3 EOR Methods of CO <sub>2</sub> Flooding.....	15
1.31 Displacement Processes.....	15
1.4 Diffusion.....	20
1.41 Diffusion coefficient and Fick's Law.....	20
<b>2. Experimental Section</b> .....	<b>23</b>
2.1 Experimental Data of CO <sub>2</sub> dissolving in Brine.....	23
2.2 Experimental Data of CO <sub>2</sub> dissolving in Crude Oil.....	28
<b>3. Phase Equilibrium Calculation</b> .....	<b>37</b>
3.1 Thermodynamic model.....	37
<b>4. Determination of Diffusion Coefficients of CO<sub>2</sub></b> .....	<b>43</b>
4.1 Introduction of Available Models.....	43
4.2 Civan and Rasmussen Model.....	44
4.21 General Formulation.....	44
4.22 Equilibrium Transport Model.....	46
4.3 Errors in Correlation Model.....	51
4.4 Application of Model.....	52
4.41 Diffusion Coefficients of CO <sub>2</sub> in Brine.....	52
4.42 Diffusion Coefficients of CO <sub>2</sub> in Oil.....	60
4.43 Summary of Results.....	73
<b>5. Conclusion</b> .....	<b>75</b>
<b>6. Future work</b> .....	<b>76</b>
<b>Nomenclature</b> .....	<b>77</b>
<b>References</b> .....	<b>79</b>

# List of Figures

Figure 1: Phase diagram of CO <sub>2</sub> as a function of pressure and temperature ( <i>1999 Chemical Logic Corporation, 99 South Bedford street, Suite 207, Burlington, MA 01803 UAS</i> ).....	12
Figure 2: Density of CO <sub>2</sub> as a function of p and T ( <i>holm and Josendal 1982; Vukalovich and Altunin 1968</i> ).....	13
Figure 3: Z factor of CO <sub>2</sub> ( <i>reamer et al. 1994</i> ).....	14
Figure 4: Viscosity of CO <sub>2</sub> as a function of p and T( <i>Goodrich 1980</i> ).....	14
Figure 5: Viscosity of several common gases at atmospheric pressure and various temperatures ( <i>Carr et al. 1954</i> ).....	15
Figure 6: CO <sub>2</sub> slug and water drive process. ....	16
Figure 7: Carbonated water flooding process.....	16
Figure 8: WAG process .....	17
Figure 9: Simultaneous injection of CO <sub>2</sub> and water process .....	17
Figure 10: Scheme of multiple-contact miscible process.....	19
Figure 11: Cylindrical PVT cell. ....	23
Figure 12: CO <sub>2</sub> in contact with brine water in PVT-cell at isothermal condition.....	25
Figure 13: Recorded pressure at 50°C & p <sub>i</sub> =40 bar .....	25
Figure 14: Recorded pressure at 50°C & p <sub>i</sub> =80 bar .....	26
Figure 15: Recorded pressure at 50°C & p <sub>i</sub> =100 bar .....	26
Figure 16: Recorded pressure at 50°C & p <sub>i</sub> =120 bar .....	26
Figure 17: Recorded pressure at 50°C & p <sub>i</sub> =160 bar .....	27
Figure 18: Recorded pressure at 70°C & p <sub>i</sub> =120 bar .....	27
Figure 19: Recorded pressure at 40°C & p <sub>i</sub> =120 bar .....	27
Figure 20: Compositional distribution of oil samples .....	28
Figure 21: Semi-plot of Fig 20 .....	29
Figure 22: Densities of oil samples @ 20°C.....	29
Figure 23: Viscosities of oil samples.....	30
Figure 24: CO <sub>2</sub> in contact with oil in PVT-cell at isothermal conditions. ....	31
Figure 25: Recorded pressure at 40°C & p <sub>i</sub> =40 bar .....	32
Figure 26: Recorded pressure at 40°C & p <sub>i</sub> =80 bar .....	32

Figure 27: Recorded pressure at 40°C & $p_i=120$ bar .....	32
Figure 28: Recorded pressure at 40°C & $p_i=160$ bar .....	33
Figure 29: Recorded pressure at 60°C & $p_i=40$ bar .....	33
Figure 30: Recorded pressure at 60°C & $p_i=80$ bar .....	33
Figure 31: Recorded pressure at 60°C & $p_i=120$ bar .....	34
Figure 32: Recorded pressure at 60°C & $p_i=160$ bar .....	34
Figure 33: Recorded pressure at 80°C & $p_i=40$ bar .....	34
Figure 34: Recorded pressure at 80°C & $p_i=80$ bar (data missing due to equipment failure).....	35
Figure 35: Recorded pressure at 80°C & $p_i=120$ bar .....	35
Figure 36: Recorded pressure at 80°C & $p_i=160$ bar (recording stopped after 25 hours due to equipment failure) .....	35
Figure 37: Data matching of CO <sub>2</sub> fraction in liquid phase at 50°C & $p_i= 40$ bar .....	40
Figure 38: Approached linear of $BIP_{H_2O-CO_2}$ vs. salinity at 50°C & $p_i=40$ bar .....	40
Figure 39: Coefficients a & b vs. pressure.....	41
Figure 40: Predicted a and b at different temperatures.....	42
Figure 41: Parameters set up in cylindrical cell .....	44
Figure 42: Pressure drop recording stoped after 20 hours of CO <sub>2</sub> dissolution test in 2% brine at 50°C, with $p_i=80$ bar .....	52
Figure 43: Pressure drops during dissolution process in brine at 50°C, with $p_i=10$ bar .....	52
Figure 44: Density difference in liquid at 50°C, with $p_i=10$ bar .....	55
Figure 45: Correlation of pressure decrease of CO <sub>2</sub> dissolution in 1% brine.....	55
Figure 46: $b_L$ determination in early and late stage for 1% brine.....	56
Figure 47: $b_L$ determination in early and late stage for 2% brine.....	56
Figure 48: $b_L$ determination in early and late stage for 5% brine.....	57
Figure 49: $b_L$ determination in early and late stage for 10% brine (LQ) .....	57
Figure 50: $b_L$ determination in early and late stage for 20% brine.....	58
Figure 51: Diffusion coefficient changes with salinity at 50°C .....	59
Figure 52: Diffusion coefficient as a function of salinity at 50°C (without the data from 10% brine) .....	59
Figure 53: $b_L$ determination in late stage for Gasoil at 60°C, $p_i=40$ bar.....	61
Figure 54: $b_L$ determination in late stage for Gasoil at 40°C, $p_i=80$ bar.....	61

---

Figure 55: $b_L$ determination in late stage for Gasoil at 60°C, $p_i=80$ bar.....	62
Figure 56: $b_L$ determination in late stage for Gasoil at 40°C, $p_i=120$ bar.....	62
Figure 57: $b_L$ determination in late stage for Gasoil at 60°C, $p_i=120$ bar.....	63
Figure 58: $b_L$ determination in late stage for Gasoil at 80°C, $p_i=120$ bar.....	63
Figure 59: $b_L$ determination in late stage for Gasoil at 60°C, $p_i=160$ bar.....	64
Figure 60: Concentration increase of CO <sub>2</sub> in Gasoil at 60°C.....	65
Figure 61: Concentration increase of CO <sub>2</sub> in Gasoil with $p_i=120$ bar.....	66
Figure 62: Pressure decrease of Hoeflein at 40°C with $p_i=40$ bar.....	67
Figure 63: Equilibrium pressure of Hoeflein changes with temperature.....	67
Figure 64: Pressure decrease of CO <sub>2</sub> dissolution in Hochleiten at 40°C.....	69
Figure 65: Pressure decrease of CO <sub>2</sub> dissolution in Hochleiten at 60°C.....	70
Figure 66: Pressure decrease of CO <sub>2</sub> dissolution in Hochleiten at 80°C.....	70
Figure 67: Short-time approximation of $b_S$ for Hochleiten at 40°C, $p_i=160$ bar.....	71
Figure 68: Short-time approximation of $b_S$ for Hochleiten at 80°C, $p_i=40$ bar.....	71
Figure 69: Short-time approximation of $b_S$ for Hochleiten at 60°C, $p_i=80$ bar.....	72
Figure 70: Short-time approximation of $b_S$ for Hochleiten at 80°C, $p_i=120$ bar.....	72
Figure 71: Diffusion coefficient decreases with viscosity.....	74

## List of Tables

Table 1: Critical properties of CO <sub>2</sub> .....	12
Table 2: Diffusion coefficients of CO <sub>2</sub> in water at atmospheric pressure .....	22
Table 3: p-T conditions of experiments for brine.....	24
Table 4: Densities and viscosities of oil samples at atmospheric pressure.....	29
Table 5: p-T conditions of experiments for oil .....	31
Table 6: Equilibrium calculation of mol fraction of CO <sub>2</sub> in brine at 50°C, p <sub>i</sub> =40 bar .....	39
Table 7: Errors of correlation equation 3.13 & 3.14 at 50°C.....	41
Table 8: Measured slopes [bar/h] of the pressure decline curves at the end of tests at 50°C....	53
Table 9: Equilibrium calculation of mol fraction of CO <sub>2</sub> in brine at 50°C, p <sub>i</sub> =10 bar .....	53
Table 10: Liquid densities at T =50°C and p=10 bar .....	54
Table 11: Slops b <sub>L</sub> and diffusion coefficients of CO <sub>2</sub> in brine at 50°C .....	58
Table 12: Selected tests from different p-T conditions.....	60
Table 13: Increased density in solution to density of Gasoil.....	60
Table 14: Diffusion coefficient [cm <sup>2</sup> /s] of CO <sub>2</sub> dissolution in Gasoil .....	64
Table 15: Slopes [bar/h] of pressure-decline curve at 60°C after a certain time .....	64
Table 16: Concentration [mol/L] of CO <sub>2</sub> dissolved in Gasoil at 60°C after a certain time (calculated by real gas equation) .....	65
Table 17: Slopes [bar/h] of pressure-decline curve with p <sub>i</sub> =120 bar after a certain time.....	65
Table 18: Concentration [mol/L] of CO <sub>2</sub> dissolved in Gasoil with p <sub>i</sub> =120 bar after a certain time (calculated by real gas equation).....	65
Table 19: Increased density in solution to density of 16TH.....	68
Table 20: Diffusion coefficients [cm <sup>2</sup> /s] of CO <sub>2</sub> dissolution in 16TH.....	68
Table 21: Increased density in solution to density of SchT .....	68
Table 22: Diffusion coefficients [cm <sup>2</sup> /s] of CO <sub>2</sub> dissolution in SchT .....	69
Table 23: Diffusion coefficients [cm <sup>2</sup> /s] of CO <sub>2</sub> dissolution in Hochleiten.....	73
Table 24: Increased density of CO <sub>2</sub> dissolved solution to density of Hochleiten.....	73
Table 25: Observation times of different tests.....	73



## Kurzfassung

Neben der Dampfinjektion gilt die CO<sub>2</sub> Injektion als eine der effektivsten EOR Methoden.

Beim CO<sub>2</sub> Fluten fungiert CO<sub>2</sub> als Lösungsmittel, indem es die leichten Kohlenwasserstoffe aufnimmt und das Ölvolumen schwellt. Dieser Effekt erniedrigt die Viskosität des Öls und erhöht die Ölsättigung. Daraus folgt eine höhere verbesserte Ölmobilität und ein wirkungsvoller Verdrängungsprozess kann erzielt werden.

Bei diesen Prozessen ist das langfristige Auflösungsverhalten of CO<sub>2</sub> von Diffusion kontrolliert. Die niedrigen Diffusionsraten können durch Ungleichgewichte die Verdrängungseffizienz herabsetzen. Deshalb ist der Diffusionskoeffizient sehr wichtig für die Beschreibung des Verdrängungsprozesses.

Die Diffusionsrate von CO<sub>2</sub> in Lagerstättenöl und Salzwasser ist ein der wichtiger Parameter, um die Effizienz während des sekundären/tertiären Förderungsprozesses zu bestimmen. Bisher wurden sehr wenige Studien experimenteller Daten zum Bestimmen des Gasdiffusionskoeffizienten von CO<sub>2</sub> in Flüssigkeiten angefertigt.

In dieser Arbeit wurden Experimente in einer zylindrischen PVT-Zelle durchgeführt, in der ein bestimmtes Volumen von CO<sub>2</sub> mit Öl oder Salzwasser in Kontakt gebracht wurde. Das Gleichgewichtsdiffusionsmodel von Civan et al. wird für die Bestimmung des Gasdiffusionskoeffizienten aus Druckabnahme bei Auflösung von CO<sub>2</sub> in Flüssigkeiten verwendet.

Mit Kenntnis der Diffusionsrate von CO<sub>2</sub>, kann man genauere Vorhersagen über die nicht-stationären Prozesse im Lagerstättenmodellsimulation treffen.

## Abstract

Along with steam injection, CO<sub>2</sub> flooding has been proved to be among the most promising EOR methods.

In CO<sub>2</sub> flooding CO<sub>2</sub> acts as a solvent, picks up lighter hydrocarbon components, resulting in swelling of oil. These effects reduce the oil viscosity and increase oil saturation. Thereby, the oil mobility improves, and a highly efficient oil displacement process can be achieved.

In all CO<sub>2</sub> recovery processes, the long term dissolution behavior of CO<sub>2</sub> in the reservoir fluid is diffusion controlled. In processes where the diffusion rates are low, non-equilibrium effects may reduce the displacement efficiency. Therefore, the diffusion coefficient is very important for the performance prediction.

The diffusion rate of CO<sub>2</sub> in reservoir oil and brine is required in reservoir simulation to predict the oil recovery for CO<sub>2</sub> miscible flooding. To our knowledge, only few studies have been carried out to experimentally investigate the gas diffusion coefficient of CO<sub>2</sub> gas into liquid phases.

This thesis describes experiments done in a cylindrical PVT-cell, where a certain volume of CO<sub>2</sub> gas was brought into contact with brine or oil. The equilibrium diffusion model by Civan et. al. is applied for determination of the gas-diffusion of CO<sub>2</sub> from pressure decline by dissolution of CO<sub>2</sub> in liquids (oil or brine water).

By knowing the rate of dissolution of CO<sub>2</sub>, the amount of CO<sub>2</sub> (including the loss of CO<sub>2</sub> to the coexisting aqueous phase) for recovery process can be predicted more accurately.

# 1. Introduction

## 1.1 CO<sub>2</sub> Flooding Modeling

Compositional models using a cubic equation of state are usually used to simulate improved oil recovery by gas injection. In general, all hydrocarbon components are assumed to stay in the oil and the gas phases and the gas solubility in the aqueous phase is ignored. This assumption could be satisfied for the case of hydrocarbon gases as their solubility in water phase is low over the range of temperature and pressure of gas injection. But high soluble gases such as CO<sub>2</sub> are an exception to this assumption. The solubility of CO<sub>2</sub> in water is much higher than that of hydrocarbon components, at moderate reservoir pressure of 300 bar at 100 °C, for example, the solubility of CO<sub>2</sub> in water could be as high as 1.25 mol CO<sub>2</sub>/ kg H<sub>2</sub>O, which is about 28 m<sup>3</sup> CO<sub>2</sub> in atmospheric condition dissolves in 1 m<sup>3</sup> water [Ref. 29]. It is therefore a factor that cannot be neglected in the flooding processes. This is especially important, when CO<sub>2</sub> is injected into a previously water flooded reservoir or when CO<sub>2</sub> is injected with water for mobility control.

The amount of CO<sub>2</sub> lost to the aqueous phase can have a significant influence on the incremental oil recovery as it affects the properties of hydrocarbon phase and change the phase behaviour of complex brine/hydrocarbon systems. So the solubility of CO<sub>2</sub> in water should be considered in the simulation process.

CO<sub>2</sub> solubility in water depends mainly on salinity, pressure, and temperature. As CO<sub>2</sub> is injected into the reservoir, the CO<sub>2</sub> contacts the reservoir water and mass transfer occurs, with CO<sub>2</sub> dissolving into water until equilibrium is reached. Injected CO<sub>2</sub> will displace CO<sub>2</sub>-saturated water during injection and hence further dissolution occurs as CO<sub>2</sub> continues to contact virgin formation water. The formation water interface between the CO<sub>2</sub> column and the formation water will become saturated with CO<sub>2</sub>. Since CO<sub>2</sub>-saturated water is under certain circumstances denser than virgin formation water, convection currents under the CO<sub>2</sub> column will occur.

To find out the solubility of CO<sub>2</sub> in brine water or crude oil during the instant equilibrium, diffusion coefficient is a very important parameter to determine the concentration distribution over time. Values of diffusion coefficients of CO<sub>2</sub> in water can be found in literature [Ref. 14, 15, 16].

## 1.2 Physical Properties of Carbon Dioxide

A reservoir simulation model has to be built to describe the reservoir and fluids it contains. Reliable input data are needed to predict the future production-pressure behavior, fluid property is one of the input data. It has a major effect on reservoir performance. Since carbon dioxide has been successfully used as an injection agent for EOR (Enhanced Oil Recovery) process, it is necessary to review its important physical properties.

CO<sub>2</sub> exists normally as a gas, but it can possibly exist as liquid at certain reservoir temperature and pressure. The p-T conditions of critical point of CO<sub>2</sub> are given in Table 1.

Property	Symbol	Value [SI Unit]	Value [Field Unit]
Critical Temperature	T <sub>c</sub>	30.978 °C	87.76 °F
Critical Pressure	p <sub>c</sub>	73.773 bar	1069.987 psia
Critical Density	ρ <sub>c</sub>	467.6 kg/m <sup>3</sup>	29.2 lb/ft <sup>3</sup>
Triple Point		-56.6°C & 5.18 bar	-69.9°F & 75.1 psia

Table 1: Critical properties of CO<sub>2</sub>

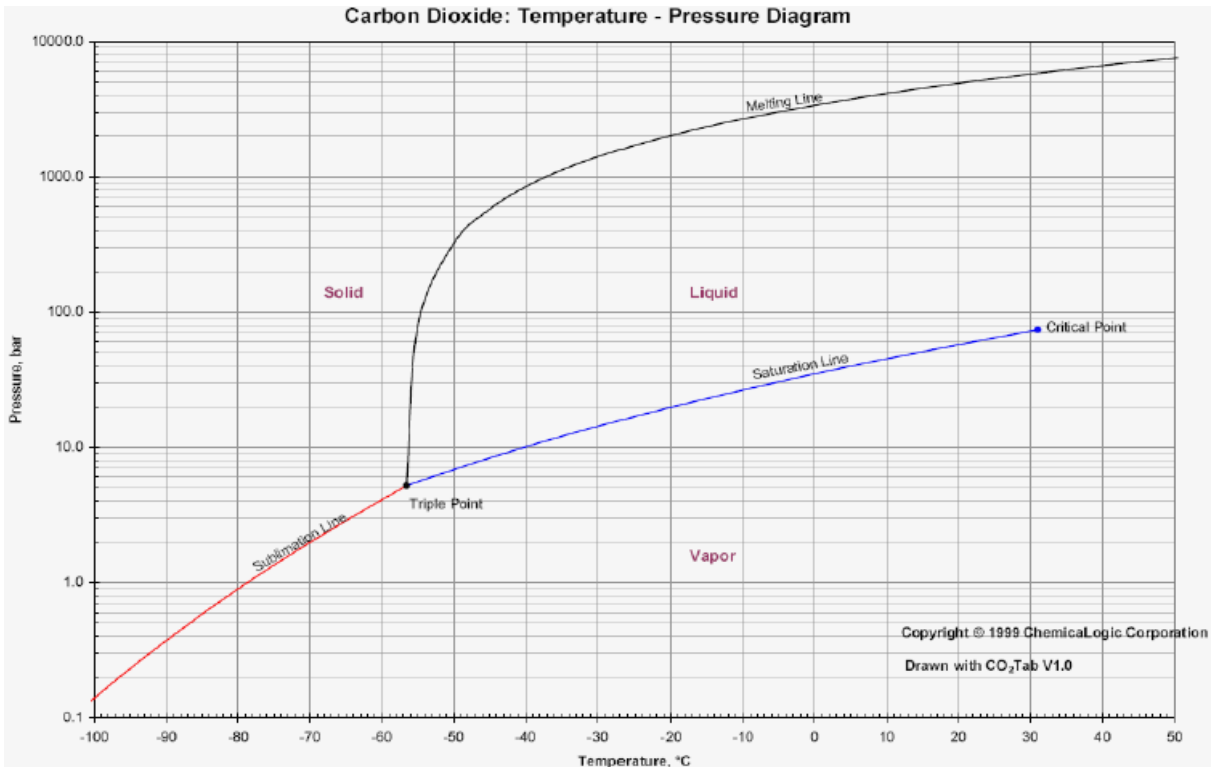


Figure 1: Phase diagram of CO<sub>2</sub> as a function of pressure and temperature (1999 Chemical Logic Corporation, 99 South Bedford street, Suite 207, Burlington, MA 01803 UAS)

Its critical temperature precludes most reservoirs from liquid CO<sub>2</sub> displacement and it has a low compressibility factor at typical reservoir conditions and is relatively dense gas with a 50% greater density than air at atmospheric condition. Fig 1 shows the phase diagram of CO<sub>2</sub> and

the solid-liquid-vapor equilibrium relationship for CO<sub>2</sub> below its critical temperature. It behaves as a vapor above the critical temperature, its density increase as pressure increases. The fluid density is a continuous function of pressure at temperature above critical conditions but the abrupt discontinuities will appear at pressures below the critical temperature (Fig 2). The CO<sub>2</sub> density near the critical region may be heavier than the resident hydrocarbon.

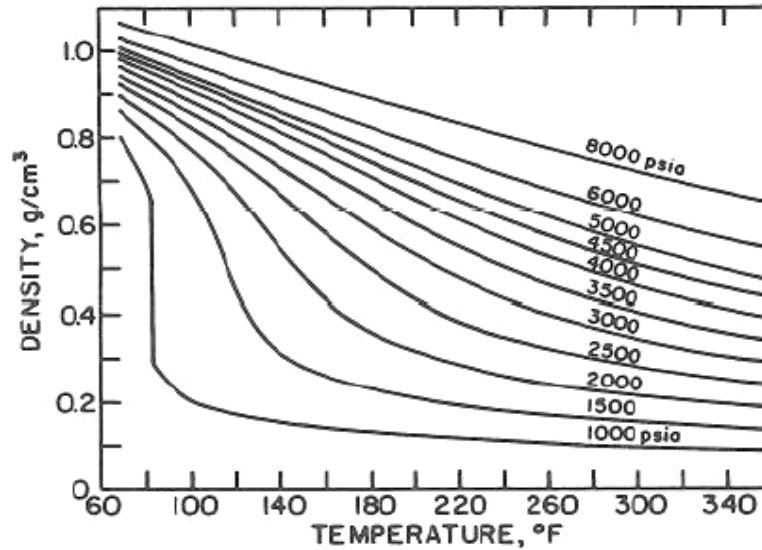


Figure 2: Density of CO<sub>2</sub> as a function of p and T (holm and Josendal 1982; Vukalovich and Altunin 1968)

Gas density at low pressures is allowed to be calculated by

$$\rho = \frac{pM}{ZRT} \quad (\text{Derivation from ideal gas law: } pV = nRT) \quad (1.1)$$

$\rho$ : Gas density [g/cm<sup>3</sup>]

p: pressure [Pa]

M: mol mass [g/mol]

R: universal gas constant 8.13 [J·K<sup>-1</sup>·mol<sup>-1</sup>]

T: temperature [K]

Z: compressibility factor

Eq 1.1 is the derived from the Real Gas Law, where Z is known as the compressibility factor. It is an empirical factor, experimentally determined, to better model the behavior of an actual gas at particular p and T, the Z factor is plotted as a function of p and T is shown in Fig 3.

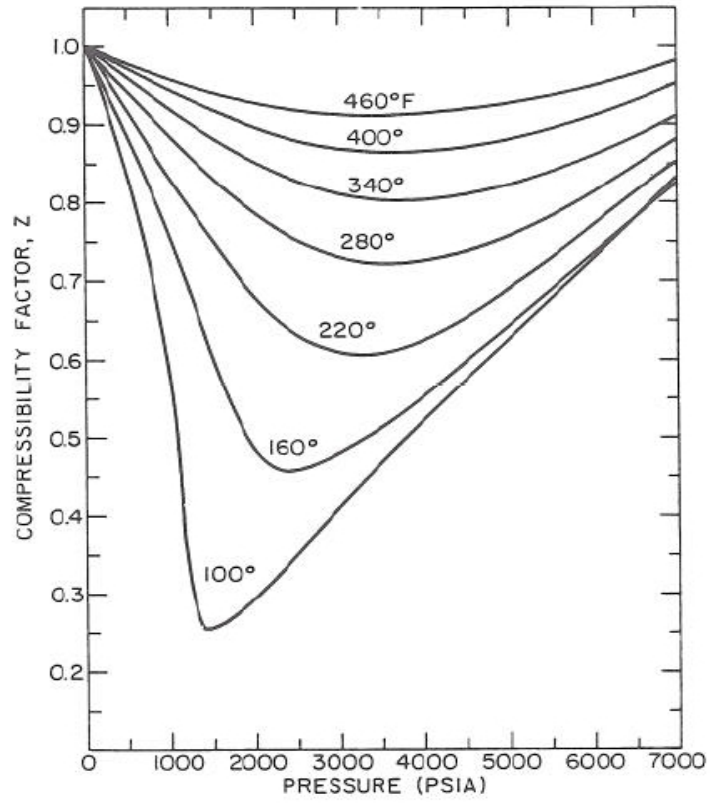


Figure 3: Z factor of CO<sub>2</sub> (reamer et al. 1994)

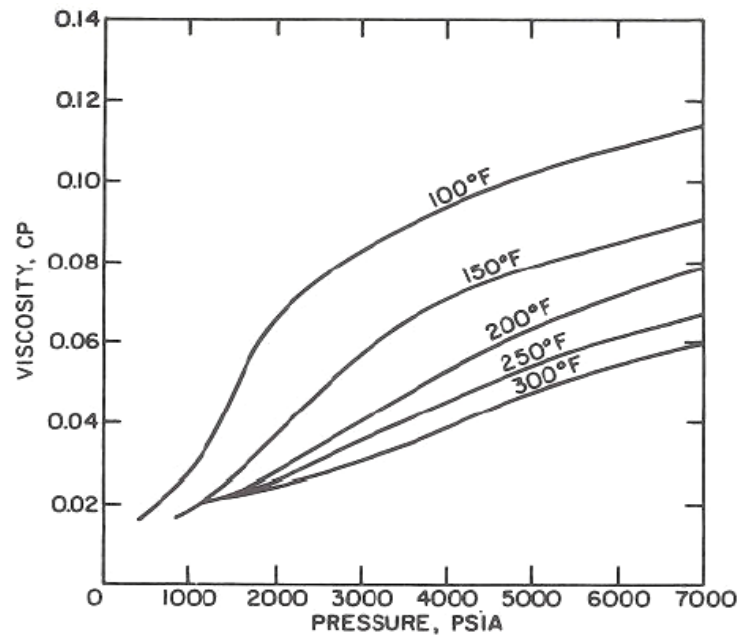


Figure 4: Viscosity of CO<sub>2</sub> as a function of p and T (Goodrich 1980)

The viscosity of CO<sub>2</sub> is a function of pressure and temperature, gas viscosity increases as pressure increases at a constant reservoir temperature. The curve of viscosity as a function of pressure and temperature is shown in Fig 4, and a comparing of viscosity of CO<sub>2</sub> with some other common gases is made in Fig 5.

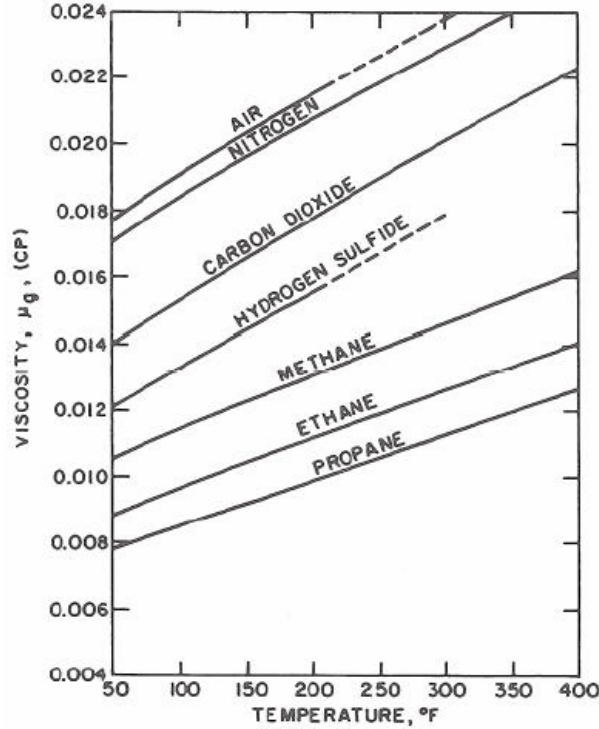


Figure 5: Viscosity of several common gases at atmospheric pressure and various temperatures (Carr et al. 1954)

## 1.3 EOR Methods of CO<sub>2</sub> Flooding

### 1.31 Displacement Processes

In recovery of oil from oil-bearing formation, we usually recover only a limited percentage of the original oil present in the reservoir by primary recovery methods in which the natural formation pressure is depleted to produce the oil through suitable production wells. To increase the oil recovery, a variety of supplementary recovery techniques has been employed, such as water flooding, miscible flooding, steam flooding, in-situ combustion. They serve either to maintain the formation pressure or to improve the displacement of oil from the porous rock matrix.

In a miscible flooding process, a solvent is injected into the reservoir to form a single phase solution with oil in place so that the oil can be removed as a more mobile phase from the reservoir. This leads to an effective displacement of oil.

Miscible recovery operations are normally carried out by a displacement procedure in which the solvent is injected into the reservoir through injection wells to displace the oil from the reservoir towards production wells from which the oil is produced. But the solvent such as liquid petroleum gas (LPG) or paraffin in the C<sub>2</sub> to C<sub>6</sub> range may be very expensive. It is often

desirable to carry out the recovery by injecting a slug of the solvent followed by a cheaper displacement liquid such as water. However, the economics of miscible recovery operations using first contact miscible solvents such as LPG or light hydrocarbons are quite unattractive.

Among all the recovery processes so far used or proposed, CO<sub>2</sub> flooding is considered to be one of the most significant recovery processes. The first patent for oil recovery using CO<sub>2</sub> was granted in 1952 [Ref. 19]. CO<sub>2</sub> was early considered as a solvent for crude oil or as a carbonated water-flood to increase oil recovery.

In the CO<sub>2</sub> flooding process, a slug of carbon dioxide is injected into the formation to mobilize the oil and permit it to be displaced towards production wells. Carbon dioxide is considered a miscible flooding agent because under supercritical conditions, usually high pressure, carbon dioxide acts as a solvent and in certain reservoir situations it has a great advantage over more common fluids as a displacement agent. Even under conditions where the carbon dioxide is not fully effective as a solvent for the oil, recovery may be improved by taking advantage of the solubility of carbon dioxide in the oil, causing a viscosity reduction and a swelling of the oil, which leads to increased recovery. These effects have been utilized at pressures much lower than the miscibility pressures for carbon dioxide and oil.

The technique of some CO<sub>2</sub> flooding process is briefly described in below.

The processes of solvent EOR methods are supposed to achieve the miscibility between the displacing and displaced fluids. Injection of CO<sub>2</sub> into oil reservoir may initiate oil displacement by different mechanisms. Although it is not usually miscible with reservoir oil on initial contact, CO<sub>2</sub> may create a miscible front. Miscibility is initiated by extraction of significant amount of hydrocarbon by CO<sub>2</sub>. If miscibility can be achieved, the interface (capillary forces) are no longer existent, the flooded oil will be swept with complete oil recovery. In general, miscible methods are applied to a reservoir in stage of depletion of high initial pressure.

CO<sub>2</sub> can be also injected in case of other miscible flooding processes:

1. continuously CO<sub>2</sub> gas injection in undiluted form,
2. alternated with water and CO<sub>2</sub> gas injection (WAG) process,
3. carbonated water injection,
4. simultaneously injection of CO<sub>2</sub> gas with water.

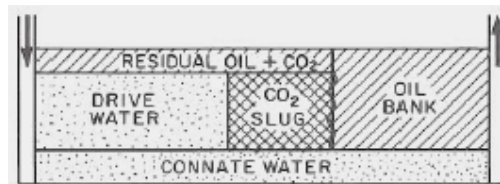


Figure 6: CO<sub>2</sub> slug and water drive process.

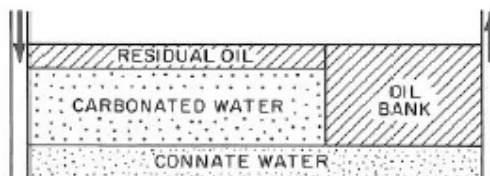


Figure 7: Carbonated water flooding process



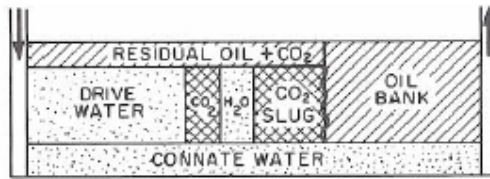


Figure 8: WAG process



Figure 9: Simultaneous injection of CO<sub>2</sub> and water process

Fig 6 shows the CO<sub>2</sub> slug process, water is continuously injected by following CO<sub>2</sub> to drive the slug through the reservoir. The water behind is immiscible, it displaces CO<sub>2</sub> leaving a residual CO<sub>2</sub> saturation in the reservoir.

Carbonated water injection is shown in Fig 7, CO<sub>2</sub> comes out of the injected water-CO<sub>2</sub> mixture when in contact with reservoir oil. The diffusion is slower than the injection of CO<sub>2</sub> slug, i.e. an effective CO<sub>2</sub> concentration at the displacement front is more likely to achieve when injected agent is a pure slug.

The WAG process is shown in Fig 8, it alternates small volume (5% PV or less) of CO<sub>2</sub> and water until the desired volume (normally 15 to 20% PV) has been injected, so that to reduce the CO<sub>2</sub> mobility and to achieve more uniform vertical entry into the reservoir.

Another process is simultaneous injection of CO<sub>2</sub> gas with water through paired injection wells to reduce unfavourable mobility ratio between solvent and oil. Water is injected in the top of the pay zone and it spreads downward as it flows through the reservoir, while CO<sub>2</sub> is injected in the bottom and able to rise (Fig 9).

Major effects of CO<sub>2</sub> injection on oil recovery in the crude oil are listed below:

- i. swelling of the net oil volume and increase in oil phase saturation,
- ii. reduction of oil viscosity,
- iii. decreasing of interfacial tension between the crude oil and CO<sub>2</sub> in the near-miscible regions,
- iv. contribution to internal solution gas drive.

### CO<sub>2</sub> injection displacement mechanisms

Fluids are miscible, if they can be mixed in all proportions and all mixtures remain in a single phase.

Some injectants for miscible flooding mix directly with reservoir oils. They are called "first contact miscible". Alcohols of low molecular weight, such as isopropyl and tertiary butyl alcohol, or LPG and light hydrocarbon which form a single phase solution with the reservoir when they are in contact. It's uneconomical, because large slugs are required to prevent the dilution of alcohol with oil and brine from non-miscible mass distribution.

Comparing with these, carbon dioxide is a multi-contact miscible solvent which forms a single phase only after a period of time during which the carbon dioxide first preferentially extracts the light hydrocarbons containing from two to six carbon atoms from the crude oil, thereby developing a hydrocarbon-containing solution at the interface between the carbon dioxide and the crude oil. This solution is able to dissolve other heavier hydrocarbons i.e. C<sub>6+</sub> hydrocarbons, and these progressively enter the solution to form the desired single phase which is then carried forward through the reservoir, and as it advances, heavier hydrocarbons are dissolved progressively. Thus, as the flooding front moves through the reservoir, the composition of the displaced fluid gradually changes from the crude oil to that of a miscible phase.

Dynamic miscibility is established above a certain and reservoir-specific MMP (minimum miscibility pressure). The multiple-contact miscibility is based on the extraction of light-to-intermediate components from oil.

The process is described on a ternary diagram, which contains the compositional information. On Fig. 10 the solvent-crude oil mixture is represented by three components while the temperature and pressure of the system are given:

- light component (CO<sub>2</sub>, methane) on the top apex
- intermediate components ,generally C<sub>2</sub> to C<sub>6</sub> (all the paraffins from ethane to hexane) on the right apex;
- heavy components, e.g. C<sub>7+</sub> on the left apex.

Under determined conditions of pressure and temperature, the dew and bubble point curves are plotted inside the ternary diagram with defined two-phase region. Point C is representative of mixture of the three pseudo-components, which has T and p as critical temperature and pressure. The high-pressure injection gas is represented by the point G, point o is composition of reservoir oil.

In the two-phase region, each point on the single tie line characterises a compositional fraction of liquid or gas in overall composition of the two-phase fluid, when they are in equilibrium.

To make sure that the miscibility is developed, the representative point of reservoir oil should be on the right side of the critical tie line (tangent to the phase envelope at point C). This implies that oil has rich intermediate components.

The displacement is not first-contact miscible. Now the dilution path passes through the two-phase region. And it's like a series of well-mixed cells that represent the permeable medium in a one-dimensional displacement. In Fig 10 the development of the multiple-contact miscible process can be described in following steps:

- I. Virgin reservoir oil and injected gas are immiscible and a representative line GO passes through the two-phase region. This implies that near the wellbore some residual oil with reservoir oil composition O remains unchanged.
- II. As oil and gas are not in equilibrium, thermodynamic exchanges occur, leading to equilibria G<sub>1</sub> (gas phase) and O<sub>1</sub> (liquid phase). The gas is enriched in intermediate and heavy components comparing with G's composition.
- III. Gas G<sub>1</sub> moves ahead due to higher mobility than liquid O<sub>1</sub>, chased by the fresh injected gas G, while the oil remains in place, and oil saturation remains behind the front.
- IV. At next step G<sub>1</sub> contacts reservoir oil O, since they are not in equilibrium, they split into two phase G<sub>2</sub> and O<sub>2</sub>, with G<sub>2</sub> being in contact with the front of injected gas. At the same time, oil O<sub>1</sub> in contact with gas G gives oil O<sub>a</sub> which is even poorer in intermediate components. This whole process will go on until the gas phase no longer form two phases on mixing with the reservoir oil, this is then the gas in contact with reservoir oil reaches point G<sub>t</sub>, defined as the intercept of the tangent to two-phase envelope from the oil representative point O. All compositions in the

displacement will be miscible by the point of tangency, this is where the fully miscibility is achieved and no residual oil remains.

In this process, CO<sub>2</sub> has been enriched in intermediate components to be miscible with the crude oil at the front of the transition zone. The miscibility is achieved by vaporizing the intermediate components from the crude oil, the process therefore called vaporizing gas drive process.

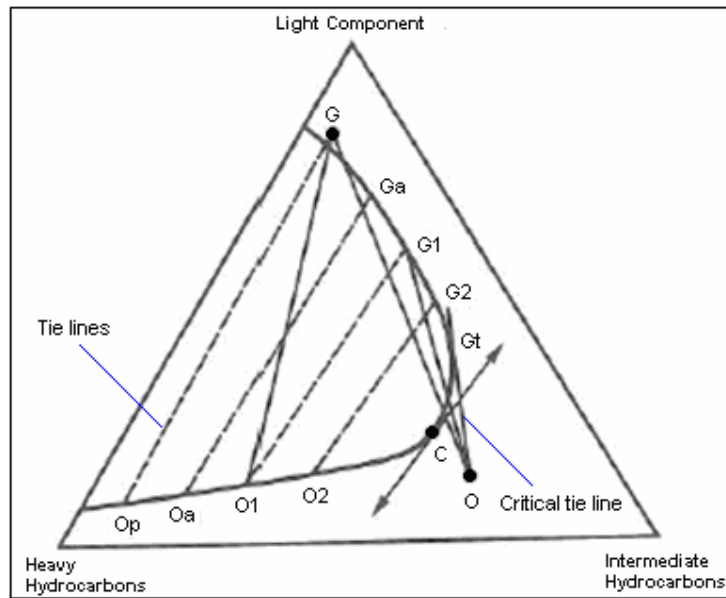


Figure 10: Scheme of multiple-contact miscible process

Multiple contact miscibility is a function of the pressure of the system and the minimum pressure required to achieve multiple contact miscibility is called the Minimum Miscibility Pressure (MMP). This varies according to the nature of the oil and of the solvent and in accordance with certain other factors. In some reservoirs, the MMP may be unattainable due to factors such as low pressure or the impracticality of pressurizing the reservoir. The presence of impurities, such as nitrogen or methane, may increase the MMP to levels beyond those attainable at reservoir conditions. If the minimum miscibility pressure cannot be achieved in the reservoir, the flooding process will be immiscible in character and recovery from the solvent injection will be low.

The multi-contact miscible flooding can be applied for reservoirs at near or above MMP. There are also positive global potential environmental benefits of CO<sub>2</sub> injection in subsurface sequestration of greenhouse gases. The MMP is an important optimization parameter in CO<sub>2</sub> floods, if the reservoir depletion pressure didn't drop below the MMP, CO<sub>2</sub> and oil can be mixed in all proportions and all mixtures remain in a single phase. CO<sub>2</sub> increases the mobility of oil by reducing the oil viscosity and by increasing the oil saturation. This can achieve a highly efficient oil displacement process.

The CO<sub>2</sub> immiscible flooding is a potentially viable method for heavy oil reservoirs. In an immiscible CO<sub>2</sub> process, part of the injected CO<sub>2</sub> is absorbed into the reservoir fluids and part forms a free-gas phase in the reservoir. CO<sub>2</sub> breakthrough occurs very early, showing the dominance of viscous forces and relatively small effect of mass transfer between CO<sub>2</sub> and oil. The total oil recovery varies considerably because of the differences in injection rates and as well the unstable displacement.

However, one of the most important limitations in the application of CO<sub>2</sub> flooding is the availability of CO<sub>2</sub>. The slug volume of 15% of the pore volume or more is required than in hydrocarbon miscible processes.

## 1.4 Diffusion

### 1.41 Diffusion coefficient and Fick's Law

#### Definitions

A confused definition of diffusion coefficient exists in the literature, because it is defined in different ways, several definitions were discussed in relation to the methods of calculation diffusion coefficient from experimental data.

Diffusion is the transfer of a substance through a homogeneous solution (single gas, liquid, or solid) resulting from a difference in concentrations at two regions in the mixture.

Molecular diffusion is defined as the transfer resulting from the random motion of the molecules and is to be distinguished from the mixing due to convection or bulk motion of the system [Ref. 15].

Thermal diffusion is another form of diffusion. A temperature gradient applied to a liquid mixture not only causes a heat flux but also gives rise to a diffusion current of the constituent components. The resulting separation of the components causes a concentration gradient parallel or antiparallel with respect to the temperature gradient. This cross-effect between temperature and concentration is known as thermal diffusion.

But obviously, we are talking about the molecular diffusion in this paper.

The diffusion coefficient or diffusivity is the proportionality constant between the rate of diffusion (diffusion flux) and the gradient of the potential causing diffusion. The diffusion potential is considered to be the concentration difference of the diffusion substance.

The typical approach to characterize diffusive transport of particles in porous materials begins with Fick's first law of diffusion that relates the bulk diffusion flux  $J$  to an apparent bulk diffusion coefficient  $D_b$  for a species with concentration  $c$ .

#### Diffusion of Gas in Liquid

The basic diffusion coefficient normally used to describe steady-state diffusion in a liquid is defined by

$$J = -D \cdot \text{grad } c \text{ or in one dimension: } J = -D \frac{dc}{dx} \quad (1.2)$$

This is the Fick's first law, Fick's laws of diffusion were derived by Adolf Fick in the year 1855. This diffusion equation of Fick's first law states that the flux per unit area (flux density),  $J$ , of a component is proportional to the concentration gradient of that component.

$J$ : the diffusion flux in dimensions of [amount of substance·length<sup>-2</sup>·time<sup>-1</sup>], e.g. [mol/(cm<sup>2</sup>s)].

$D$ : the diffusion coefficient or diffusivity in dimensions of [length<sup>2</sup>·time<sup>-1</sup>], e.g. [cm<sup>2</sup>/s].

$c$ : the concentration in dimensions of [amount of substance·length<sup>-3</sup>], e.g. [mol/cm<sup>3</sup>].

$x$ : the position [length], e.g. [cm].

This equation is applied to each diffusing substance in one phase.

Diffusion coefficient is proportional to the velocity of the diffusing particles, which depends on the temperature, viscosity of the fluid and the size of the particles according to the Stokes-Einstein relation. The value of  $D$  is in the range 0.5 to 4 × 10<sup>-5</sup> cm<sup>2</sup>/s for a wide variety of solutes and solvents at normal temperatures.

Diffusion coefficient increases with temperature and diffusion coefficient of gas in liquid is found to vary (usually decrease) due to the increasing of concentration of solute.

One-dimensional diffusion occurs, when we have two infinite parallel boundary planes and concentrations that are constant along any plane parallel to these boundaries. It can also be used exactly for diffusion in a straight tube of constant diameter. Such situations are steady-state diffusion, in which  $\frac{dVc}{dt} = 0$ . In simple cases, steady-state solutions for the diffusion

equation are usually easier to find than complete, time-dependent solutions. However, in more complex situations, the easiest way to find the steady-state solution may be by numerical integration (with a computer) of the complete equation until equilibrium is reached.

The time-dependent diffusion is non-steady or continually changing state diffusion, in which  $dc/dt \neq 0$ , i.e., the concentration within the diffusion volume changes with time.

This is Fick's second law:

$$\frac{\partial c}{\partial t} = D \cdot \nabla^2 c, \text{ or in one dimension, } \frac{\partial c}{\partial t} = D \frac{\partial^2 c}{\partial x^2} \quad (1.3)$$

where  $t$  is time [s].

It can be derived from the Fick's First law and the mass balance:

$$\frac{\partial c}{\partial t} = -\frac{\partial J}{\partial x} = \frac{\partial}{\partial x} \left( D \frac{\partial c}{\partial x} \right) \quad (1.4)$$

The diffusion coefficient of carbon dioxide was well correlated by the equation that was found by *Timmerhaus & Drickamer*:

$$D = D_o \exp\left(-\frac{e}{RT}\right) \quad \text{or} \quad \ln D = \ln D_o - e/RT \quad (1.5)$$

where

$e$ : the activation energy for diffusion. [J/mol], [eV/mol]

$D_o$ : pre-exponential factor or diffusion coefficient based on molecular concentration

Eq 1.5 shows that  $D$  increases with temperature. An increase in temperature represents an increase in the average molecular speed, diffusion occurs faster at higher temperatures. At a prescribed temperature, small, light molecules (such as H<sub>2</sub>, hydrogen gas) diffuse faster than larger, more massive molecules on the average. According to Graham's law (Eq1.6), the gas diffusion rate is inversely proportional to the square root of the mass of its particles.

$$\frac{q_1}{q_2} = \sqrt{\frac{M_2}{M_1}} \quad (1.6)$$

$q$  :the diffusion rate.

And another equation with viscosity involved is Einstein relation (also Sutherland, Nernst), Eq 1.8 shows D decreases with viscosity.

$$D = \frac{kT}{f'} \quad (1.7)$$

$k$  : Boltzmann gas constant [J/K]

$f'$  : molecular friction coefficient []

For large spheres,  $f'$  may be eliminated by the Stokes equation,

$$D = \frac{kT}{6\pi\eta r} \quad (1.8)$$

$\eta$  : viscosity of solution [mPa.s]

$r$  : particle radius [m]

During the diffusion process, the concentration gradient is minimized until the equilibrium of system is reached, the diffusion coefficient is a very important parameter to characterize the diffusion process, and this can help us better simulate the thermodynamic equilibrium of CO<sub>2</sub> flooded reservoir by considering the factor that how fast and how much CO<sub>2</sub> is diffused in reservoir fluid.

Several values of the diffusion coefficient of CO<sub>2</sub> in water can be found in the literature and are listed in the table below (in atmospheric pressure):

$D_{CO_2-water} [cm^2/s]$	$T [K]$	Literature
$1.96 \times 10^{-5}$	298	Chemical Engineerings' Handbook <i>Perry, R.H</i>
$1.6 \times 10^{-5}$	N/A	Wikipedia
$1.62 \times 10^{-5}$	293.15	Handbook of Physics and Chemistry (76 <sup>th</sup> Edition)
$1.71 \times 10^{-5}$	298	Properties of Gases and Liquids <i>Robert C. Reid</i>

Table 2: Diffusion coefficients of CO<sub>2</sub> in water at atmospheric pressure

## 2. Experimental Section

The experiments took place in OMV's laboratory for exploration and production.

Goal of the experimental work is to measure the pressure decline in the PVT cell during CO<sub>2</sub> dissolves in reservoir fluid (oil, brine) in order to be able to determine the diffusion coefficients of CO<sub>2</sub>.

The diffusion-cell method is a simple experimental method which is very commonly used to get average values of D over a finite concentration range.

### 2.1 Experimental Data of CO<sub>2</sub> dissolving in Brine

PVT cells were selected for monitoring the pressure change during the equilibration of gas-liquid phase of CO<sub>2</sub> and brine water, the diffusion processes were carried out in six PVT cells simultaneously, in each cell CO<sub>2</sub> was in contact with brine with different salinities. To make sure the whole process was isothermal, the cells were placed in a tank filled with Gasoil (synthetic condensate), which was thermo-regulated by a thermo-generator. A high pressure pump was also needed to initiate high pressures to the cells.

#### Equipment

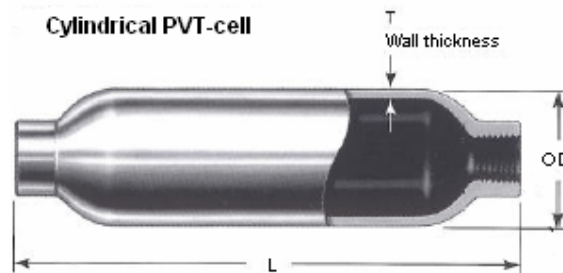


Figure 11: Cylindrical PVT cell.

- PTV-cells (Fig 11)
  - Outside diameter OD = 48.2 mm
  - Wall thickness T = 6.1 mm
  - Length L = 203 mm
  - Weight = 1.4 kg
  - Standard volume = 150 cm<sup>3</sup>
- Mercury pumps
- Gasoil (Thermo-transfer medium)
- Thermostat
- Temperature bath (liquid bath) with mounted thermocouple

Pressed CO<sub>2</sub> was prepared in high pressure gas cylinder, the distilled water was according to the required salinity (weight percentage) mixed with KCl solution.

Valves were mounted on each side of the PV-cell, during the operation both valves were closed, and the PVT-cells were submersed in a temperature bath (liquid bath) filled with Gasoil which was thermo-regulated by a thermostat. The thermocouple was mounted on the wall of the liquid bath to measure the liquid bath temperature, and at the top of the tube a pressure gauge was mounted which measured the pressure at the tube. These data were recorded by a computer.

**Experimental Procedure:**

The schematic procedure (Fig 12) is summarized as follows:

1. First the liquid bath was heated by thermostat to the required temperature. After cleaning the PVT-cell with ethanol, vacuum was applied to the PVT-cell, 100 cm<sup>3</sup> brine water was sucked from a measuring cylinder into the cell through a valve at the bottom due to the pressure difference, and the pressure in the cell was released to atmospheric pressure when it was finished.
2. Mercury was then injected into the cell from the valve at the bottom by a mercury pump, and brine was displaced towards to the top of the cell. The displacement was stopped when the cell fulfilled with liquid, and the bottom and top valves were closed.
3. To make sure the operations were carried out in isothermal condition, all cells were submersed in the liquid bath. 30-minute waiting time was respected for liquid in cells coming into thermal equilibrium with liquid bath.
4. Before CO<sub>2</sub> was brought in the cell, CO<sub>2</sub> in the gas tank was adjusted to the desired initial pressure. The last step was to shift CO<sub>2</sub> into the PVT-cell from the valve at the top, and the exact shifting volume was 15 cm<sup>3</sup> which was achieved by removing 15 cm<sup>3</sup> of mercury from the bottom of the cell by the mercury pump. In the next step, the pressure in the cell should more or less reach the same required pressure as the one in the gas cylinder.
5. The pressure decline due to CO<sub>2</sub> dissolution in brine was recorded until it reached the equilibrium condition.

Data of pressure declines were recorded every minute in the first hour after test started, then every 10 minutes afterwards.

Since 5 PVT-cells fitted in the liquid bath at a time, 5 cells filled with brines with different salinities were tested at one time.

The experiments were carried out at 50°C with 5 different brine salinities, at 5 different initial pressures. The experiments for temperature at 40°C and 70°C were only completed at 120 bar.

<i>Salinities of Brine</i>	<i>Initial Pressures</i>				
<i>[KCl Weight %]</i>	40 bar	80 bar	100 bar	120 bar	160 bar
1%	50°C	50°C	50°C	40°C,50°C,70°C	50°C
2%	50°C	50°C	50°C	40°C,50°C,70°C	50°C
5%	50°C	50°C	50°C	40°C,50°C,70°C	50°C
10%	50°C	50°C	50°C	40°C,50°C,70°C	50°C
20%	50°C	50°C	50°C	40°C,50°C,70°C	50°C

Table 3: p-T conditions of experiments for brine



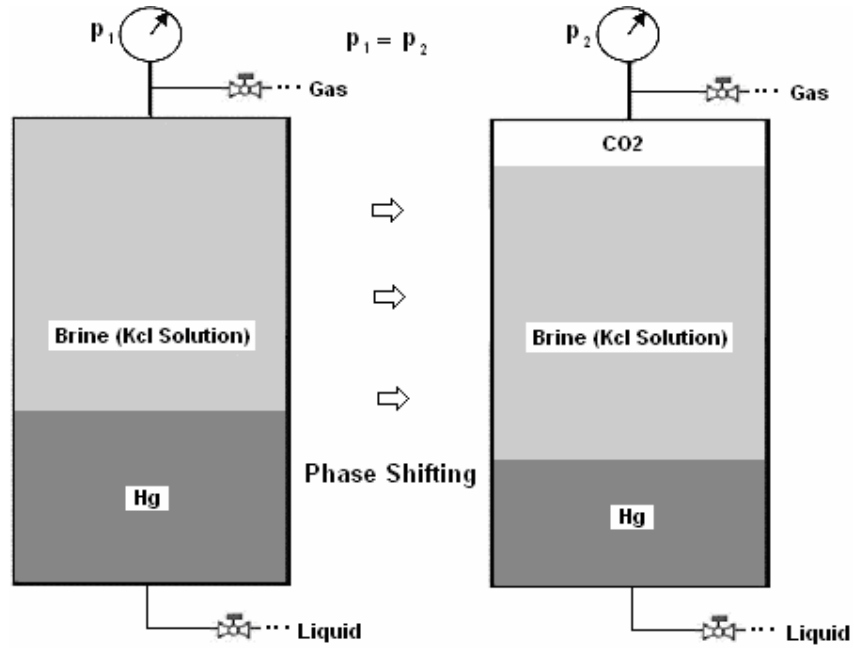


Figure 12: CO<sub>2</sub> in contact with brine water in PVT-cell at isothermal condition.

The monitored pressure decline of each cell is shown below (Figure 13 - 19):

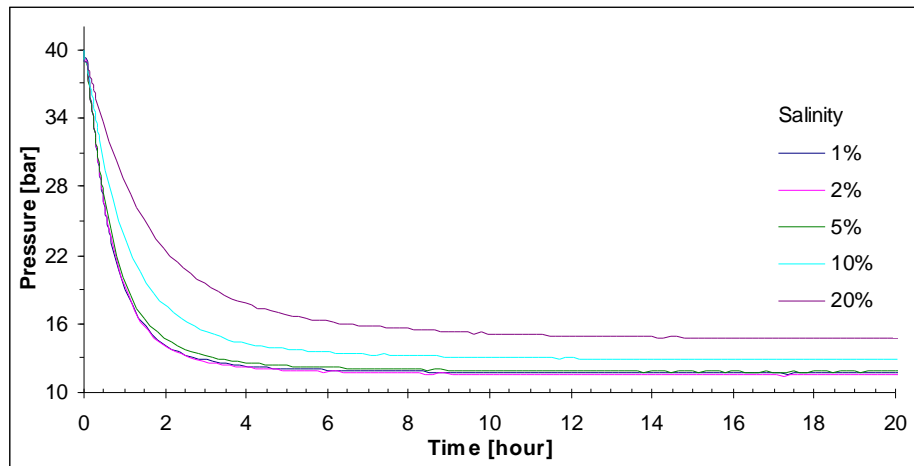


Figure 13: Recorded pressure at 50°C & p<sub>i</sub>=40 bar

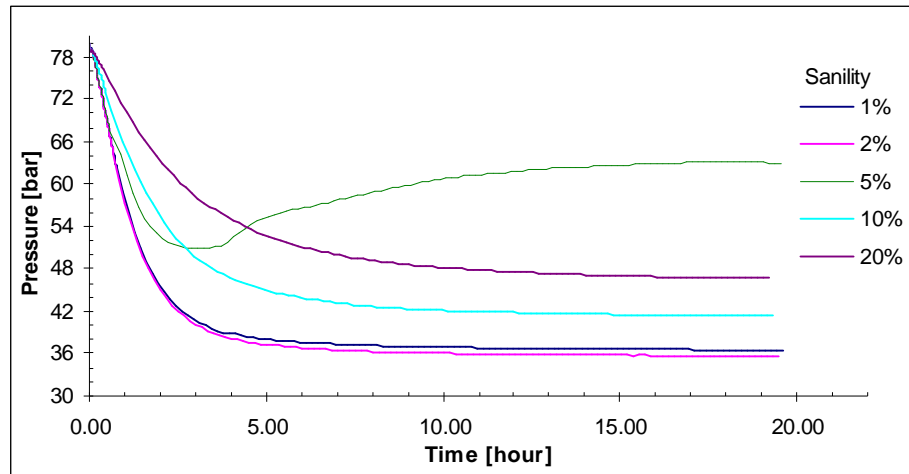


Figure 14: Recorded pressure at 50°C &  $p_i=80$  bar

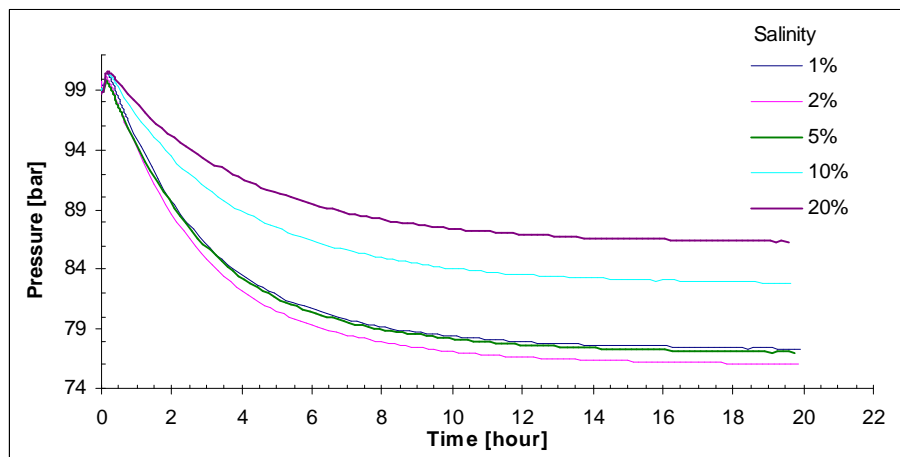


Figure 15: Recorded pressure at 50°C &  $p_i=100$  bar

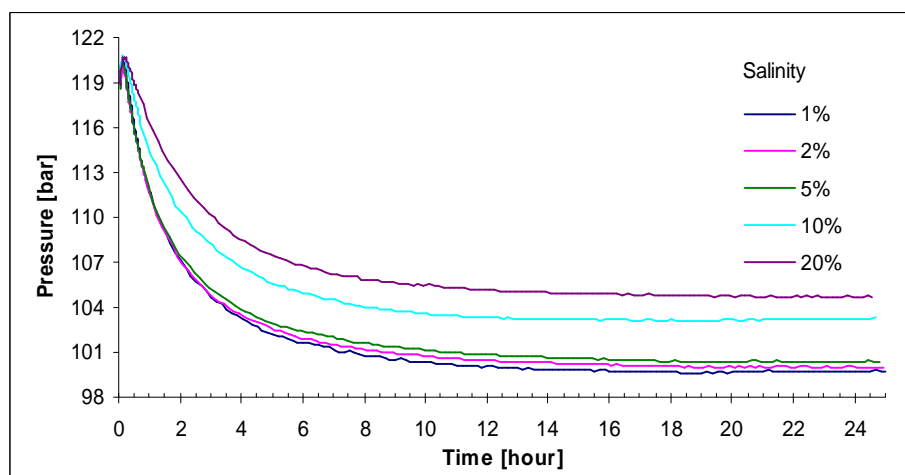


Figure 16: Recorded pressure at 50°C &  $p_i=120$  bar

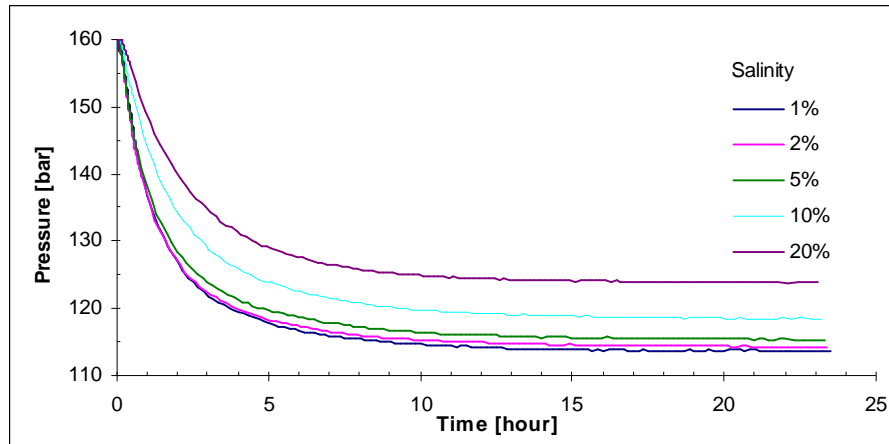


Figure 17: Recorded pressure at 50°C &  $p_i=160$  bar

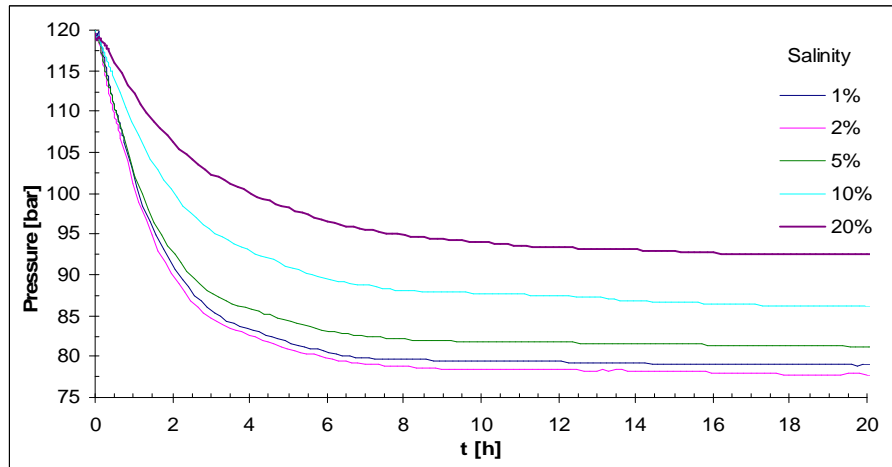


Figure 18: Recorded pressure at 70°C &  $p_i=120$  bar

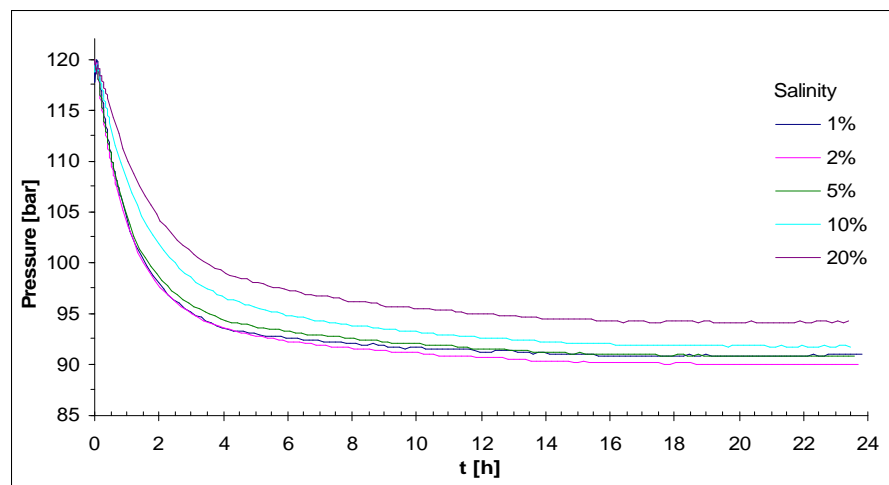


Figure 19: Recorded pressure at 40°C &  $p_i=120$  bar

We know that CO<sub>2</sub> solubility decreases with salinity which means that the less pressure drop should be expected in brine with higher salinities, but in Fig 14, 15, 18 and 19, larger pressure declines were observed in brine of 2% salinity than the ones in brine of 1% salinity. So the data obtained in brine of 2% salinity might have poor quality, this can be seen in further data evaluation.

In Figure 14, the pressure decline in 5% brine is incorrect due to leak of the PVT cell during the measurement; this pressure-decline data was not evaluated.

The final pressure of each experiment reached very close to its equilibrium pressures. These values were used in equation of state calculations for water-CO<sub>2</sub> system.

## 2.2 Experimental Data of CO<sub>2</sub> dissolving in Crude Oil

### Oil Samples

CO<sub>2</sub> was brought into contact with 5 different oil samples separately, the samples are Gasoil, Hoefflein condensate, Schoenkirchen Tief (SchT), Hochleiten (HI) and 16TH, and they are all taken from Vienna Basin except Gasoil, which is a synthetic condensate.

Gas chromatography has been used to analyse the compositions of oil samples. The result is displayed below:

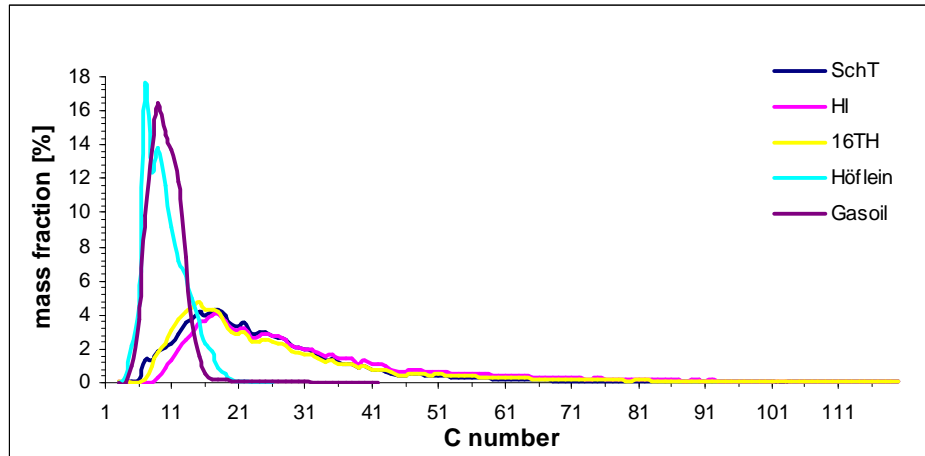


Figure 20: Compositional distribution of oil samples

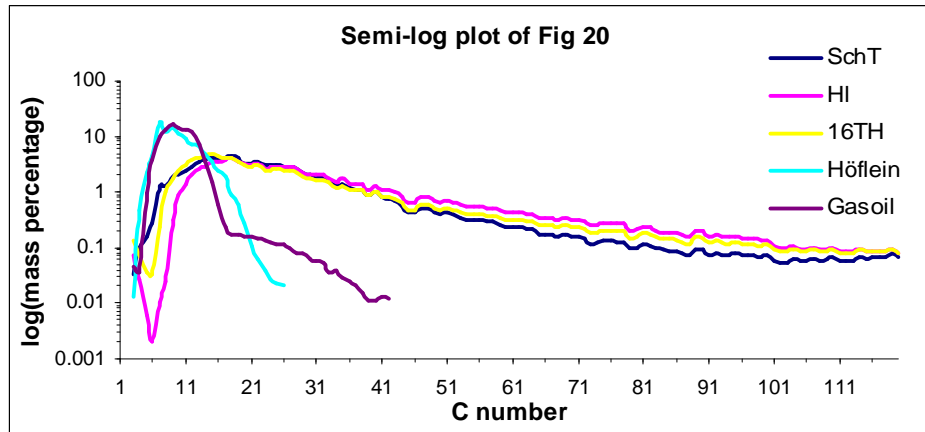


Figure 21: Semi-plot of Fig 20

According to the composition analyses, oil samples can be characterized in two groups:

1. Hoeflein and Gasoil (light oil)
2. Schoenkirchen Tief, 16TH and Hochleiten (heavy oil).

The viscosities, densities, and API gravities of oil samples are shown in Table 4 and Fig 22 and 23. The same sequence has been observed in density and in viscosity; oil with higher density has a higher viscosity.

Oil Sample	Density (20°C) [g/cm <sup>3</sup> ]	Viscosity (40°C) [mPa.s]	Viscosity (60°C) [mPa.s]	Viscosity (80°C) [mPa.s]
Hoeflein	0.7602	0.6080	0.4781	0.3589
Gasoil	0.8773	4.0901	2.5617	1.7634
Schoenkirchen Tief	0.8827	12.903	6.8636	4.1609
16 TH	0.9091	25.814	12.163	6.7182
Hochleiten	0.9399	131.17	44.847	19.964

Table 4: Densities and viscosities of oil samples at atmospheric pressure

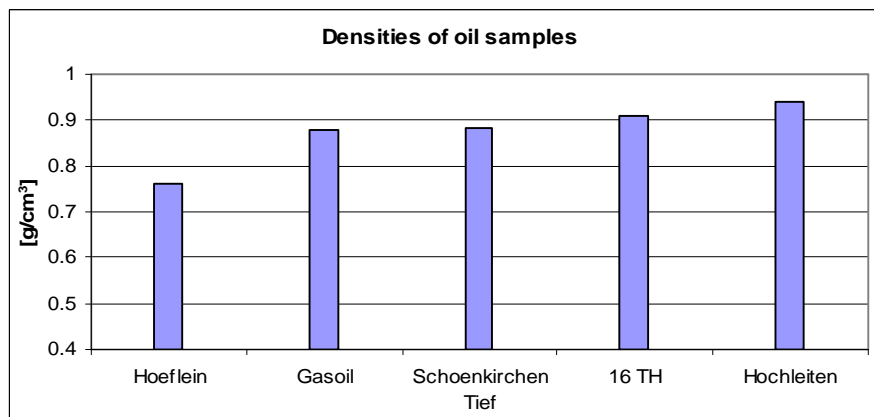


Figure 22: Densities of oil samples @ 20°C

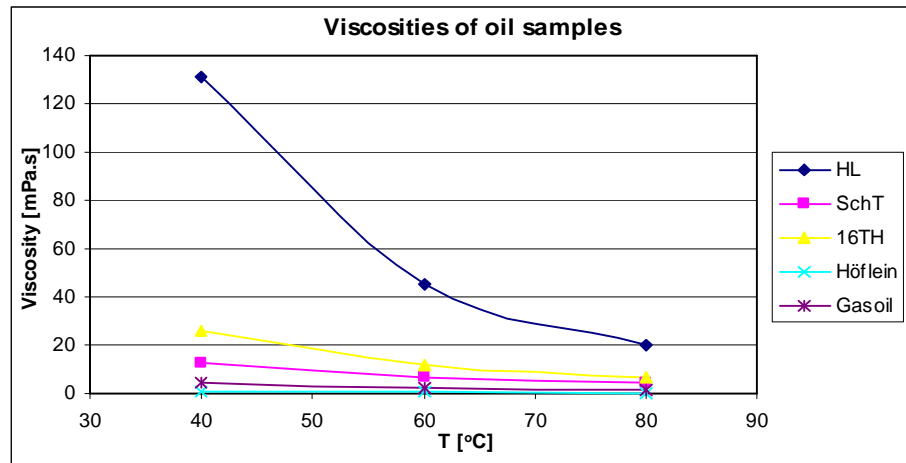


Figure 23: Viscosities of oil samples

#### Experimental procedure:

The same equipment was used in this experiment. The procedures was a little different from the one carried out with brine water. The schematic procedure (Fig 24) is summarized as follows:

1. The liquid bath was first heated by thermostat to required temperature. After cleaning the PVT-cell with ethanol, vacuum was applied. Then 100 cm<sup>3</sup> of oil sample carried by a measuring cylinder was sucked into the cell through a valve at the bottom due to the pressure difference, and the pressure in the cell was brought to atmospheric pressure.
2. Mercury was then injected into the cell through the valve at bottom and oil was displaced to the top of the cell. The displacement was stopped when the cell was full with liquid, and the both valves were closed afterward.
3. Top valve was then open again and connected with a nitrogen pump at low pressure. 15 cm<sup>3</sup> N<sub>2</sub> was shifted into the cell from the top valve by removing exact 15 cm<sup>3</sup> of mercury from the bottom by mercury pump. The pressure in the cell was released to atmospheric pressure. The gas volume made in the cell was for CO<sub>2</sub> to fill in.
4. To make sure the operations were carried out in isothermal condition, all cells were submersed in the liquid bath. 20-minute waiting time was required for fluid in cells becoming thermal equilibrium with liquid bath.
5. After the pressure of CO<sub>2</sub> in the gas tank was adjusted to the required initial pressure, CO<sub>2</sub> was filled in the cell from the top valve until the PVT-cell reached the same required initial pressure (the valve at the bottom was closed). The volume of CO<sub>2</sub> in the cell should be more or less also 15 cm<sup>3</sup>. Then the pressure decline during the dissolution was recorded.

5 cells filled with 5 different oil samples were tested at one time.

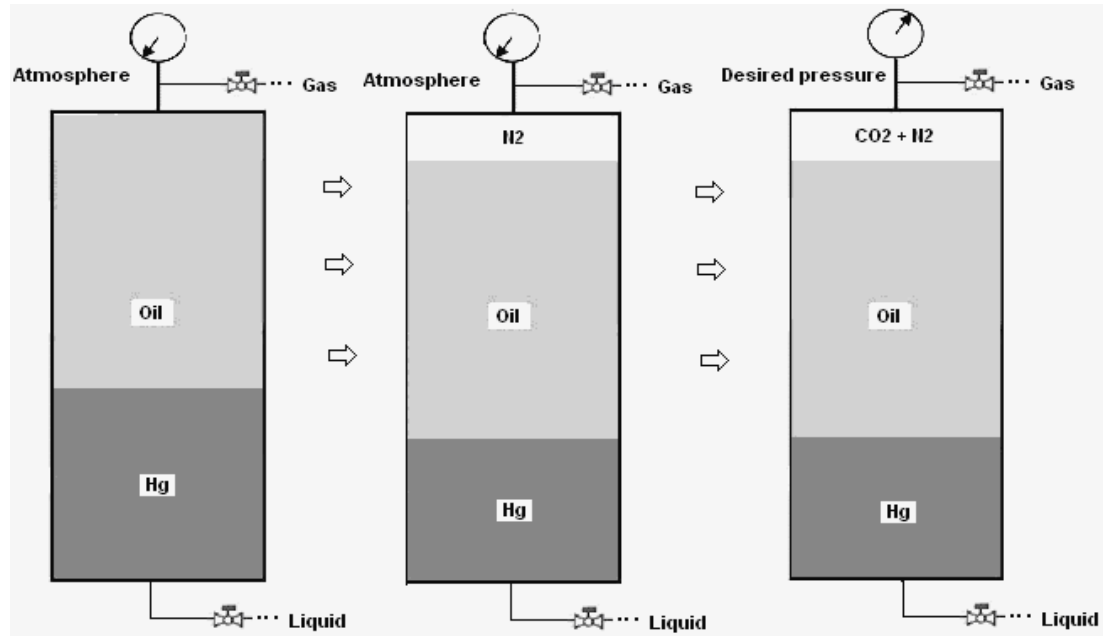


Figure 24: CO<sub>2</sub> in contact with oil in PVT-cell at isothermal conditions.

The experiments were carried out in different p-T conditions for all oil samples.

$T \backslash p_i$	40 bar	80 bar	120 bar	160 bar
40°C	r	r	r	r
60°C	r	r	r	r
80°C	r	r	r	r

Table 5: p-T conditions of experiments for oil

Pressure change was recorded every minute in the first hour after test started, then recorded in every hour from the second hour on.

It's very important that the pressure was continuously recorded until the pressure stabilized in the cell. A few samples didn't reach the stabilization due to the time limit or equipment failures during the experiment, these values will be considered as low quality data.

The monitored pressure declines in cells are shown from Figure 25 to 36.

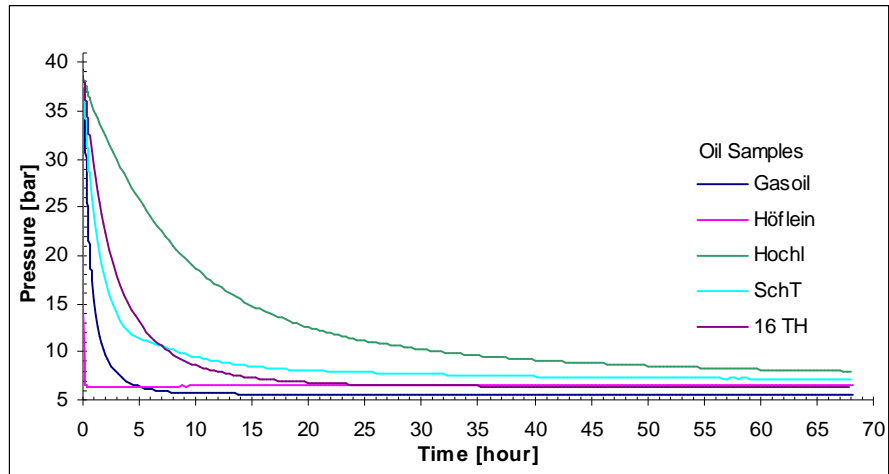


Figure 25: Recorded pressure at 40°C &  $p_i=40$  bar

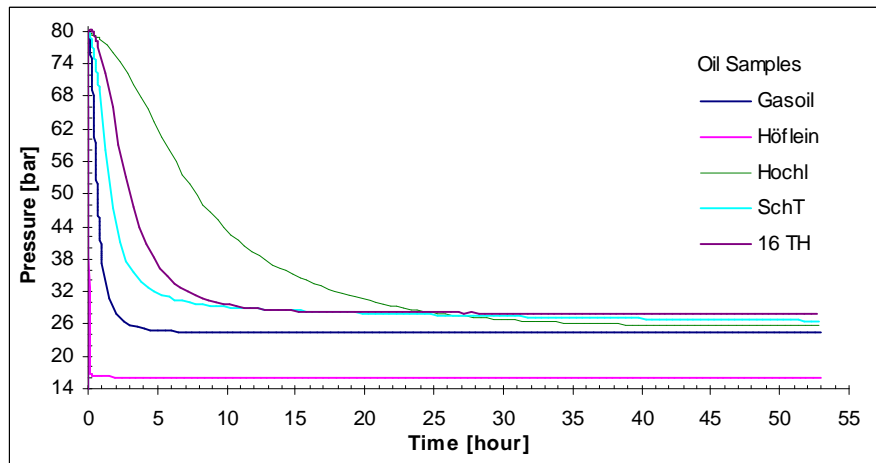


Figure 26: Recorded pressure at 40°C &  $p_i=80$  bar

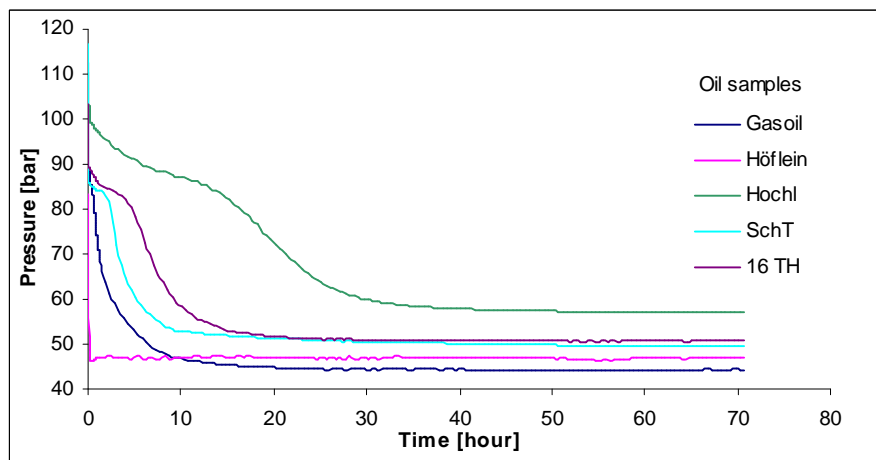


Figure 27: Recorded pressure at 40°C &  $p_i=120$  bar



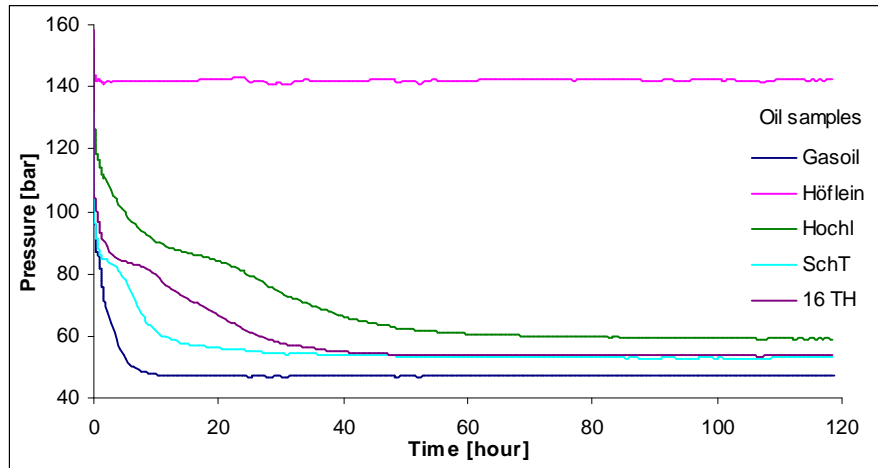


Figure 28: Recorded pressure at 40°C &  $p_i=160$  bar

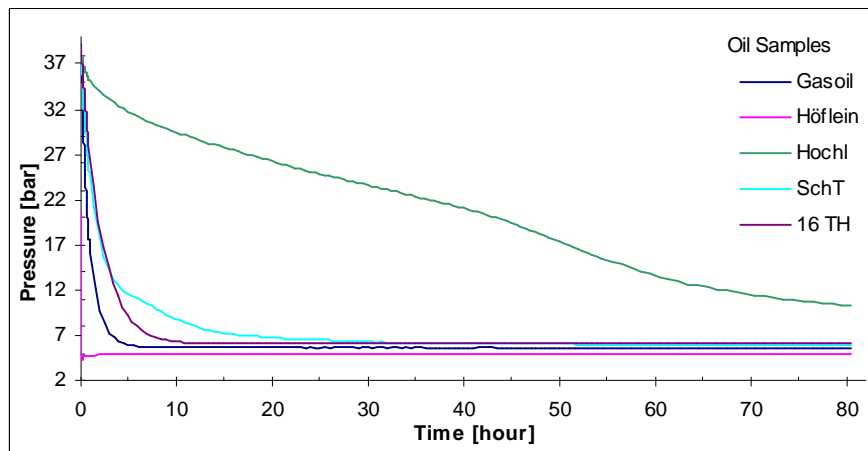


Figure 29: Recorded pressure at 60°C &  $p_i=40$  bar

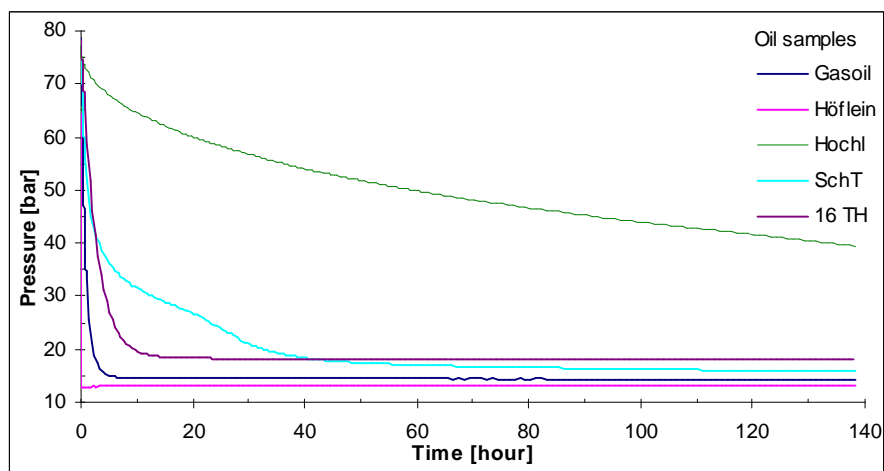


Figure 30: Recorded pressure at 60°C &  $p_i=80$  bar

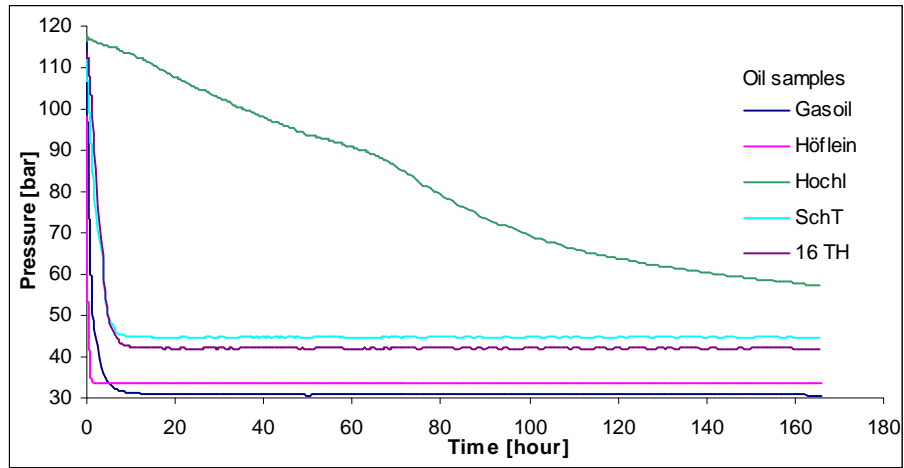


Figure 31: Recorded pressure at 60°C &  $p_i=120$  bar

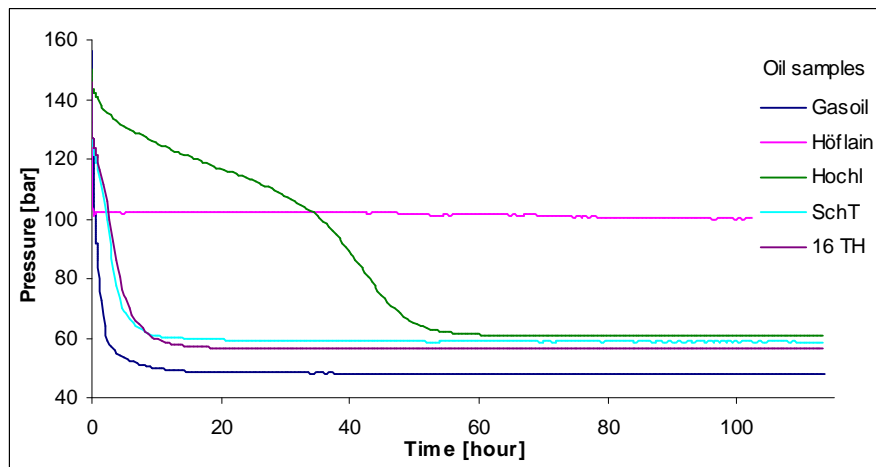


Figure 32: Recorded pressure at 60°C &  $p_i=160$  bar

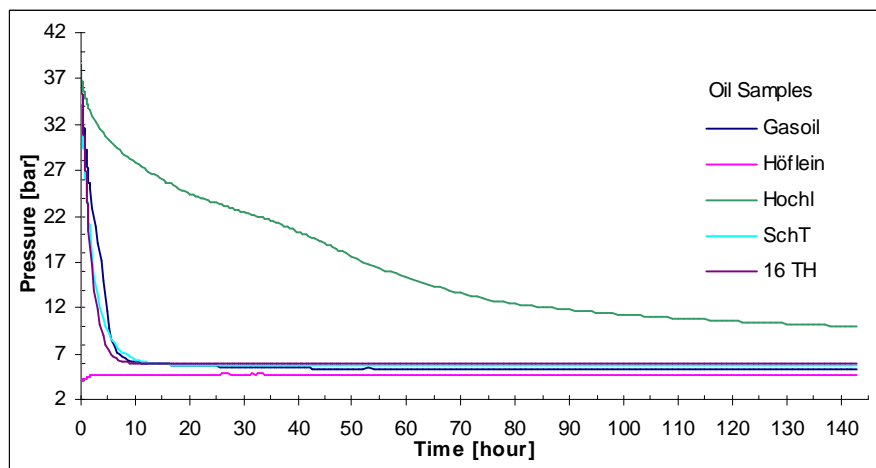


Figure 33: Recorded pressure at 80°C &  $p_i=40$  bar

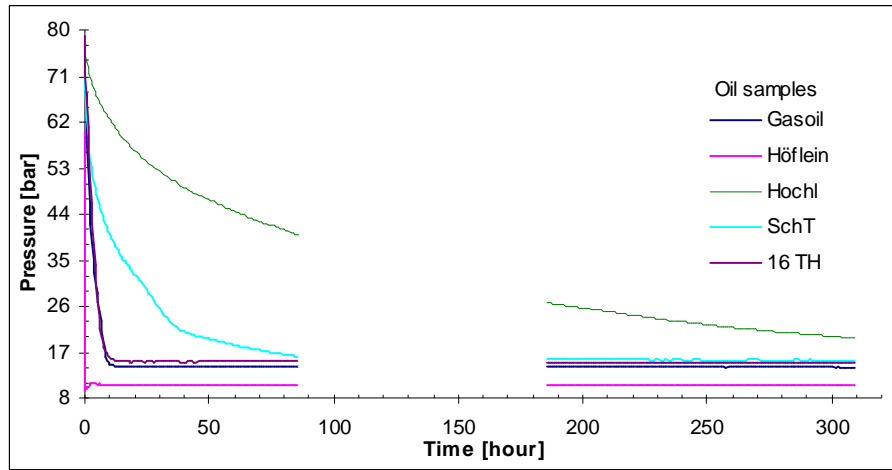


Figure 34: Recorded pressure at 80°C &  $p_i=80$  bar (data missing due to equipment failure)

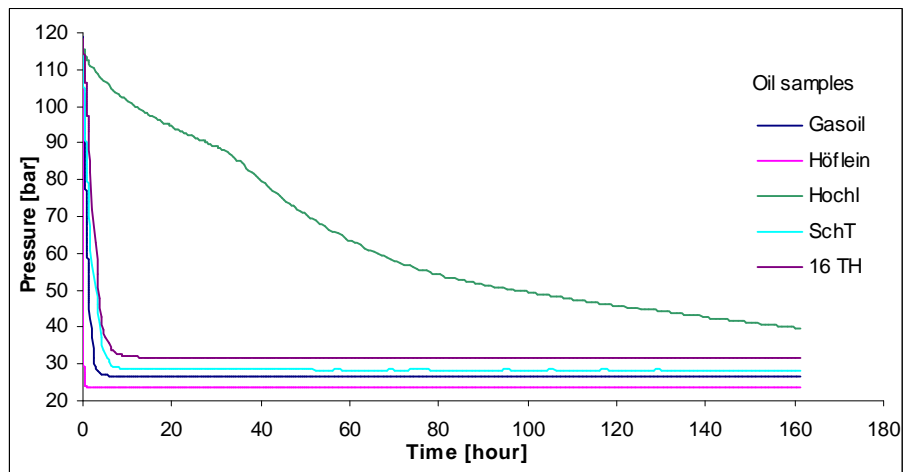


Figure 35: Recorded pressure at 80°C &  $p_i=120$  bar

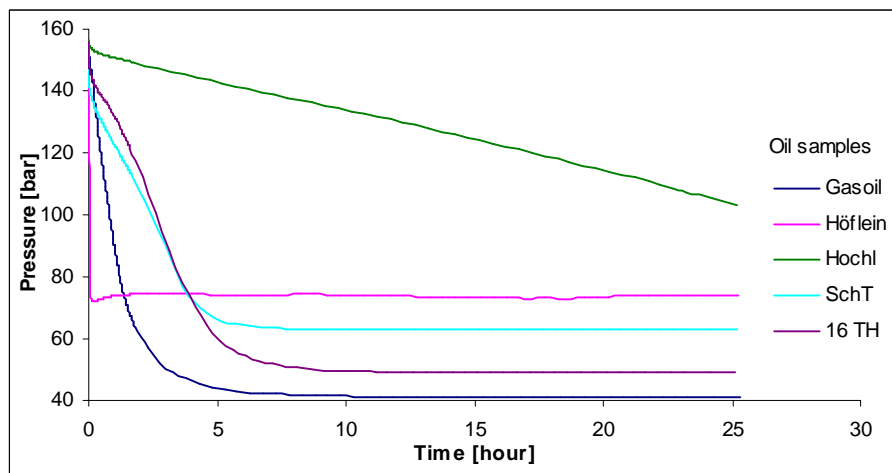


Figure 36: Recorded pressure at 80°C &  $p_i=160$  bar (recording stopped after 25 hours due to equipment failure)

Pressure drop during the dissolution of CO<sub>2</sub> in Hoeflein was very rapid, in most cases it reached the lowest pressure within 10 minutes after test started, and the pressure didn't decrease anymore. This kind of pressure slump could be caused by a relative high dissolution rate of CO<sub>2</sub> in Hoeflein, and CO<sub>2</sub> became less miscible with Hoeflein in higher pressure and lower temperature.

The final pressures of pressure decline curves for Gasoil, 16 TH and SchT were stabilized in the end of the most tests, and these values can be considered very close to the equilibrium values, which was an important requirement of data evaluation.

The pressure decrease during dissolution of CO<sub>2</sub> in Hochleiten was very slow, and the slopes of the pressure decline curves were relative high by the end of the tests, and they increased at higher temperature. Much more observation time would be required for these tests. But we have our time limitation, such longer test was not expected.

The convex and concave shapes were found in one single pressure decline curve in some of the tests especially in higher initial pressure and lower temperature (Fig 27 & 28). One explanation could be that a third phase occurred at a certain T-p region during the dissolution process. The pressure decline curves with this kind of shape will be applied carefully.

## 3. Phase Equilibrium Calculation

### 3.1 Thermodynamic model

The cubic equation of state can be used to model the phase behaviour of CO<sub>2</sub>-brine water fluid system, but the influence of salinity on brine water properties is a difficulty in modelling the binary system.

*Binary Interaction Parameters* are used in the cubic equation of state as empirical parameters for modelling the CO<sub>2</sub>-brine fluid system.

The binary interaction parameters can be generalized as a function of temperature pressure and salinity, and this will be used to predict equilibria of CO<sub>2</sub>-brine binary systems.

SPECS V4.0 is a separation and phase equilibrium calculation program and selected to match our measured data.

SPECS is developed at IVC-SEP (Centre for Phase Equilibria and Separation Processes, Department of Chemical Engineering, Technical University of Denmark) for the Windows 32bit environment. The program integrates different thermodynamic models and algorithms that perform phase equilibrium calculations for different systems. SPECS can model complex mixtures. The algorithms available in the program allow the user to calculate multiphase pT-flashes, phase envelopes, dew and bubble points, p-x and T-x diagrams and other types of calculations which also include the regression of binary interaction parameters for different thermodynamic models. SPECS can be used to characterize oils, perform PVT experiment and slim-tube simulations, calculate viscosities, minimum miscibility pressures and investigate equilibria in reservoirs. Phase diagrams of aqueous electrolyte systems can also be generated with the program [Ref. 22].

#### SPECS configuration:

- *Components:* CO<sub>2</sub> (T<sub>c</sub>: 304.21 K, P<sub>c</sub>: 72.865 bar);  
H<sub>2</sub>O (T<sub>c</sub>: 647.13 K, P<sub>c</sub>: 217.66 bar)
- *Equation of State:* Soave-Redlich-Kwong + Cubic-Plus-Association Equation of State (CPA)
- *Mixing rule:* Quadratic mixing rule with a K<sub>ij</sub> as a parameter
- *Vapour pressure function:* Vapour pressure with use of acentric factor

Soave-Redlich-Kwong + CPA is an equation of state, which combines the physical term of the classical SRK equation of state (Soave, 1972) with the association term based on the perturbation theory of Wertheim (1984, 1986), was developed as the Cubic Plus Association (CPA) equation of state (Kontogeorgis et al., 1996) [Ref. 21].

The development of CPA started in 1995 as a research project funded by Shell, and the model was first published in 1996. Since then, it has been successfully applied to a variety of complex phase equilibria, including mixtures containing alcohols, glycols, organic acids, water, and hydrocarbons. Focus has been placed on cases of industrial importance, e.g., systems with gas-hydrate inhibitors (methanol, glycols), glycol regeneration and gas dehydration units, oxygenate additives in gasoline, alcohol separation, etc. The current focused areas are the estimation of pure compound parameters, alcohol-hydrocarbon vapor-liquid equilibria (VLE) and solid-liquid equilibria (SLE), as well as aqueous systems [Ref. 21].

Soave-Redlich-Kwong EOS:

$$p = \frac{RT}{V-b} - \frac{a(T)}{V(V+b)} \quad (3.1)$$

The Soave-Redlich-Kwong EOS was the first modification of the simple Redlich-Kwong EOS which is based on the van der Waals equation ( $p = \frac{RT}{v-b} - \frac{a}{v^2}$ ).

It has two pure component parameters  $a$  and  $b$ . The parameter  $a$  is a measure of the attractive forces between the molecules, and  $b$  can be interpreted as the inherent volume of the molecules. The van der Waals equation is regarded as a "sphere term + attractive term" equation of state composed from the contribution of repulsive and attractive intermolecular interactions. The Soave-Redlich-Kwong EOS was proposed as an empirical modification of the van der Waals equation to make the attractive term temperature-dependent.

The Soave-Redlich-Kwong EOS requires three input parameters per component:  $T_c$ ,  $P_c$  and  $\omega$ . Constants  $a$  and  $b$  in Eq. 3.1 are functions of  $T_c$ ,  $P_c$  and  $\omega$ . The constant  $a$  of a mixture is related to the  $a$  values of each component,  $a_i$  and  $a_j$ ,

$$a(T) = a_c \cdot a(T) \quad (3.2)$$

$$\text{where } a_c = 0.42747 \frac{R^2 T_c^2}{P_c} \quad (3.3)$$

$$a(T) = [1 + m(1 - \sqrt{T_r})]^2 \quad (3.4)$$

$$\text{with } m = 0.48 + 1.574\omega - 0.176\omega^2 \quad (3.5)$$

$$\& \quad T_r = \frac{T}{T_c} \quad (3.6)$$

where  $\omega$  is the acentric factor.

$$b = 0.08664 \frac{RT_c}{P_c} \quad (3.7)$$

The Soave-Redlich-Kwong EOS is able to predict the phase behaviour of mixtures (vapour-liquid) in the critical region.

*Quadratic mixing rule:*

The quadratic mixing rule is the only mixing rule described here which only two binary interaction parameters per binary system, where only one is used to adjust the parameter  $a$ .

$$a = \sum_{i=1}^k \sum_{j=1}^k x_i x_j (1 - k_{ij}) \sqrt{a_i a_j} \quad \text{with } k_{ij} = k_{ji}, \quad k_{ii} = k_{jj} = 0 \quad (3.8)$$

$$b = \sum_{i=1}^k x_i b_i \quad (3.9)$$

where  $k_{ij}$  is the binary interaction parameter (BIP) between component  $i$  and  $j$ .

The binary interaction coefficients are assumed to be independent of pressure and temperature

**CPA:**

The applications of the CPA (Cubic-Plus-Association) equation of state, is placed on cross-associating systems. Various mixtures are investigated, including systems with two self-associating compounds (e.g., water-alcohol systems or glycols, mixtures with organic acids, or two alcohols) but also binaries with only one self-associating substance, where solvation is expected (e.g., CO<sub>2</sub> or styrene with water).

In the CO<sub>2</sub> dissolution process, the volume decrease of CO<sub>2</sub> is considered to be small. This allows us to use the real gas equation to calculate the amount of dissolved gas  $n_{dis}$ :

Gas Constant:  $R = 83.145 \text{ bar}\cdot\text{cm}^3/\text{mol}\cdot\text{K}$

Gas Volume:  $15 \text{ cm}^3$

$$n = \frac{pV}{RTZ} \quad (\text{real gas equation}) \quad (3.10)$$

$n_{dis}$  at 50 °C with initial pressure at 40 bar can be calculated from data of Fig. 13.

Experimental Data						Calculated Data				
Salinity	T	p <sub>1</sub>	Z <sub>1</sub>	p <sub>2</sub>	Z <sub>2</sub>	n <sub>1</sub>	N <sub>2</sub>	n <sub>dis</sub>	n <sub>brine</sub>	F <sub>CO2</sub>
[%]	[°C]	[bar]		[bar]		[mol]	[mol]	[mol]	[mol]	[mol%]
1%	50	40	0.8307	11.23	0.95394	0.0268	0.0066	0.0202	5.435	0.00370
2%	50	40	0.8307	11.44	0.95394	0.0269	0.0067	0.0202	5.494	0.00366
5%	50	40	0.8307	11.75	0.95394	0.0268	0.0069	0.0199	5.448	0.00364
10%	50	40	0.8307	12.86	0.94985	0.0269	0.0076	0.0193	5.405	0.00355
20%	50	40	0.8307	14.76	0.94117	0.0262	0.0088	0.0175	5.274	0.00331

Table 6: Equilibrium calculation of mol fraction of CO<sub>2</sub> in brine at 50°C, p<sub>i</sub>=40 bar

p<sub>1</sub>: initial pressure

p<sub>2</sub>: final pressure at the end of test

n<sub>1</sub>: mol number of CO<sub>2</sub> in vapour phase at p<sub>1</sub>

n<sub>2</sub>: mol number of CO<sub>2</sub> in vapour phase at p<sub>2</sub>

n<sub>brine</sub>: mol number of brine at start

n<sub>dis</sub>: amount of dissolved CO<sub>2</sub>

F<sub>CO2</sub>: mol fraction of CO<sub>2</sub> in liquid phase.

BIP will be used to tune the program to match the CO<sub>2</sub> mol fraction calculated by experimental data and by SPECS program.

The matching results are shown in Fig 37 and 38.

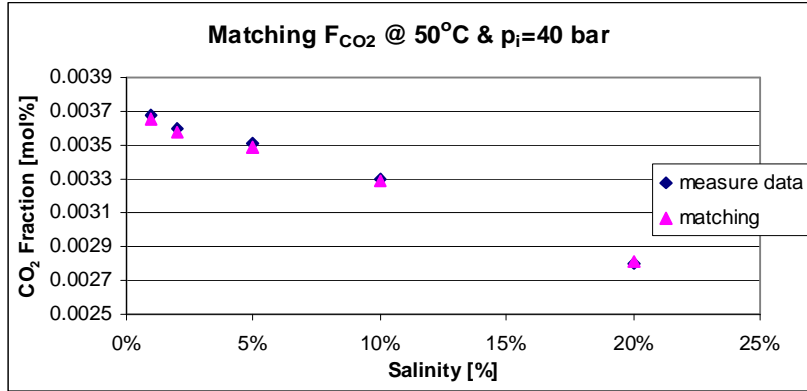


Figure 37: Data matching of CO<sub>2</sub> fraction in liquid phase at 50°C & p<sub>i</sub>= 40 bar

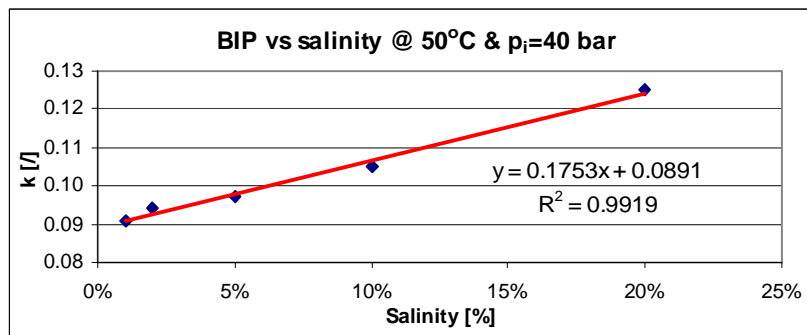


Figure 38: Approached linear of BIP<sub>H<sub>2</sub>O-CO<sub>2</sub></sub> vs. salinity at 50°C & p<sub>i</sub>=40 bar

A general linear equation can be defined as:

$$k = aC + b \quad (3.11)$$

Our correlation equation as a linear function of salinity for BIP at 50°C and 40 bar can be written then:

$$k = 0.1753 \cdot C + 0.0891 \quad (3.12)$$

C : Salinity [weight%]

k : BIP

Correlation equations for BIP for other conditions can be determined by doing the same matching procedure:

50°C and 80 bar:  $k = 0.2122 \cdot C + 0.0318$

50°C and 100 bar:  $k = 0.245 \cdot C + 0.0161$

50°C and 120 bar:  $k = 0.2726 \cdot C + 0.0135$

50°C and 160 bar:  $k = 0.3211 \cdot C + 0.0044$

40°C and 120 bar:  $k = 0.2614 \cdot C + 0.0137$

70°C and 120 bar:  $k = 0.36 \cdot C + 0.0322$



The coefficients a, b can be plotted as a function of pressure at 50°C in Fig 39.

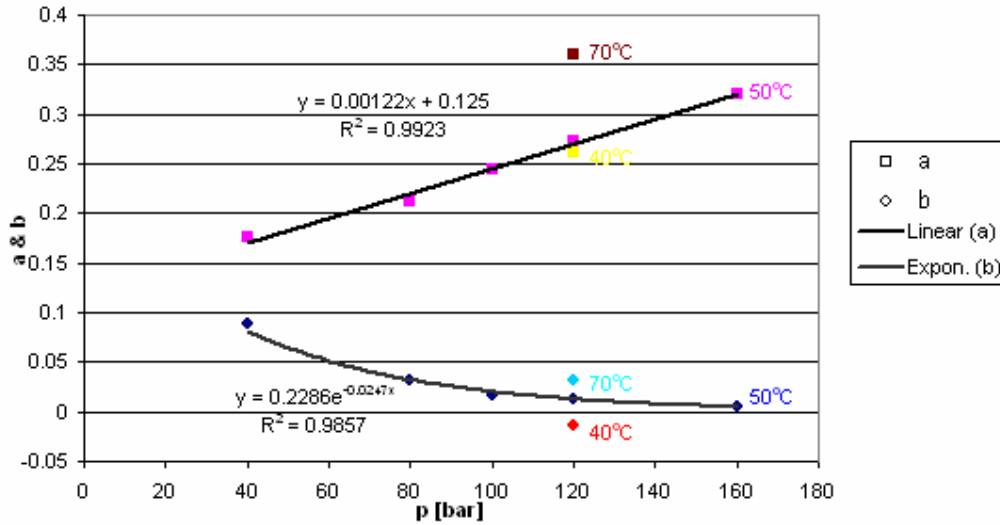


Figure 39: Coefficients a & b vs. pressure

The correlation equation of a and b as a function of pressure at 50°C can be defined (Fig 39) and expressed as:

$$a = 0.00122p + 0.125 \tag{3.13}$$

$$b = 0.2286e^{-0.0247p} \tag{3.14}$$

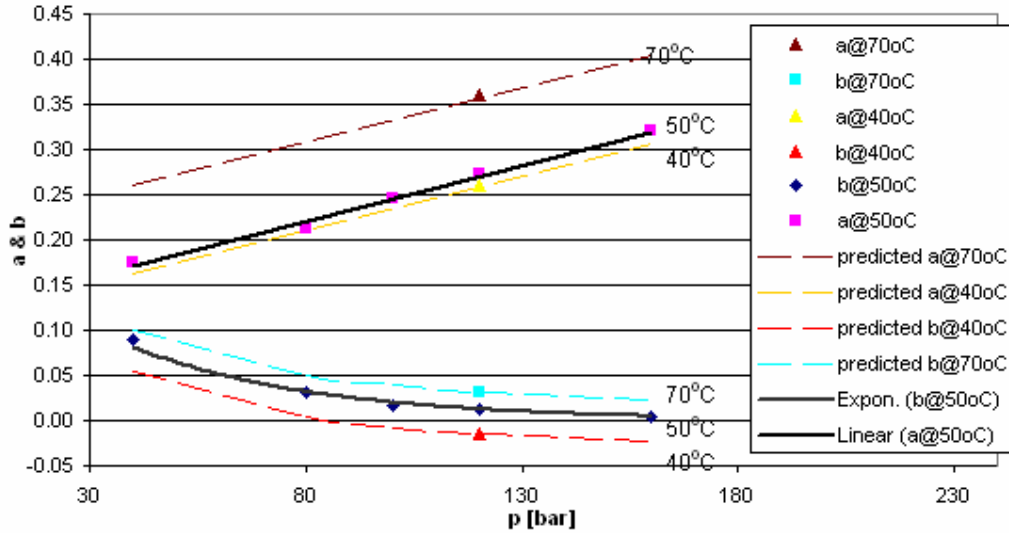
The correlation equations (Eq 3.13 & 3.14) of BIP are expected to give a reasonable prediction of binary CO<sub>2</sub>-brine water equilibrium for temperature at 50°C. The errors of correlated results at tested pressures are shown below.

Errors	40 bar	80 bar	100 bar	120 bar	160 bar	P / Salinity
						Salinity
$error = \frac{ BIP_{matched} - BIP_{correlated} }{BIP_{matched}} [\%]$	4.56%	0.25%	27.12%	9.30%	8.50%	<b>1%</b>
	5.76%	0.98%	15.00%	36.20%	16.95%	<b>2%</b>
	3.30%	4.44%	12.31%	6.04%	2.84%	<b>5%</b>
	2.39%	0.09%	2.17%	9.45%	4.18%	<b>10%</b>
	4.10%	2.99%	6.16%	1.38%	0.82%	<b>20%</b>

Table 7: Errors of correlation equation 3.13 & 3.14 at 50°C

The relative larger errors can be found in brine with 2% salinity at higher pressures, and the reason could be that this brine sample might not be 2% salinity brine. We know that CO<sub>2</sub> solubility decreases with salinity; this means that the less pressure drop should be expected in brine with higher salinity, but in some of the pressure decline profiles of the CO<sub>2</sub> dissolution in brine (Fig 14, 15, 18 & 19), there were larger pressure declines in brine of 2% salinity than the ones in brine of 1% salinity. So the data obtained in brine of 2% salinity could be unreliable.

The predicted coefficients a and b changed with temperatures are shown in Fig 40.


 Figure 40: Predicted  $a$  and  $b$  at different temperatures

Based on Eq 3.13 and 3.14, the equation for the correlation coefficients now can be written as functions of not just pressure but also temperature.

$$a = 0.00122x + 0.1629e^{0.0111T} - 0.1546 \quad (3.15)$$

$$b = 0.2286e^{-0.0247p} + 0.0014T - 0.0699 \quad (3.16)$$

Now  $a$  and  $b$  can be calculated with given the pressure, temperature by Eq 3.15 and 3.16, and BIP can be determined by Eq 3.11, if we know the salinity  $C$ .

But for the lack of our experimental data at 40°C and 70°C, there is a big uncertainty in Eq 3.15 and 3.16 having temperature involved. It's a speculation by predict the BIP both equations. To prove the availability of Eq 3.15 and 3.16, more tests with different initial pressures should be done at a constant temperature.

Although the interaction parameters calculated using those methods may fail to predict the complex phase behaviour at high pressures. The motivation behind this correlation was to estimate an interaction parameter using a fixed point in the phase space and evaluate its effect on the ability of the cubic equation of state to give correct predictions in the region of interest.

The matching of phase behavior of CO<sub>2</sub>-oil system was more complicated than CO<sub>2</sub>-brine system, general correlation of BIP could not be obtained with our experimental data.

## 4. Determination of Diffusion Coefficients of CO<sub>2</sub>

### 4.1 Introduction of Available Models

Laboratory measurement of gas diffusion coefficient in liquid is usually done by measuring the pressure of gas in contact with certain liquids in a PVT-cell during the two-phase equilibration. Several models for determination of gas diffusion coefficient in gas-liquid phase are available, such as models by *Riazi*, *Sachs*, *Zhang et al.*, but the accuracy of their models is limited by simplifying analytical assumptions and subsequent interpretation of experimental data. No consensus is found among their simplified models used for experimental measurement.

The best way to estimate the diffusion coefficient of gas in a given liquid medium is usually by matching the prediction of an appropriate mathematical model including the mass transfer by diffusion to experimental data under prescribed conditions.

*Sach* (1980) used the numerical solution of the nonlinear model equations incorporating the dependency of the diffusion coefficient on concentration without clearly describing the boundary conditions. *Zhang et al.* provided the simplified analytical solutions under special conditions which is more practical. They have determined the diffusion coefficient for gas diffusing into heavy oil using a transient-state diffusion model. It allows for determination of the amount of gas dissolved in the liquid phase, which is then used as the gas/liquid-interface boundary condition in the liquid phase to determine the diffusion coefficient. The reported diffusion coefficients are significantly different from each other. The interpretation methods used to analyse the experimental data are different. *Zhang et al.* used an improper gas/liquid interface boundary assuming a fixed saturation gas concentration value for the liquid phase near the interface is to be obtained only when the equilibrium pressure is achieved. And a constant value is used as the real gas deviation factor, although it might deviate significantly from the unity at elevated pressures. When additional errors are introduced for practical reasons in parameter estimation by inducing the lower order functional approximations, the accuracy of the value of the gas diffusion coefficient becomes unreliable.

The general interface flux continuity condition has been applied by *Civan and Rasmussen*. *Tharanivasan et al.* (2004) determined that this condition yields the best result in determination of the diffusion coefficient for the CO<sub>2</sub>/oil system, it should be pointed out that the flux continuity is a general interface condition that simplifies to the point value condition (Dirichlet boundary condition) considered as the interface mass-transfer coefficient assumes a sufficiently large value.

Based on previous *Civan and Rasmussen* studies, some extensions have been applied in this section, physical and mathematical models have been improved, considering equilibrium and non-equilibrium diffusion gas transport in a non-volatile liquid phase and resistance of the gas/liquid interface to gas dissolution. The models can be solved analytically under various conditions. Practical procedures are developed for accurate estimation of the gas diffusion coefficient by fitting analytical solution to experimental data. The short- and long-time solutions of these models are reformulated for direct determination of gas-diffusivity for the best estimation by regression of analytical expressions to experimental data. The various experimental data are analysed by means of the present improved methods [Ref 24, 26].

## 4.2 Civan and Rasmussen Model

The laboratory measurement of CO<sub>2</sub>-diffusivity in liquids is usually obtained by measuring the pressure of gas in contact with liquids (such as brine, oil, drilling mud) during gas dissolution in the liquid phase.

The pressure in the cell is assumed to be independent of the position. During the dissolution process, we admit a pressure dependence of time in case of diffusion transport is:

$$\frac{dp(t)}{dx} = 0 \quad (4.1)$$

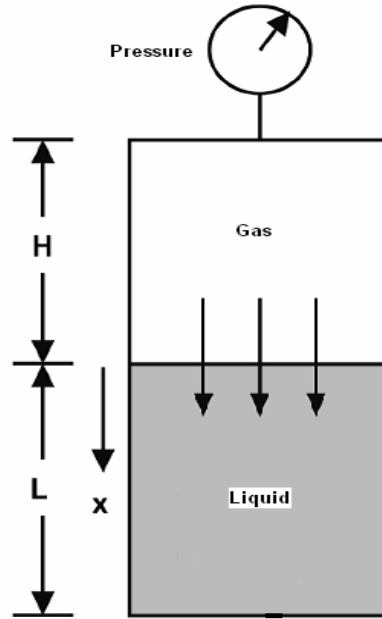


Figure 41: Parameters set up in cylindrical cell

### 4.21 General Formulation

Mathematical model (Civan and Rasmussen *et al.*)

Assuming in the thermodynamic equilibrium throughout the gas phase, the gas properties are considered uniform. The gas density can be calculated by applying the real gas equation of state (derived from Eq 3.7):

$$\rho_g = \frac{M_g p}{ZRT} \quad (4.2)$$

where

$r_g$  : density of gas [kg/m<sup>3</sup>]

p: pressure [bar]

$M_g$ : molecular weight of gas ( $M_{CO_2} = 44.01$ kg/mol)

Z: gas deviation/compressibility factor

T: temperature [K]

R: universal gas constant, 8.31 [J/K/mol]

And  $Z=Z(p,T)$  represents the Z factor, Z is correlated empirically as a function of pressure and temperature. The volume V and mass m of the gas phase are:

$$V = AH \quad (4.3)$$

$$m = r_g V \quad (4.4)$$

where

A: the cross-section area of the test cylinder

H: the length of the gas column (see Fig 41)

m: mass of gas [g]

And the mass flux of gas diffusing from the gas phase into the liquid phase at the gas/liquid interface can be described in the gas-phase mass balance.

$$\frac{dm}{dt} = -AJ|_{x=0}, \quad t > 0 \quad (4.5)$$

The initial gas mass is

$$m = m_o, \quad t = 0 \quad (4.6)$$

Solving Eq 4.5 & Eq 4.6:

$$\frac{m_o - m}{A} = \int_0^t J|_{x=0} dt = Q, \quad t > 0 \quad (4.7)$$

Q: the cumulative mass of gas dissolved in the liquid phase per unit cross-sectional area of the gas/liquid interface [g/cm<sup>2</sup>].

Then substituting Eq 4.2 to Eq 4.4 into Eq 4.7 can result the following operating equation for gas phase:

$$\frac{M_g H}{RT} \left[ \frac{P_o}{Z_o} - \frac{P}{Z} \right] = Q, \quad t > 0 \quad (4.8)$$

An alternative expression to Eq 4.7 can be derived. If  $c(x,t)$  [g/cm<sup>3</sup>] is the concentration of the gas that is dissolved in the liquid phase, and we let  $c_o$  be the initial value, Q can be then expressed as:

$$Q(t) = \int_0^L [c(x,t) - c_o] dx = L \int_0^1 [c(\frac{x}{L}, t) - c_o] d(\frac{x}{L}) \quad (4.9)$$

where  $L$  is the length of the liquid column (see Fig 41), it varies with time when the gas/liquid solution swells by the gas dissolution, i.e.  $L = L(t)$ .

$Q(t)$  can be interpreted as the average gas accumulation in the liquid-phase region (per unit area of cross section).

## 4.22 Equilibrium Transport Model

Moreover, it was assumed that there is no swelling effect due to the dissolution of CO<sub>2</sub> into liquid phase, i.e., the gas/liquid-boundary remains unchanged., and take our diffusion coefficient as a constant.

We apply the second Fick's Law for our case, Eq 1.3 for one dimension can be written as:

$$\frac{\partial c}{\partial t} = D \frac{\partial^2 c}{\partial x^2}, \quad 0 \leq x \leq L, \quad t > 0 \quad (4.10)$$

### Initial condition and boundary condition (IC & BC)

The initial condition is:

$$c = c_o, \quad 0 \leq x \leq L, \quad t = 0 \quad (4.11)$$

The gas/liquid interface-resistive or hindered gas mass-transfer boundary condition is:

$$J|_{x=0} = k(c^* - c), \quad x = 0, \quad t > 0 \quad (4.12)$$

$k$ : the film mass-transfer coefficient at the gas/liquid interface.

$c^*$ : denotes the saturation or equilibrium gas concentration of the liquid phase.

The sealed boundary condition at the bottom of the test cylinder is:

$$J = 0, \quad x = L, \quad t > 0 \quad (4.13)$$

Insert it to Eq 1.2 (first Fick's Law), we get finite-distance condition:

$$\frac{\partial c}{\partial x} = 0, \quad x = L, \quad t > 0 \quad (4.14)$$

The infinite-distance condition is (Dirichlet condition):

$$c = c_o, \quad x \rightarrow \infty, \quad t > 0 \quad (4.15)$$

Boundary condition in gas/liquid interface:

$$-D \frac{\partial c}{\partial x} = k(c^* - c), \quad x = 0, \quad t > 0 \quad (4.16)$$

As  $k \rightarrow \infty$ , the Robin-type Eq 4.15 simplified to the case for the surface Dirichlet-type boundary, given by:

$$c = c^*, \quad x = 0, \quad t > 0 \quad (4.17)$$

### Dimensionless variables

For convenience in the analysis, the concentration, distance and time are expressed in dimensionless form respectively:

$$c_D = \frac{c - c_o}{c^* - c_o} \quad (4.18)$$

$$x_D = \frac{x}{L} \quad (4.19)$$

$$t_D = \frac{Dt}{L^2} \quad (4.20)$$

Subsequently, the second Fick's law and IC & BC (Eq 4.10, 4.11, 4.14, 4.15 and 4.16) can be transformed into the dimensionless forms:

$$\frac{\partial c_D}{\partial t_D} = \frac{\partial^2 c_D}{\partial x_D^2}, \quad 0 \leq x_D \leq 1, \quad t_D > 0 \quad (4.21)$$

$$c_D = 0, \quad 0 \leq x_D \leq 1, \quad t_D = 0 \quad (4.22)$$

$$\frac{\partial c_D}{\partial x_D} = 0, \quad x_D = 1, \quad t_D > 0 \quad (4.23)$$

or

$$c_D = 0, \quad x_D \rightarrow \infty, \quad t_D > 0 \quad (4.24)$$

$$-\frac{\partial c_D}{\partial x_D} = k_D(1 - c_D), \quad x_D = 0, \quad t_D > 0 \quad (4.25)$$

The parameter  $k_D$  appearing in Eq 4.22 can be referred to as a mass-transfer Boit number:

$$k_D \equiv kL/D \quad (4.26)$$

In terms of the non-dimensional variables, the mass accumulation function  $Q(t)$  can be expressed as:

$$Q(t) = L(c^* - c_o)Q_D(t_D) \quad (4.27)$$

where  $Q_D(t)$  is the average of the gas concentration in the liquid-gas mixture region:

$$Q_D(t_D) = \int_0^1 c_D(x_D, t_D) dx_D \quad (4.28)$$

And now Eq 4.8 can be written in dimensionless terms:

$$\frac{MH}{RTL(c^* - c_o)} \left[ \frac{P_o}{Z_o} - \frac{P}{Z} \right] = Q_D(t) \quad (4.29)$$

This is the key equation for determination of diffusion coefficient  $D$ , and it is only valid when the final pressure reaches the equilibrium pressure after an effectively long time.

We assume that the equilibrium condition is obtained after a sufficient long time and P reaches P\*, when  $Q_D = 1$ , we have:

$$\frac{MH}{RTL(c^* - c_o)} \left[ \frac{P_o}{Z_o} - \frac{P^*}{Z^*} \right] = 1 \quad (4.30)$$

And now Eq 4.29 is divided by Eq 4.30, the new equation can be written as:

$$\frac{\frac{P_o}{Z_o} - \frac{P}{Z}}{\frac{P_o}{Z_o} - \frac{P^*}{Z^*}} = Q_D \quad (4.31)$$

Now the terms on the left side can be determined by the measured data of pressure at a given temperature as a function of time, and the function  $Q_D(t)$  on the right is a time function on the right side is assumed to represent the physical process and correlate the data, it is established using the analytical solutions which are described in the following solution section.

## Analytical Solutions

The gas diffusion coefficient D of the binary mixture in the gas/liquid solution can be determined by solving Eq 4.21 with the IC and BC.

### Long-time (finite-length) solution

When the length L is finite, Eq 4.21 can be solved together with the initial condition (Eq 4.22) and boundary condition (Eq 4.23 and 4.25).

A Fourier-series analytical solution can be obtained which is valid for large time:

$$c_D = 1 - 4 \sum_{m=1}^{\infty} \frac{\sin I_m}{2I_m + \sin(2I_m)} \exp(-I_m^2 t_D) \cos[I_m(1 - x_D)] \quad (4.32)$$

and  $\lambda_m$  denotes the root of

$$\tan I = k_D / I \quad (4.33)$$

when  $k_D = p$ , the first four smallest positive roots can be:  $\lambda_1 = 1.2046$ ,  $\lambda_2 = 3.828$ ,  $\lambda_3 = 6.7205$ , and  $\lambda_4 = 9.7369$ ...

Subsequently, the expression for  $c_D$  (Eq 4.30) is substituted into Eq (4.28) for  $Q_D$  and the integration is then made for  $x_D$ , the result is:

$$Q_D(t_D) = 1 - 4 \sum_{m=1}^{\infty} \frac{\sin^2 I_m}{I_m [2I_m + \sin(2I_m)]} e^{-I_m^2 t_D} \quad (4.34)$$

The complete infinite series satisfies the relation  $Q_D(0) = 0$ . The same result is found when the time integral of the mass-flux term is used in accordance with Eq 4.7.

When the time  $t_D$  is large, we can neglect the rest terms of the infinite series, and take the leading one as the significant term, and the Eq 4.32 is then:



$$Q_D^L(t_D) = 1 - \frac{4 \sin^2 I_1}{I_1 [2I_1 + \sin(2I_1)]} e^{-I_1^2 t_D} \quad (4.35)$$

or

$$1 - Q_D^L(t_D) = \frac{4 \sin^2 I_1}{I_1 [2I_1 + \sin(2I_1)]} e^{-I_1^2 t_D} \quad (4.36)$$

$\lambda_1$ : the smallest positive root of the equation  $\tan I_1 = k_D / I_1$ .

The upper bound corresponds to  $k_D \rightarrow \infty$ , which is coming up to the case for the surface Dirichlet-type boundary condition  $c(0,t)=c^*$  in Eq 4.12.

This is known as the long-time approximation, this approximation is used to determine a least-squares estimate of coefficient of gas diffusion coefficient  $D$  in the liquid phase by using the measure data of pressure values during the gas diffusion in a liquid.

For the non-equilibrium case for the finite region, the long-time approximation can not be applied, it does not satisfy the IC & BC.

We note that if we take the natural logarithm of the Eq 4.34, the equation becomes:

$$\ln[1 - Q_D^L(t_D)] = \ln\left(\frac{4 \sin^2 I_1}{I_1 [2I_1 + \sin(2I_1)]}\right) - I_1^2 t_D \quad (4.37)$$

In which the term  $\ln\left(\frac{4 \sin^2 I_1}{I_1 [2I_1 + \sin(2I_1)]}\right)$  is a constant.

This indicates that plotting the natural logarithm of  $[1 - Q_D^L(t_D)]$  against  $t_D$  should give us a straight-line relation. The gas diffusion coefficient will be extracted from this method with a given set of a pressure-decline data.

The data can be correlated with the straight line by means of regression analysis in this form which is a general form of Eq 4.35:

$$\ln[1 - Q_D^L(t_D)] = a_L + b_L t \quad (4.38)$$

where

a: the y-axis intercept

b: the slope of the line

These two variables can be expressed by comparing between Eq 4.35 and 4.36:

$$a_L = \ln\left(\frac{4 \sin^2 I_1}{I_1 [2I_1 + \sin(2I_1)]}\right) \quad (4.39)$$

$$b_L = -\frac{DI_1^2}{L^2} \quad (4.40)$$

For the limiting case  $k_D \rightarrow \infty$  and  $I_1 = p / 2$ , the diffusion coefficient can be solved from Eq 4.40:

$$D = -\frac{4b_L L^2}{p^2} \quad (4.41)$$

### Short-time (Semi-infinite) solution

For semi-infinite region, the Eq 4.21 can be solved together with the initial condition (Eq 4.22) and boundary condition (Eq 4.24 and 4.25). The analytical short-time solution for semi-infinite region can be obtained as follow:

$$Q_D^S(t_D) = \frac{1}{k_D} \left[ \exp(k_D^2 t_D) \operatorname{erfc}(k_D \sqrt{t_D}) - 1 + 2k_D \sqrt{\frac{t_D}{p}} \right] \quad (4.42)$$

When the mass-transfer Biot number  $k_D \rightarrow \infty$ , Eq 4.32 can be simplified to

$$Q_D^S(t_D) = 2\sqrt{\frac{t_D}{p}} \quad (4.43)$$

This result could be obtained if the Dirichlet boundary condition has been imposed at the interface. The length  $L$  cancels out the problem for semi-infinite region. This result is considered as small-time approximations, these solutions can be used with fluid with low diffusion rate or test time is sufficient short that the diffusing gas can not reach the bottom of the test cylinder.

The result of Eq 4.42 can be obtained formally from the small-time inversion of the Laplace-transform analysis for the finite-length condition. For very small times, Eq 4.42 can be expanded with small  $z = k_D \sqrt{t_D}$ :

$$Q_D^S(t_D) \cong \frac{1}{k_D} \left[ z^2 - \frac{4}{3\sqrt{p}} z^3 + \frac{z^4}{2} - \frac{8}{15\sqrt{p}} z^5 + \frac{z^6}{6} + \dots \right], \quad z \rightarrow \infty \quad (4.44)$$

For finite  $k_D$ , the initial slope of plotting  $Q_D$  against  $\sqrt{t_D}$  is always zero, but when  $t_D$  is very large, the short-time approximation approaches the asymptote.

$$Q_D^S(t_D) \cong 2\sqrt{\frac{t_D}{p}} - \frac{1}{k_D}, \quad k_D \sqrt{t_D} \rightarrow \infty \quad (4.45)$$

The straight-line character of the curves for asymptotic long-time behavior can be applied for the short-time solution on  $Q_D(t_D)$  vs.  $\sqrt{t}$  plots, if we express Eq 4.45 as:

$$Q_D^S(t_D) = a_s + b_s \sqrt{t} \quad (4.46)$$

In which the slope can be given by:

$$b_s = \frac{2}{L} \sqrt{\frac{D}{p}} \quad (4.47)$$

Diffusion coefficient is then calculated as follows:

$$D = \frac{pL^2 b_s^2}{4} \quad (4.48)$$

### 4.3 Errors in Correlation Model

By using the straight line correlation method of long-time data and the calculation of diffusion coefficient D from experimental data, some errors are introduced.

#### Errors from Assumptions

In order to be able to derive the analytical solutions, we neglected the swelling effect caused by gas dissolution and we assumed the mass-transfer Biot number to be constant. In reality, the values of the parameters may vary and cause errors. Diffusion often contains gravitational effects, there is a bulk motion resulting from the change densities of the solutions, and the change of density in gas-liquid mixture may cause convection, which may also affect the accuracy of diffusion coefficient calculation. In our case, we actually considered the gas diffusion in quiescent liquid.

#### Errors from long-time data

Cumulative mass of gas dissolved in liquid Q could cause significant errors at long times compared to short time. We assume that the error occurs in obtaining the experimental value of the dimensionless cumulative gas dissolution is a certain percent of the true value, this can be expressed as:

$$Q_{D'exp} = (1 + \epsilon)Q_{D'true} \quad (4.49)$$

$\epsilon$ : percentage of error.

If the true value of the dimensionless cumulative gas dissolution is already available, we can express  $Q_{D'true}$  (true dimensionless cumulative gas dissolution) in Eq 4.35:

$$Q_{D'true} = 1 - Q(h)e^{-h^2 t_D} \quad (4.50)$$

$$Q(h) = \frac{4 \sin^2(h)}{h[2h + \sin(2h)]} \quad (4.51)$$

The experimental value of the dimensionless cumulative gas dissolution  $Q_{D'exp}$  is then:

$$\begin{aligned} Q_{D'exp} &= 1 - Q(h)e^{-h^2 t_D} + \epsilon[1 - Q(h)e^{-h^2 t_D}] \\ &= 1 - Q(h)e^{-h^2 t_D} \left[ 1 - \epsilon \left( \frac{e^{h^2 t_D}}{Q(h)} - 1 \right) \right] \end{aligned} \quad (4.52)$$

After taking the natural logarithm, the equation is now:

$$\ln(1 - Q_{D'exp}) = \ln Q(h) - h^2 t_D + \ln \left[ 1 - \epsilon \left( \frac{e^{h^2 t_D}}{Q(h)} - 1 \right) \right] \quad (4.53)$$

Eq 4.53 shows the effect of error.

Therefore, the scatter in data increases as time increases. Thus, every effort should be taken to obtain data with special accuracy at long times.

## 4.4 Application of Model

### 4.41 Diffusion Coefficients of CO<sub>2</sub> in Brine

Unfortunately we have not given sufficient observation time for previous brine tests, none of the pressure drop have reached the equilibrium pressure closely enough to satisfy our diffusion model. One typical pressure drop by the end of the test with 2% brine at 50°C with an initial pressure of 80 bar is shown below, by the time we stopped the test, the pressure still had the tendency to decrease.

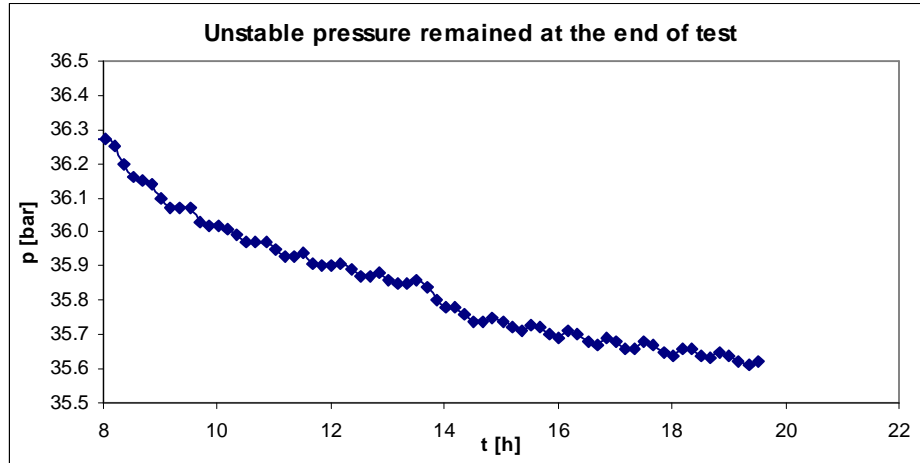


Figure 42: Pressure drop recording stopped after 20 hours of CO<sub>2</sub> dissolution test in 2% brine at 50°C, with  $p_i=80$  bar

In order to minimize the error, we omitted the data from previous brine tests due to insufficient observation time. Another test with an initial pressure of 10 bar was ran at 50°C, and the observation time was extended up to about 70 hours, this could make the pressure getting closer to equilibrium pressure. Again the pressure decreases of CO<sub>2</sub> dissolution in different salinity of brine are shown in Fig 43.

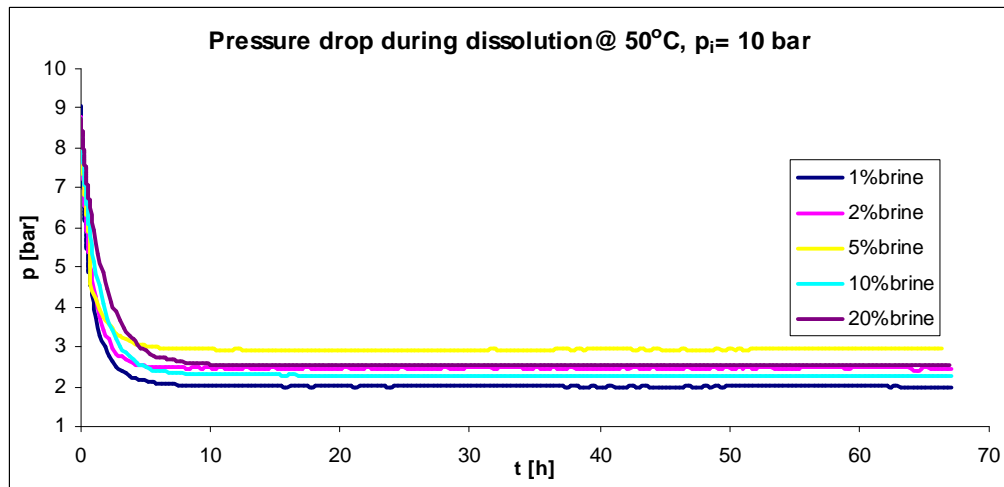


Figure 43: Pressure drops during dissolution process in brine at 50°C, with  $p_i=10$  bar

The slopes of the pressure curves by the end of these test and the previous tests have been made:

Salinity	10 bar	40 bar	80 bar	100 bar	120 bar	160 bar
1%	-0.0001	-0.011	-0.023	-0.034	-0.037	-0.025
2%	-0.0002	-0.014	-0.026	-0.038	-0.044	-0.034
5%	-0.0001	-0.011	N/A	-0.038	-0.054	-0.046
10%	-0.0001	-0.013	-0.046	-0.045	-0.048	-0.060
20%	-0.0001	-0.023	-0.086	-0.038	-0.028	-0.374
Observation time	67 hours	22 hours	20 hours	20 hours	25 hours	23 hours

Table 8: Measured slopes [bar/h] of the pressure decline curves at the end of tests at 50°C

The test carried out at 10 bar shows that the pressure became much more stable at the end than the ones in the previous tests with shorter observation time and higher initial pressures. Therefore the data from the new tests were chosen to be used for the evaluation.

Unfortunately the mass transfer rate is not only caused by diffusion but also by convection. Convection is another mechanism that refers to the movement of currents within fluids; it is also one of the major modes of mass transfer. Convection mechanism can result from difference of densities in inhomogeneous fluids, which induces fluid motion and this enables the mass transfer.

Generally, the dissolution of CO<sub>2</sub> into water will cause a density increase. The density difference can cause natural convection, and this natural convection mechanism dominates in the short term in the CO<sub>2</sub> dissolution process, which enhances the mass transfer rate across the interface at high initial pressure.

Density calculations were run to estimate the effect of natural convection mechanism during the dissolution process. The phase density of the CO<sub>2</sub>-brine solution can be determined by EOS. The phase equilibrium calculation program SPECS was used to perform the phase behavior computation of CO<sub>2</sub>-brine system.

Experimental Data							Calculated Data				
Salinity	T	p <sub>1</sub>	Z <sub>1</sub>	p <sub>2</sub>	Z <sub>2</sub>	V <sub>CO<sub>2</sub></sub>	n <sub>1</sub>	n <sub>2</sub>	n <sub>dis</sub>	brine	F <sub>CO<sub>2</sub></sub>
	[°C]	[bar]		[bar]		[cm <sup>3</sup> ]	[mol]	[mol]	[mol]	[mol]	[mol%]
1%	50	9.05	0.9632	1.99	0.9951	15	0.00525	0.0009	0.0044	5.5389	0.0785
2%	50	8.79	0.9640	2.42	0.9922	15	0.00509	0.0014	0.0037	5.5267	0.0674
5%	50	8.77	0.9641	2.93	0.9889	15	0.00508	0.0017	0.0034	5.5164	0.0620
10%	50	8.73	0.9642	2.25	0.9934	15	0.00506	0.0013	0.0038	5.4242	0.0698
20%	50	8.74	0.9641	2.53	0.9915	15	0.00506	0.0014	0.0036	5.3432	0.0680

Table 9: Equilibrium calculation of mol fraction of CO<sub>2</sub> in brine at 50°C, p<sub>i</sub>=10 bar

The equilibrium density of CO<sub>2</sub> dissolved in brine can be obtained by matching the mol fraction of CO<sub>2</sub> in liquid phase.

And the density of brine at 50°C and 10 bar can be estimated by Eq 4.54. This equation is also valid to calculate the density of oil samples.

$$r = r_0 \cdot e^{(T_0-T)a} \cdot e^{(p-p_0)b} \quad (4.54)$$

$\alpha$  : thermal expansion coefficient,  $a = \frac{1}{V} \left( \frac{\partial V}{\partial T} \right)$

$\beta$  : isothermal compressibility coefficient,  $b = -\frac{1}{V} \left( \frac{\partial V}{\partial p} \right)$

$\alpha_w = 4.57 \times 10^{-4} \text{ [K}^{-1}]$        $\alpha_o = 1 \times 10^{-3} \text{ [K}^{-1}]$       for  $T = 50^\circ\text{C}$

$\beta_w = 4.64 \times 10^{-5} \text{ [bar}^{-1}]$        $\beta_o = 1 \times 10^{-4} \text{ [bar}^{-1}]$       for  $T = 50^\circ\text{C}$ .

$\alpha_w$  &  $\beta_w$  are taken from the value of water, and used for the calculation of density of brine, and  $\alpha_o$  and  $\beta_o$  are experience values for the oil density calculation (see Chapter 4.22).

The results for brine are shown below:

Salinity [%]	Density of brine + CO <sub>2</sub> [kg/m <sup>3</sup> ]	Density of brine [kg/m <sup>3</sup> ]	Increased density [%]
1%	1006.54	991.33	1.53%
2%	1011.73	996.76	1.50%
5%	1033.50	1018.37	1.49%
10%	1057.97	1042.35	1.50%
20%	1134.88	1118.34	1.48%

Table 10: Liquid densities at T =50°C and p=10 bar

In Fig 44, we can see the liquid density difference between the one on top region close to the interface which is saturated with CO<sub>2</sub> and the one at the bottom which is equal to the brine density.

The unstable densities in liquid cause the natural convection, in a gravity field such differences cause movement forces due to buoyancy of the less-dense particles of fluid. This movement force drives the less-dense fluid moving to the upper region.

However a sufficient long time is needed until the mass transfer becomes diffusion like, and also very important for obtaining the equilibrium pressure. The mass transfer rate can be controlled only by diffusion in long term process. This allows us to do the following determination of diffusion coefficient of CO<sub>2</sub> in brine.

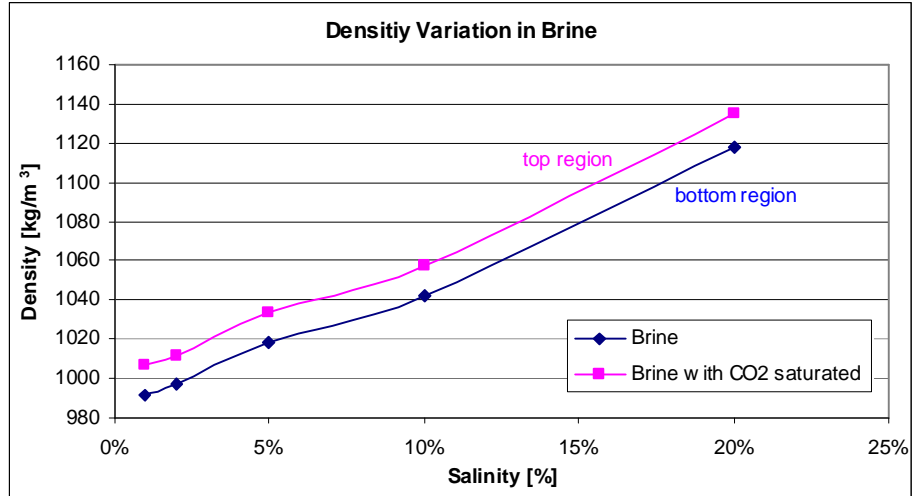


Figure 44: Density difference in liquid at 50°C, with p=10 bar

Data we gained from CO<sub>2</sub> dissolution in brine at 50°C and 10bar was used to determine the diffusion coefficient of CO<sub>2</sub> in brine by applying Civan's analytical model based on Fick's law.

### Data Correlation

During the longer observation time, the final pressure was stabilized. Unfortunately the pressure drop  $\Delta p$  was not monotonously decreasing at the late stage due to the limitation in accuracy of equipment, the pressure can be precise in the range of 0.01 bar. To be able to predict diffusion coefficient properly, the pressure drop in late hours had to be correlated to be monotonously decreasing. For example, the pressure correlation of CO<sub>2</sub> dissolution in 1% brine is shown in Fig 45.

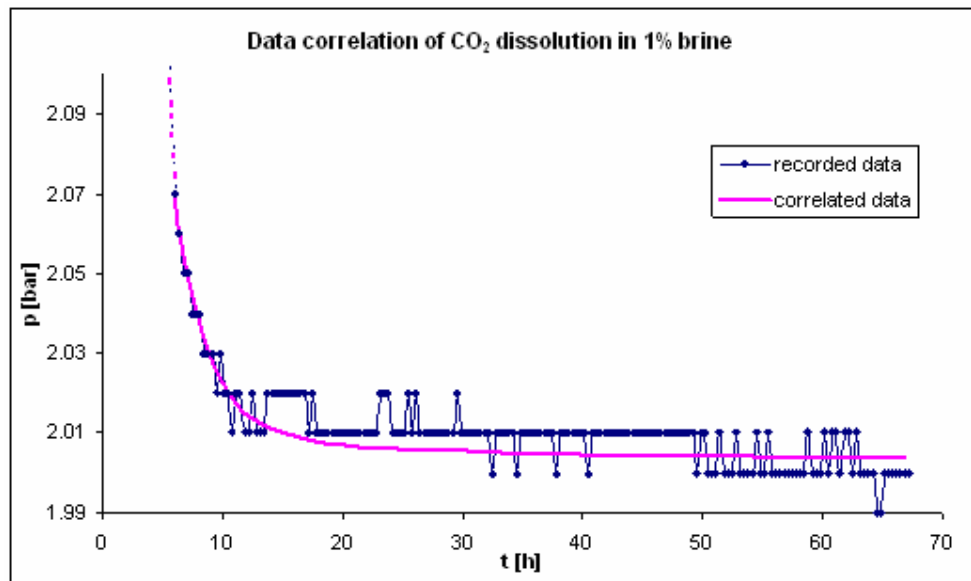


Figure 45: Correlation of pressure decrease of CO<sub>2</sub> dissolution in 1% brine

Long-time (finite-length) approximation was used to determine the diffusion coefficients of brine. As we showed before, the natural convection is the dominant mechanism in the early phase of dissolution process, the mass transfer is controlled by diffusion only in the late hours, therefore we divided the process in two stages: early stage where the pressure decline curve has high slope in the early hours; late stage for pressure starts to get stable in the late hours, this is where our effective data is taken from to determine the value of diffusion coefficient of CO<sub>2</sub>.

The key equations to do the graphic determination are Eq 4.37 & 4.38.

$b_L$  of the long-time approximation can be obtained by plotting the following figures (46-50):

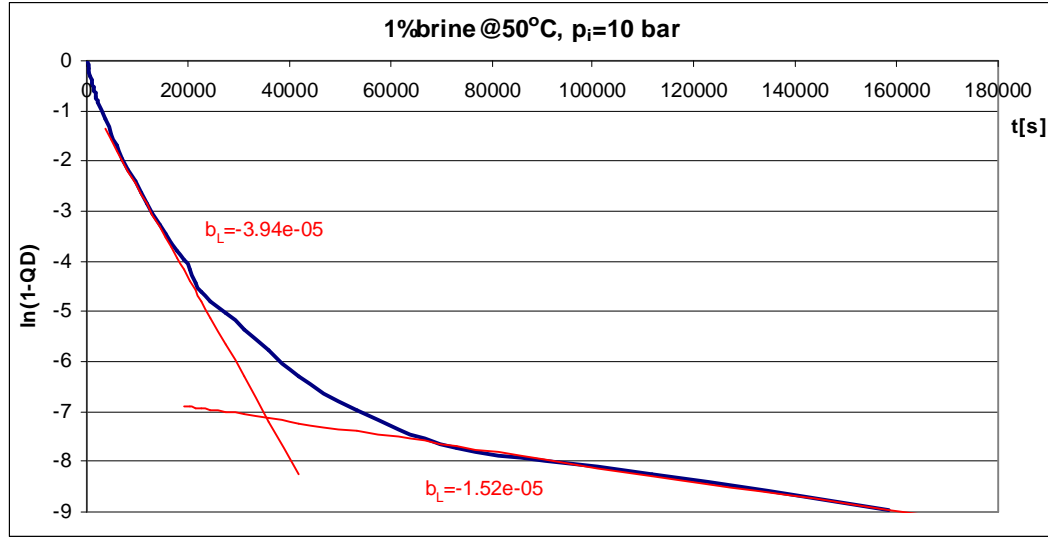


Figure 46:  $b_L$  determination in early and late stage for 1% brine

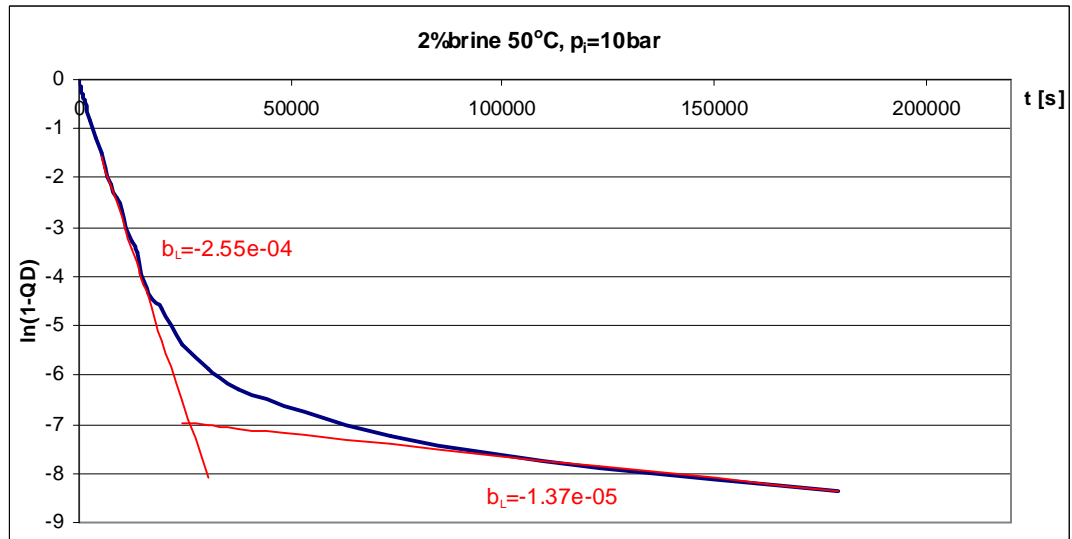


Figure 47:  $b_L$  determination in early and late stage for 2% brine



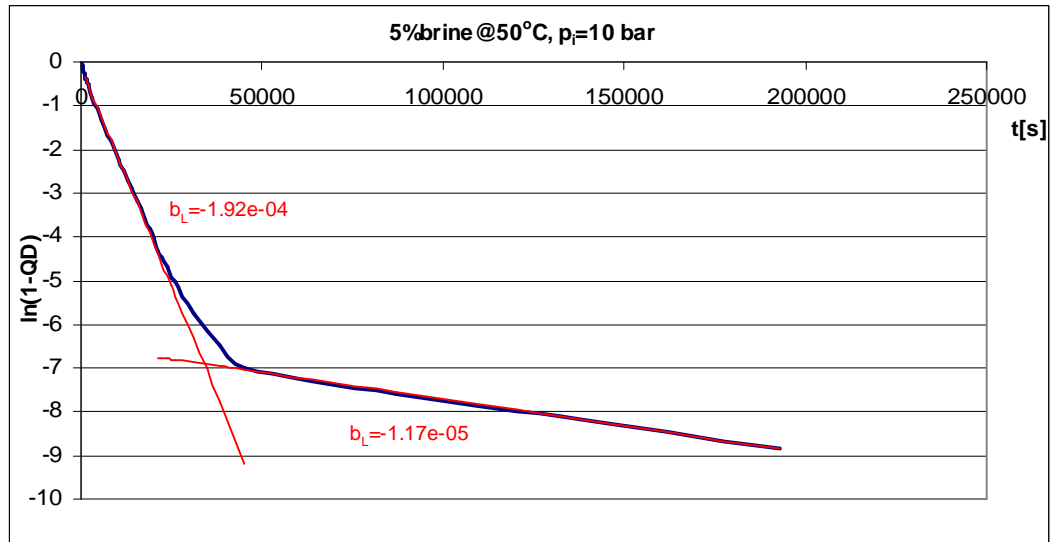


Figure 48:  $b_L$  determination in early and late stage for 5% brine

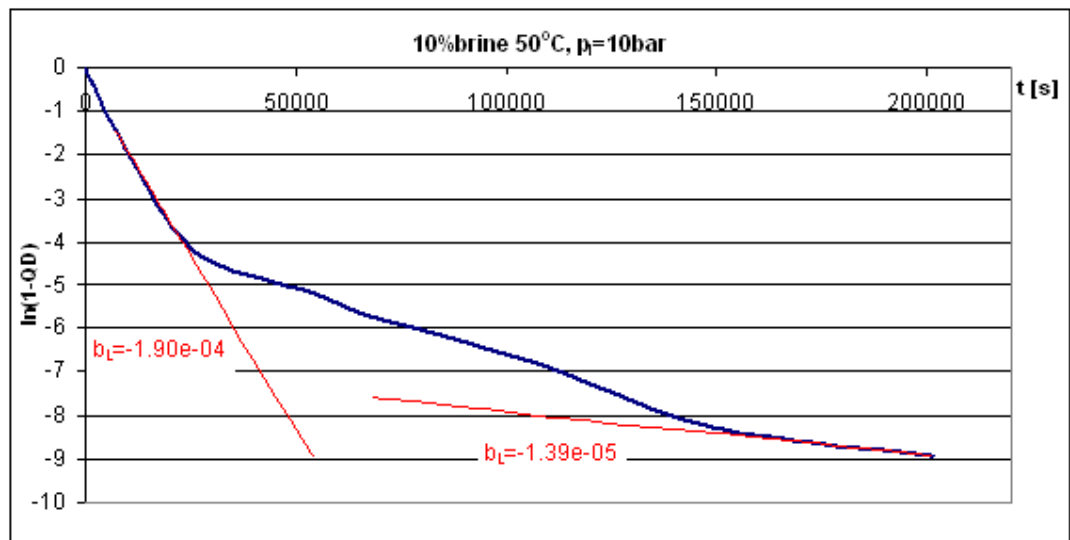


Figure 49:  $b_L$  determination in early and late stage for 10% brine (LO)

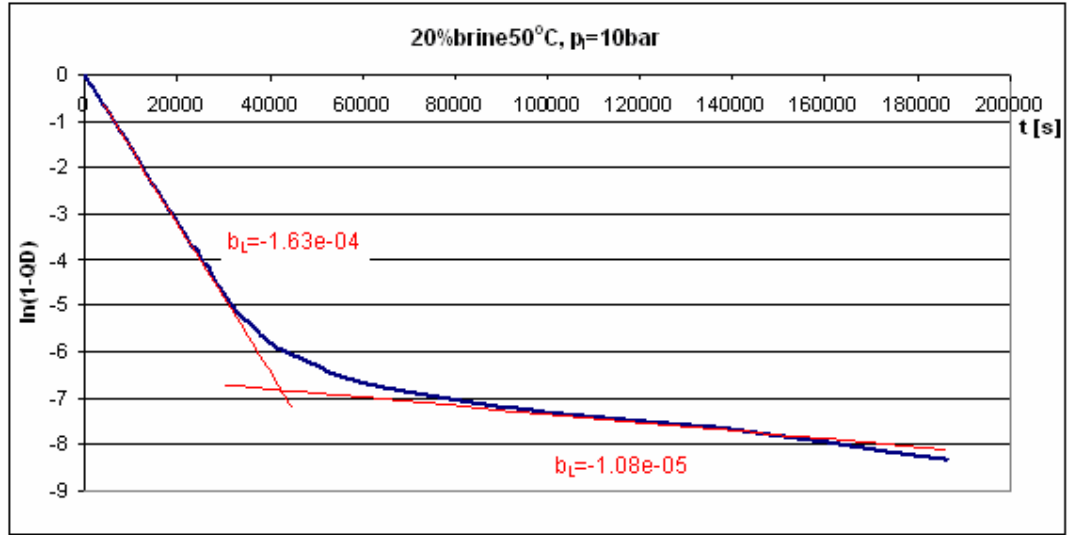


Figure 50:  $b_L$  determination in early and late stage for 20% brine

The long-time solution for diffusion coefficient can be calculated by using Eq 4.41, and the results are displayed below:

Salinity	$b_L$ (early stage)	$D_L$ (early stage) [cm <sup>2</sup> /s]	$b_L$ (late stage) [bar/h]	$D_L$ (late stage) [cm <sup>2</sup> /s]
1%	3.94E-04	1.54E-02	1.52E-05	5.94E-04
2%	2.55E-04	9.96E-03	1.37E-05	5.37E-04
5%	1.92E-04	7.50E-03	1.17E-05	4.59E-04
10%	1.90E-04	7.45E-03	1.39E-05	5.43E-04
20%	1.63E-04	6.36E-03	1.08E-05	4.24E-04

Table 11: Slops  $b_L$  and diffusion coefficients of CO<sub>2</sub> in brine at 50°C

The diffusion coefficient of CO<sub>2</sub> in brine at early stage is at least one order of magnitude higher than the values at late stage. This can be interpreted as the enhancement of the diffusion mechanism of CO<sub>2</sub> in brine by convection at early stage.

The experimental data of pressure drop in 10% brine shows an outlier of the D values, which could lead to high error of D value. This can be seen in Fig 49, the D value of CO<sub>2</sub> in 10% brine didn't fit in the graphic as a function of salinity (Fig 51). Therefore we ignore this one and displayed the curve again in Fig 52, it shows the diffusion coefficients of CO<sub>2</sub> in brine decreases with salinity, and the slope of curve decreases with higher salinity.

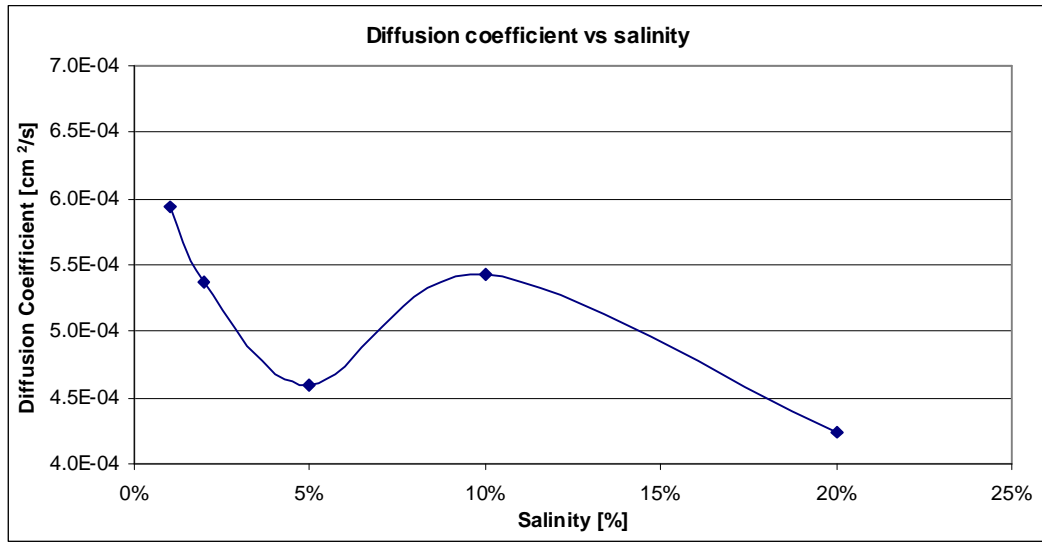


Figure 51: Diffusion coefficient changes with salinity at 50°C

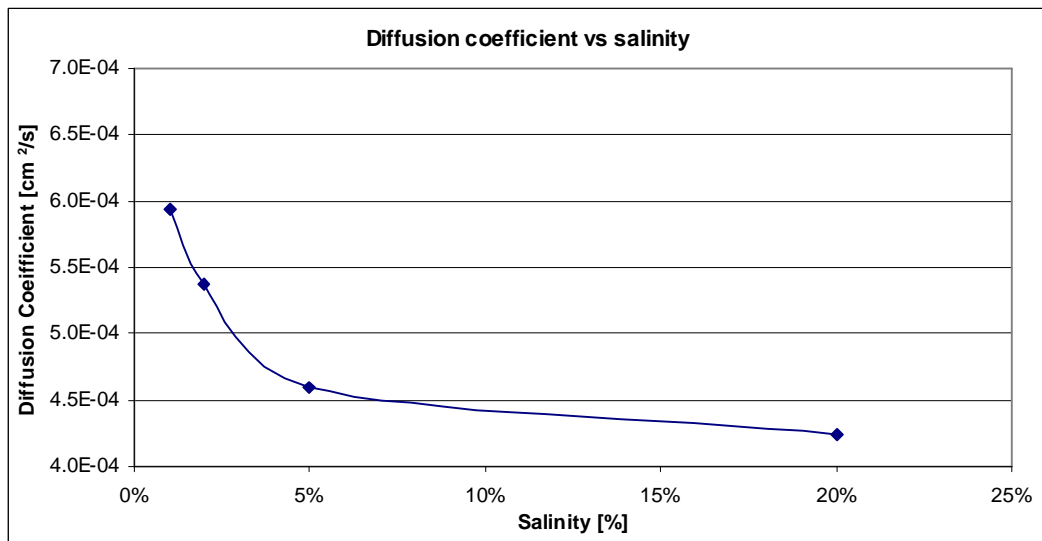


Figure 52: Diffusion coefficient as a function of salinity at 50°C (without the data from 10% brine)

### 4.42 Diffusion Coefficients of CO<sub>2</sub> in Oil

A whole series of tests of CO<sub>2</sub> dissolving in oil have been carried out, but not all the data are able to be used by Civan's model. The quality check has been done for each pressure drop profile. It should have a long observation time in order for the pressure to reach the equilibrium pressure.

#### Gasoil

Gasoil is a synthetic condensate, it's one of the light oils among our oil samples, quite transparent. It has low liquid viscosity (higher than Hoefflein), and is second lightest oil sample. The pressure drop profiles of CO<sub>2</sub> dissolution in Gasoil in different p-T conditions have been checked, the data from the tests were chosen, in which the pressure decreased to the equilibrium pressure in a sufficiently long observation time. The selected tests are shown below:

T \ p <sub>i</sub>	40 bar	80 bar	120 bar	160 bar
40°C	IT	ü	ü	error
60°C	ü	ü	ü	ü
80°C	IT	DD	ü	IT

IT: insufficient time for obtaining equilibrium pressure; DD: discontinuity in data.

Table 12: Selected tests from different p-T conditions

And also the density effects in those tests were evaluated. The equilibrium densities of Gasoil with CO<sub>2</sub> dissolved were calculated by EOS (SPECS). The Gasoil density at different p-T conditions can be calculated with Eq 4.54, and the increase from Gasoil density at the bottom to the upper region near the interface is displayed below in percentage:

T \ p <sub>i</sub>	40 bar	80 bar	120 bar	160 bar
40°C	IT	3.72%	5.37%	error
60°C	2.57%	3.10%	3.96%	5.01%
80°C	IT	DD	6.48%	IT

Table 13: Increased density in solution to density of Gasoil

Table 13 shows the density increases occurred in the solution during the solution process, this caused natural convection, which enhanced the mass transfer rate in CO<sub>2</sub> dissolution in Gasoil.

We also see convection effects by applying the Civan's model.

b<sub>l</sub> was graphically determined in Figures (53-59) by using Civan's long-time approximation with Eq 4.37 and 4.38.

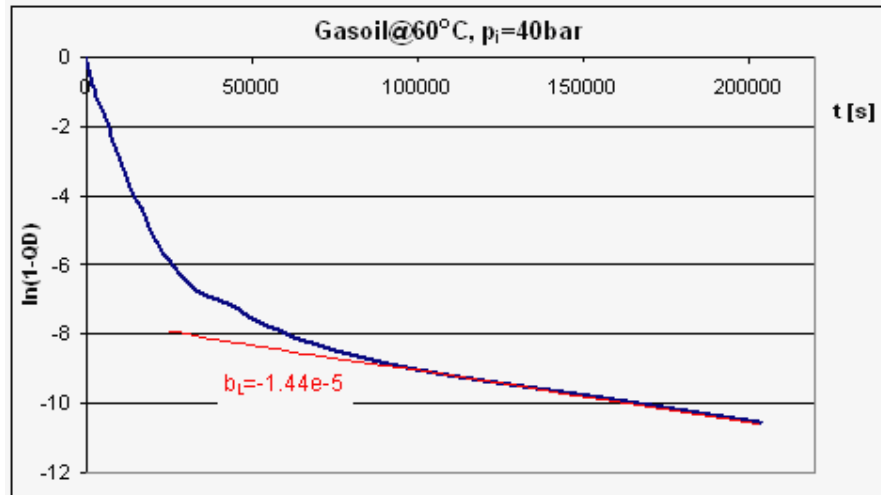


Figure 53:  $b_L$  determination in late stage for Gasoil at 60°C,  $p_i=40$  bar

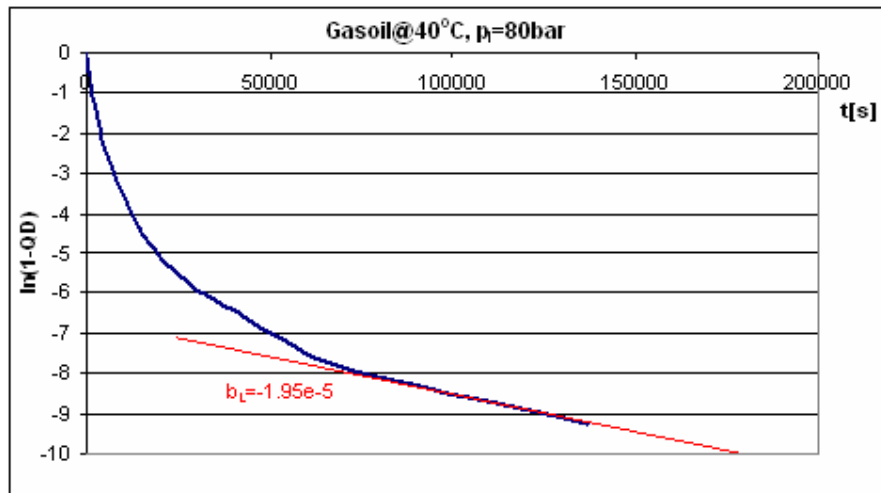


Figure 54:  $b_L$  determination in late stage for Gasoil at 40°C,  $p_i=80$  bar

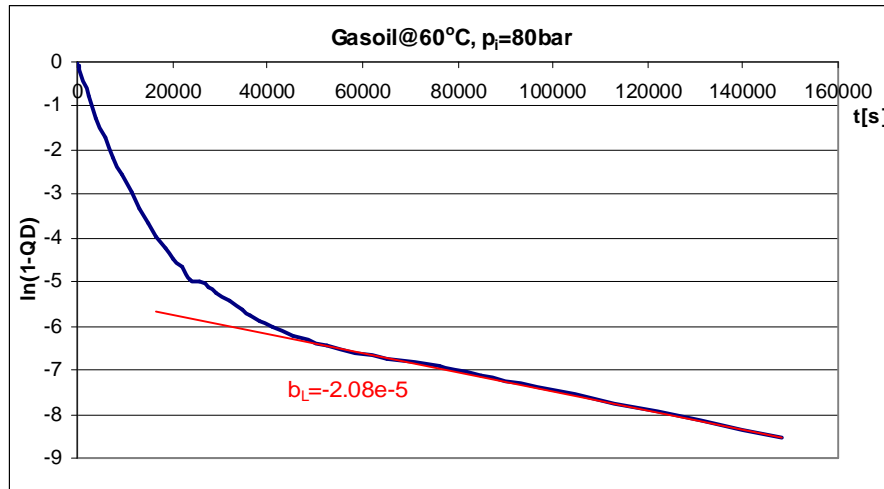


Figure 55:  $b_L$  determination in late stage for Gasoil at 60°C,  $p_i=80$  bar

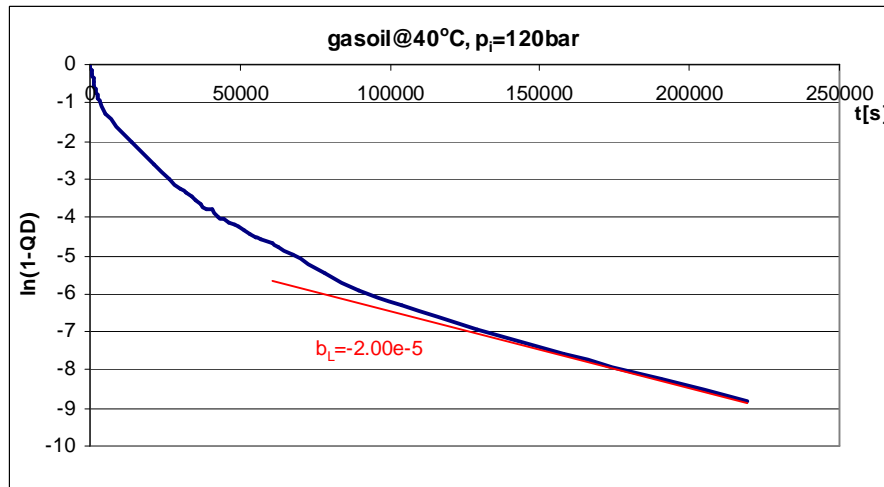


Figure 56:  $b_L$  determination in late stage for Gasoil at 40°C,  $p_i=120$  bar

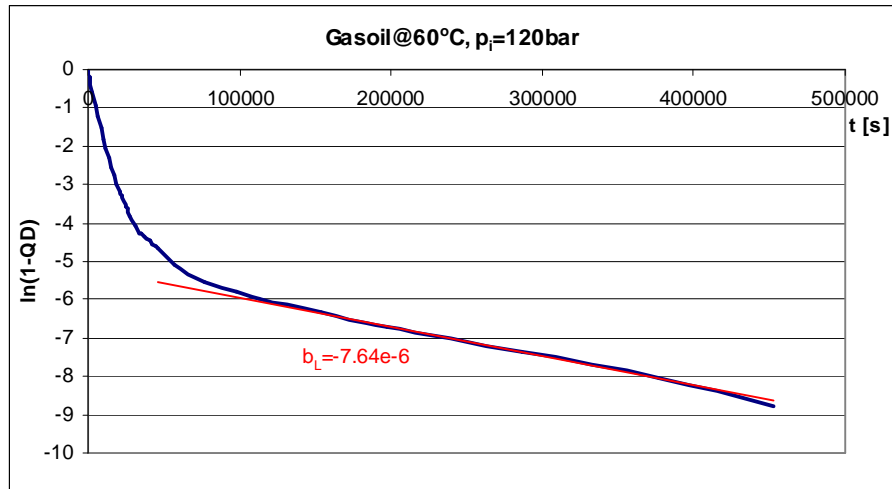


Figure 57:  $b_L$  determination in late stage for Gasoil at 60°C,  $p_i=120$  bar

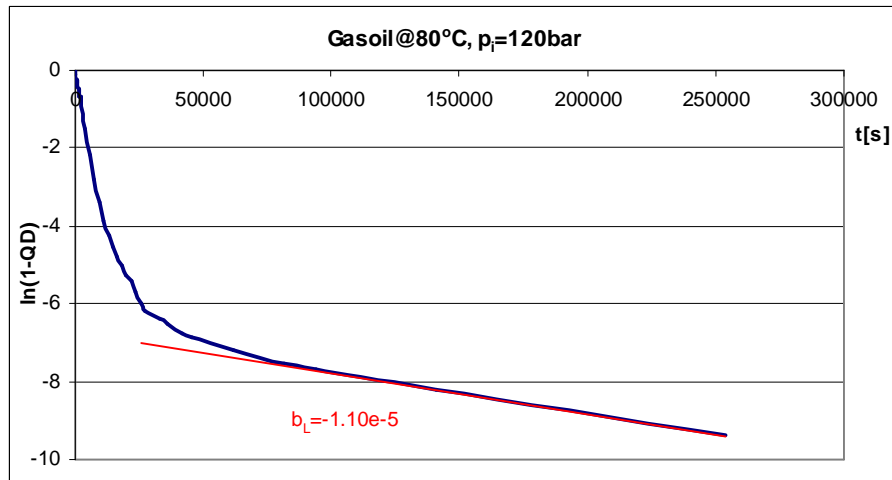


Figure 58:  $b_L$  determination in late stage for Gasoil at 80°C,  $p_i=120$  bar

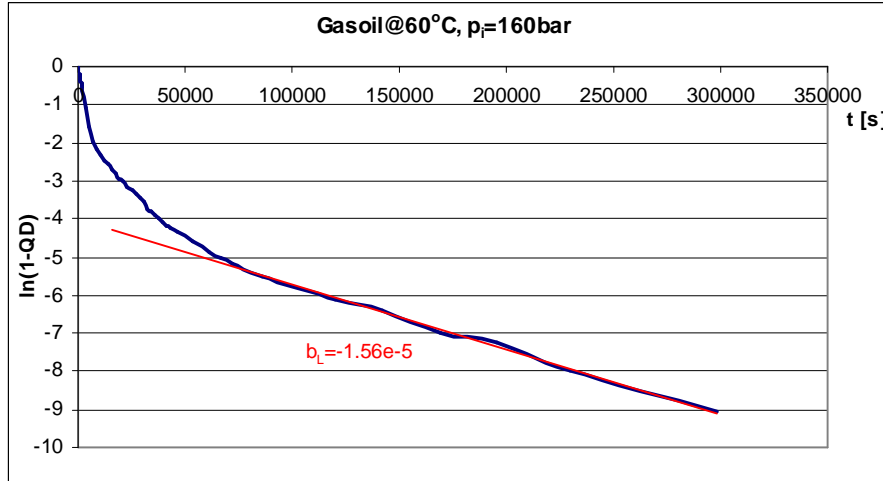


Figure 59:  $b_L$  determination in late stage for Gasoil at 60°C,  $p_i=160$  bar

The long-time solution for diffusion coefficients in the late stage are calculated by Eq 4.41 and the results are displayed below.

$T \backslash p_i$	40 bar	80 bar	120 bar	160 bar
40°C	IT	$7.63 \times 10^{-4}$	$7.82 \times 10^{-4}$	Error
60°C	$5.63 \times 10^{-4}$	$8.14 \times 10^{-4}$	$2.99 \times 10^{-4}$	$6.11 \times 10^{-4}$
80°C	IT	DD	$4.32 \times 10^{-4}$	IT

Table 14: Diffusion coefficient [cm<sup>2</sup>/s] of CO<sub>2</sub> dissolution in Gasoil

To see how the temperature and pressure affect the dissolution rate of CO<sub>2</sub>, two series of tests were selected to make the following calculations.

Tests carried out at 60°C by different initial pressures.

$p_i \backslash t$	0 hour	1.5 hours	80 hours
40 bar	-42.257	-5.14	-0.0005
80 bar	-72.611	-12.27	-0.0005
120 bar	-96.578	-13.16	-0.0007
160 bar	-104.37	-18.16	-0.003

Table 15: Slopes [bar/h] of pressure-decline curve at 60°C after a certain time



$p_i$ \ $t$	0 hour	1.5 hours	80 hours
40 bar	0	0.1791	0.2170
80 bar	0	0.4837	0.5539
120 bar	0	1.0063	1.1677
160 bar	0	1.2365	1.4525

Table 16: Concentration [mol/L] of CO<sub>2</sub> dissolved in Gasoil at 60°C after a certain time (calculated by real gas equation)

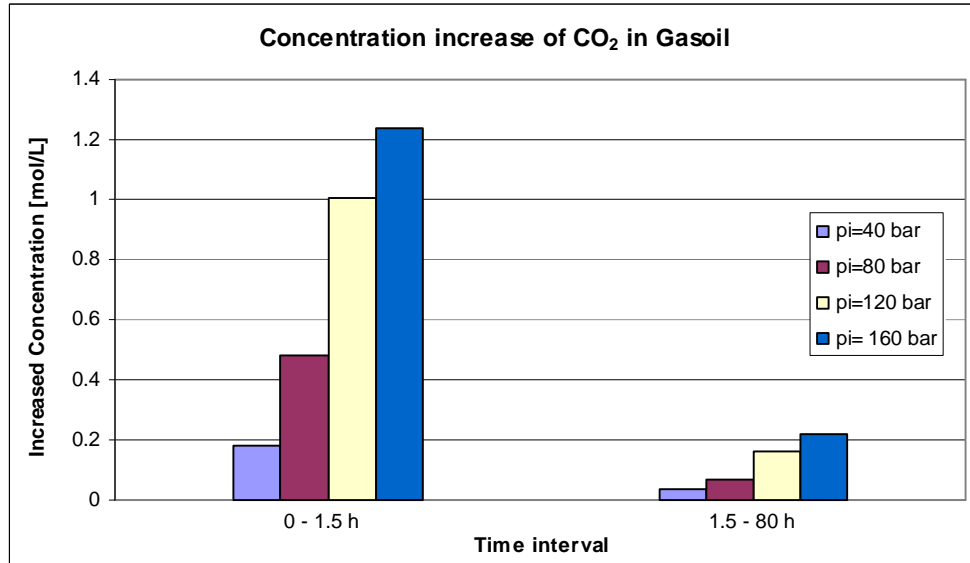


Figure 60: Concentration increase of CO<sub>2</sub> in Gasoil at 60°C

Tests carried out at 120 bar at different temperatures.

$T$ \ $t$	0 hour	1.5 hours	80 hours
40°C	-64.20	-9.74	-0.006
60°C	-96.58	-13.16	-0.0007
80°C	-74.71	-19.56	-0.0005

Table 17: Slopes [bar/h] of pressure-decline curve with  $p_i=120$  bar after a certain time

$T$ \ $t$	0 hour	1.5 hours	80 hours
40°C	0	0.7961	0.9880
60°C	0	1.0063	1.1677
80°C	0	1.1236	1.2523

Table 18: Concentration [mol/L] of CO<sub>2</sub> dissolved in Gasoil with  $p_i=120$  bar after a certain time (calculated by real gas equation)

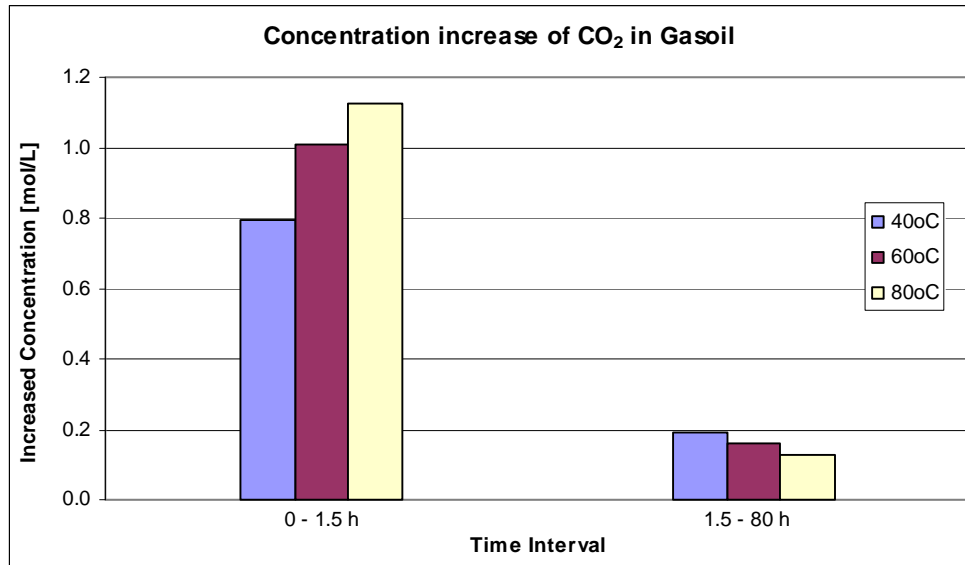


Figure 61: Concentration increase of CO<sub>2</sub> in Gasoil with p<sub>i</sub>=120 bar

In table 15, we see that the sufficient amount of CO<sub>2</sub> dissolution in Gasoil at higher the initial pressure has a less stable final pressure after 80 hours, but the dissolution process started at the same initial pressure has a more stable final pressure with higher temperature after 80 hours (table 17), thus the dissolution rate is increasing with temperature.

Fig 60 and 61 show the dissolution rate is higher at higher initial pressure in early and late stage of the dissolution process at the constant temperature, and at the same initial pressure the dissolution rate is also higher at higher temperature at early stage but the rate decreases faster at higher temperature at late stage.

## Hoeflein

Hoeflein is the lightest oil sample, half-transparent. It has the lowest viscosity. The pressure drop of CO<sub>2</sub> in Hoeflein showed a very different way, in the most cases the pressure fell rapidly within the first 10 minutes, and it started to increase a little before it reached its equilibrium pressure. Fig 62 is one of the typical pressure drops of Hoeflein.

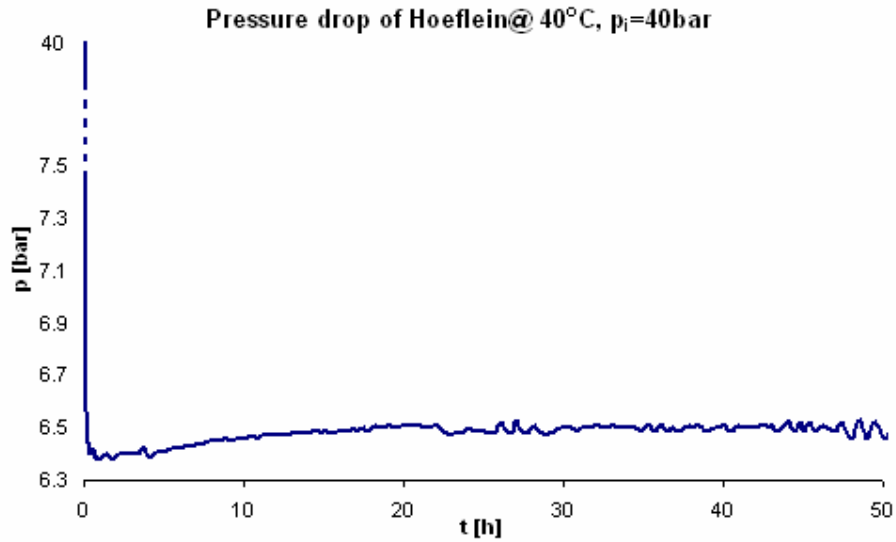


Figure 62: Pressure decrease of Hoeflein at 40°C with  $p_i=40$  bar

This shape of curve is not able to be handled by Civan's model, so the data from Hoeflein will not be used to evaluate the diffusion coefficient of CO<sub>2</sub> in Hoeflein for this case.

However the rapid pressure drop as CO<sub>2</sub> get contacted with Hoeflein would mean that the dissolution rate of CO<sub>2</sub> could be very high at the beginning of the phase contact, and a short dissolution process completes when equilibrium reaches.

Fig 63 shows at the same final pressure the equilibrium pressure increases with increased temperature.

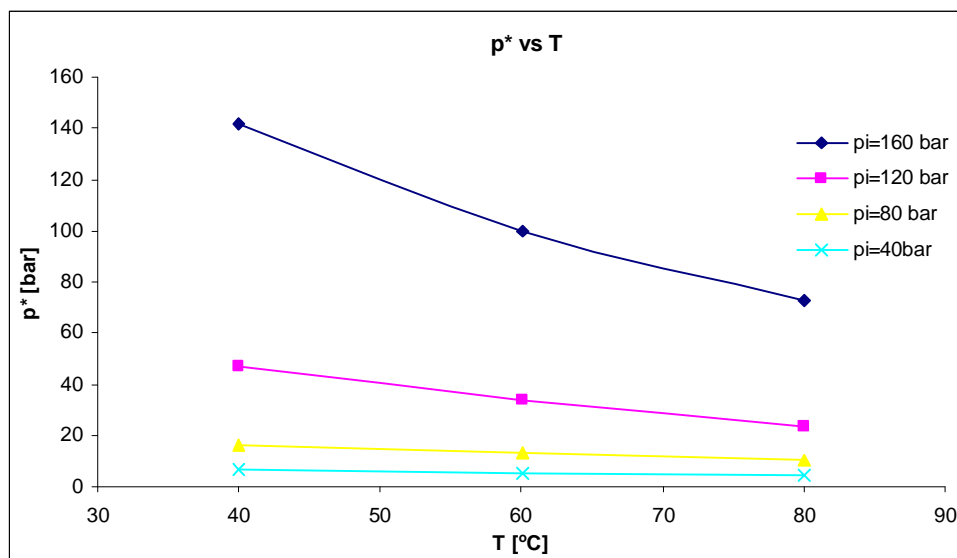


Figure 63: Equilibrium pressure of Hoeflein changes with temperature

## 16 TH

16TH is the second heaviest oil sample, and its viscosity is very higher than other samples except Hochleiten.

The pressure drop profiles of CO<sub>2</sub> dissolution in 16TH contain two inflection points in each in Fig 27 and 28. The reason why a convex-concave shape occurred in single pressure decline curve in the dissolution process is difficult to explain just by knowing the pressure data, but these data can not be used as evaluation data.

The qualified tests were selected and the density calculation for these test were done with SPECS program again, and the increases of equilibrium densities to 16TH densities at corresponding p-t conditions are displayed below:

T \ p <sub>i</sub>	40 bar	80 bar	120 bar	160 bar
40°C	IT	IT	MIP	MIP
60°C	2.12%	1.72%	0.65%	1.00%
80 °C	3.48%	DD	2.73%	IT

MIP: Multi-inflection points in pressure decline curve during dissolution process.

Table 19: Increased density in solution to density of 16TH

The natural convection enhanced the CO<sub>2</sub> dissolution process, b<sub>L</sub> was taken from the late stage, and the diffusion coefficients calculated by Eq 4.41 with long-time approximation was shown below:

T \ p <sub>i</sub>	40 bar	80 bar	120 bar	160 bar
40°C	IT	IT	MIP	MIP
60°C	6.85x10 <sup>-4</sup>	6.82x10 <sup>-4</sup>	2.58x10 <sup>-4</sup>	3.57x10 <sup>-4</sup>
80 °C	3.07x10 <sup>-4</sup>	DD	3.48x10 <sup>-4</sup>	IT

Table 20: Diffusion coefficients [cm<sup>2</sup>/s] of CO<sub>2</sub> dissolution in 16TH

## Schoenkirchen Tief

Schoenkirchen Tief is the third heaviest oil, with a viscosity higher than Hoeflein and Gasoil.

The same procedure was done here for Schoenkirchen Tief.

T \ p <sub>i</sub>	40 bar	80 bar	120 bar	160 bar
40°C	IT	IT	IT & MIP	IT & MIP
60°C	IT	error	1.64%	1.32%
80 °C	3.35%	DD	2.90%	IT

Table 21: Increased density in solution to density of SchT

T \ p <sub>i</sub>	40 bar	80 bar	120 bar	160 bar
40°C	IT	IT	IT & MIP	IT & MIP
60°C	IT	error	1.78x10 <sup>-4</sup>	3.10x10 <sup>-4</sup>
80 °C	4.23x10 <sup>-4</sup>	DD	8.70x10 <sup>-5</sup>	IT

Table 22: Diffusion coefficients [cm<sup>2</sup>/s] of CO<sub>2</sub> dissolution in SchT

### Hochleiten

Hochleiten is the heaviest oil with the highest viscosity of all.

The pressure drops of CO<sub>2</sub> dissolution in Hochleiten took the most time, during our limited observation time, none of the pressure profiles has reached the equilibrium pressure, and there are two inflection points in the pressure decreasing curve in most of the tests, except the test started at 80 bar and 60°C and another one at 40 bar and 40°C. These two tests have no inflection point in the pressure drop curves.

Civan's short-time approximation solution has been used to estimate the diffusion coefficient of CO<sub>2</sub> dissolution in Hochleiten. But test with insufficient observation time and inflection points in pressure curves are the major difficulties in applying the model.

Fig 64-66 shows the pressure decrease curve have two inflection points in most cases. This type of pressure drop profile can not be handled with our model.

The idea for those type of pressure profiles is to assume the pressure drop starts after the second or the last inflection point, the pressure drop from the second or the last inflection point is valid to be used to the short-time approximation except the pressure did not become stable at the end of the test. The observation time is playing an important role in the estimation.

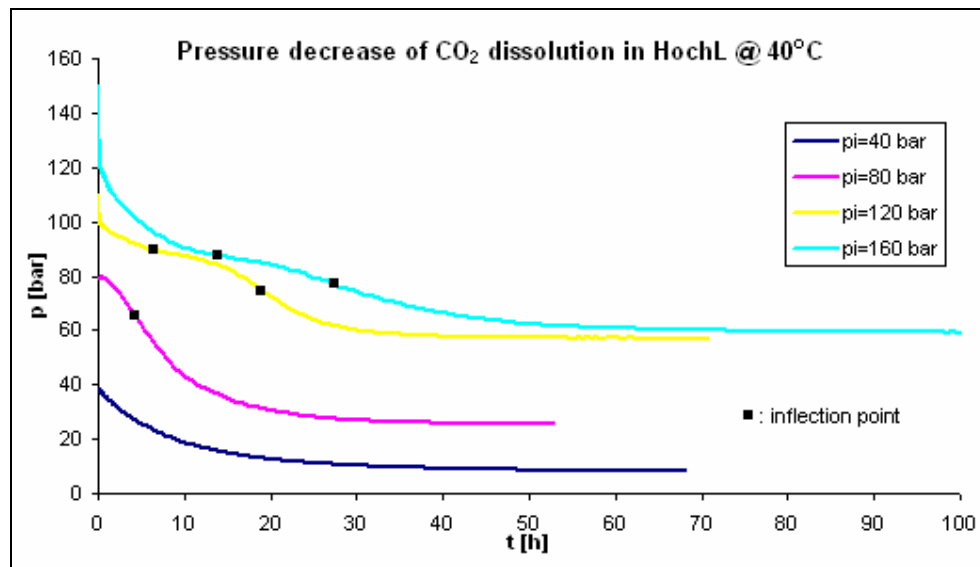


Figure 64: Pressure decrease of CO<sub>2</sub> dissolution in Hochleiten at 40°C

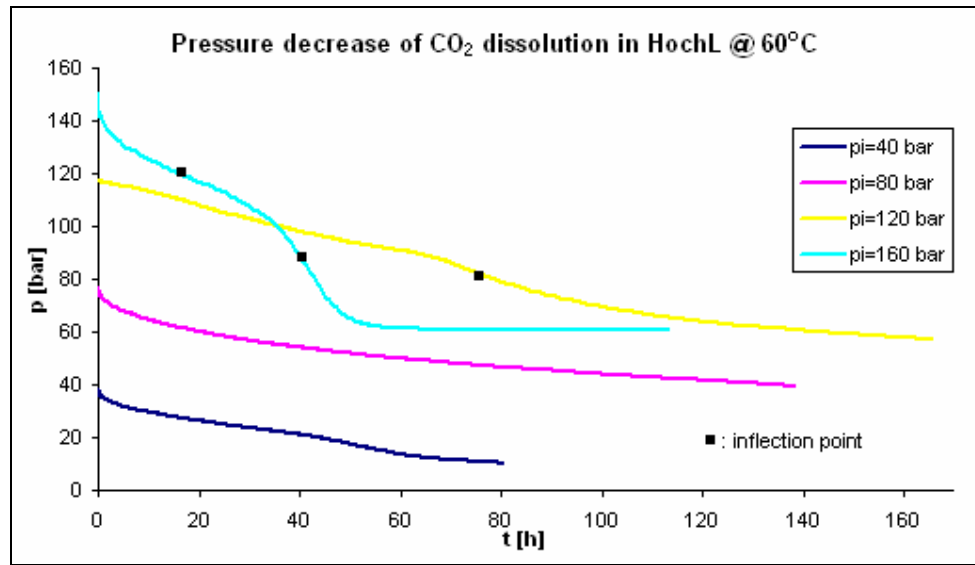


Figure 65: Pressure decrease of CO<sub>2</sub> dissolution in Hochleiten at 60°C

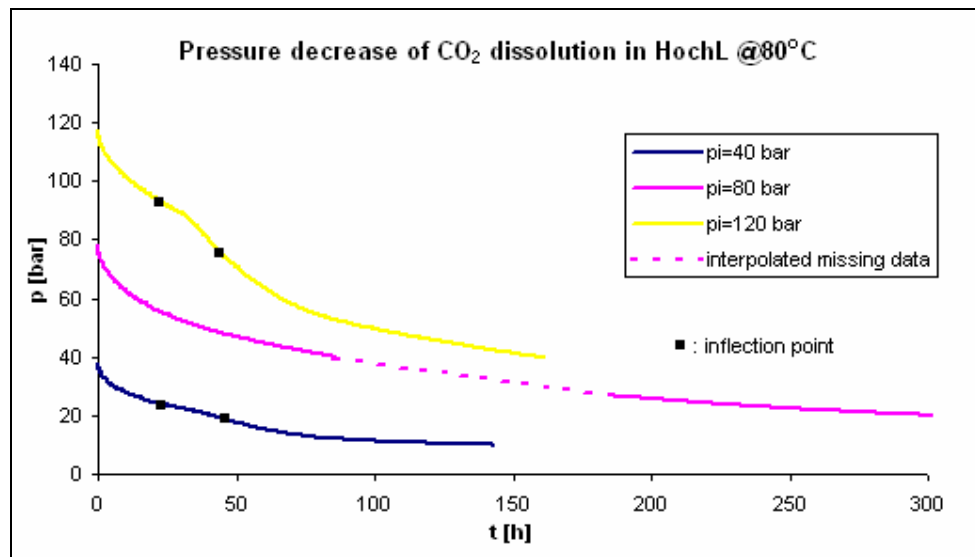


Figure 66: Pressure decrease of CO<sub>2</sub> dissolution in Hochleiten at 80°C

Graphical estimation of  $b_S$  is shown below (Figs 67 - 70)

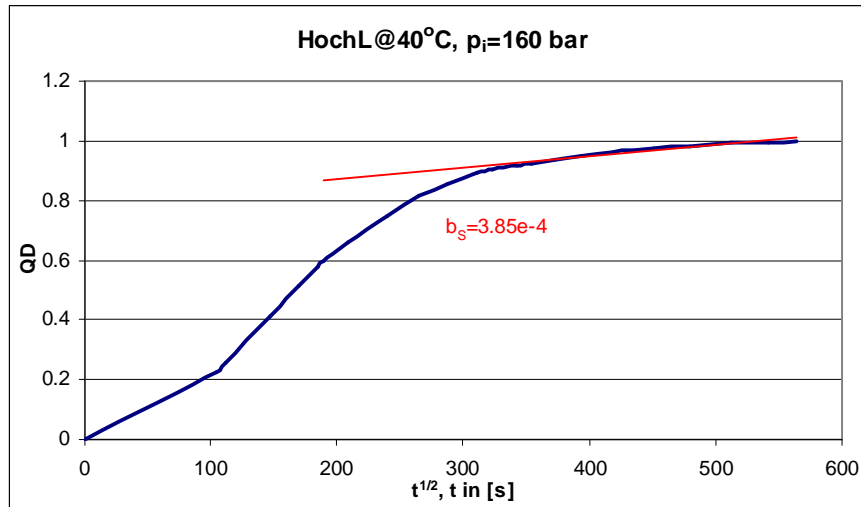


Figure 67: Short-time approximation of  $b_s$  for Hochleiten at 40°C,  $p_i=160$  bar

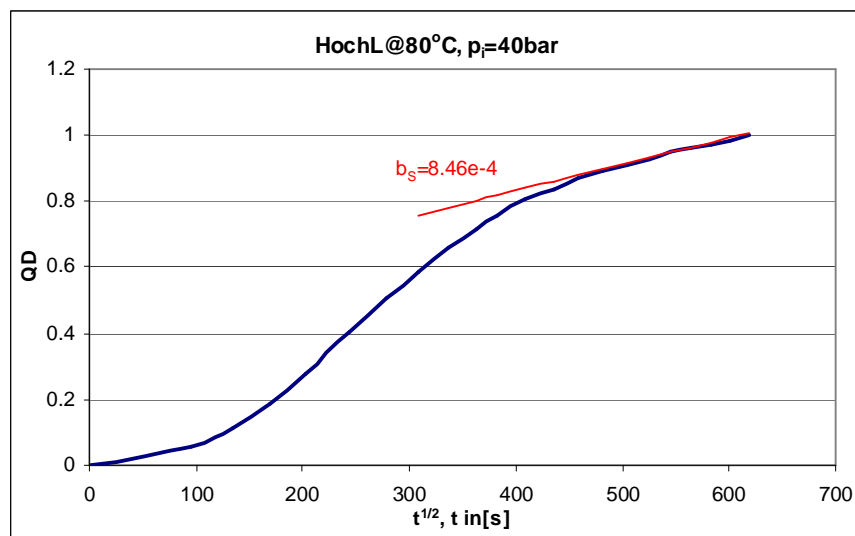


Figure 68: Short-time approximation of  $b_s$  for Hochleiten at 80°C,  $p_i=40$  bar

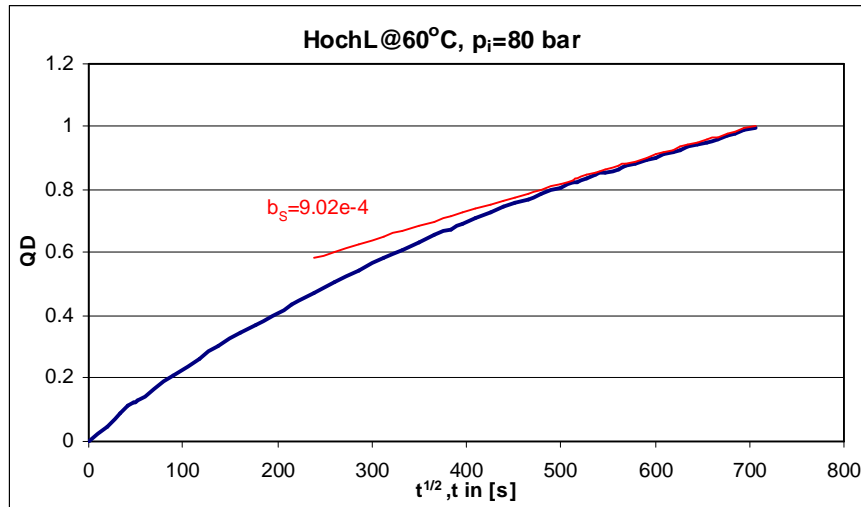


Figure 69: Short-time approximation of  $b_s$  for Hochleiten at 60°C,  $p_i=80$  bar

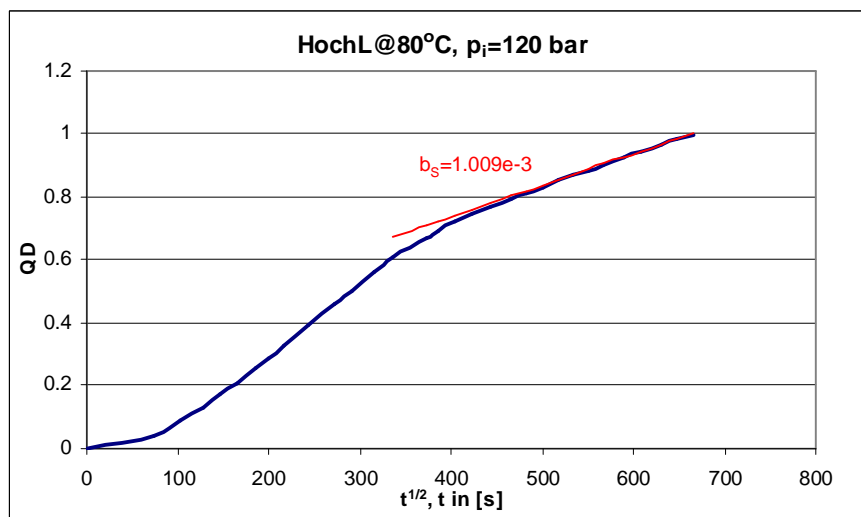


Figure 70: Short-time approximation of  $b_s$  for Hochleiten at 80°C,  $p_i=120$  bar

The diffusion coefficients of CO<sub>2</sub> dissolution in Hochleiten were calculated with short-time approximation by Eq 4.48 in table 23. Few results were evaluated, because the pressure drop of CO<sub>2</sub> dissolution in Hochleiten took the most time to get the pressure stabilized among all the samples. This is not achieved in most of the tests, and there were only a few tests, where the pressure drop data can be used in short-time approximation to do the graphical determination. Much longer observation time is required to obtain better results.



T \ p <sub>i</sub>	40 bar	80 bar	120 bar	160 bar
40°C	IT	IT	IT	1.12x10 <sup>-5</sup>
60°C	IT	6.16x10 <sup>-5</sup>	IT	IT
80 °C	5.43x10 <sup>-5</sup>	ID	7.72x10 <sup>-5</sup>	IT

 Table 23: Diffusion coefficients [cm<sup>2</sup>/s] of CO<sub>2</sub> dissolution in Hochleiten

The density increases of Hochleiten solution were calculated below.

T \ p <sub>i</sub>	40 bar	80 bar	120 bar	160 bar
40°C	IT	IT	IT	0.39%
60°C	IT	2.4%	IT	IT
80 °C	4.92%	ID	3.05%	IT

 Table 24: Increased density of CO<sub>2</sub> dissolved solution to density of Hochleiten

#### 4.43 Summary of Results

The observation times of the test are shown in table 25:

T \ P <sub>i</sub>	40 bar	80 bar	120 bar	160 bar
40°C	68 hours	55 hours	70 hours	120 hours
60°C	80 hours	135 hours	165 hours	115 hours
80 °C	142 hours	310 hours	160 hours	25 hours

Table 25: Observation times of different tests

The tests with observation time less than 100 hours are difficult to evaluate for heavy oil. The pressure decline curve of those tests exhibited no constant final value and the final pressure could not be used for diffusion coefficient calculation. Some of the tests that took longer than 100 hours were also considered as invalid, due to lower dissolution rate in the solvent. Longer observation time was required to have final pressure stabilized.

CO<sub>2</sub> has higher diffusion coefficient in brine than in oil.

Diffusion coefficient of CO<sub>2</sub> in Gasoil has the highest average value of all oil samples.

Result of 16 TH has a lower average value comparing to Gasoil value. It is closer to the value obtained from Schoenkirchen Tief.

Hochleiten has the slowest pressure decline and the CO<sub>2</sub> diffusion coefficient in Hochleiten is the lowest of all, it is an order of magnitude small than other oil samples.

The diffusion coefficients of CO<sub>2</sub> in oil samples and the average values are displayed together with the viscosities of oil samples in Fig 71. The results show the diffusion coefficient decreases with viscosity, which proved the tendency of D and  $\mu$  in Eq 1.8.

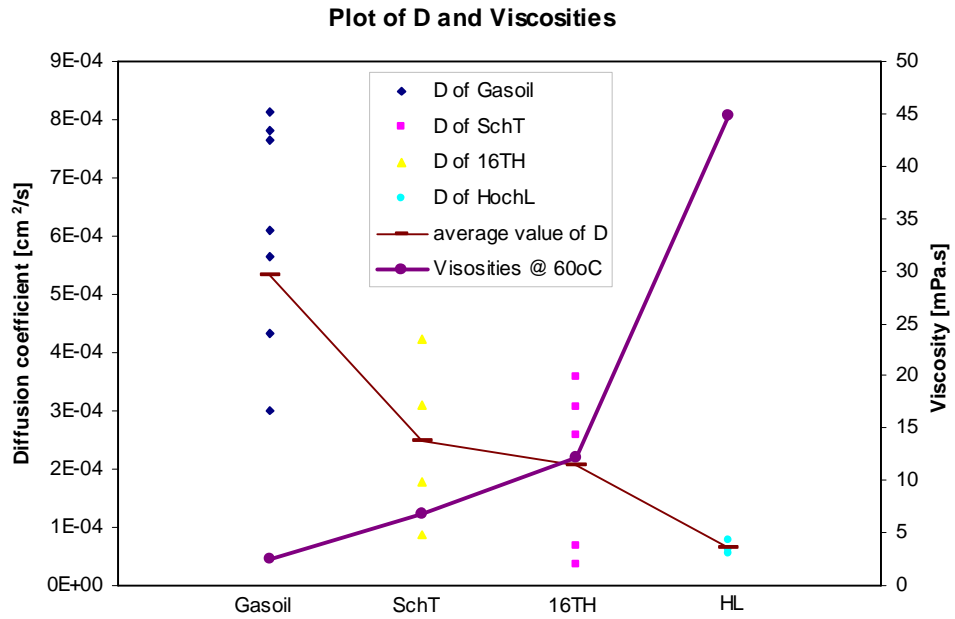


Figure 71: Diffusion coefficient decreases with viscosity

## 5. Conclusion

In this work, a certain volume of gaseous CO<sub>2</sub> was brought into contact with brine water and crude oil in PVT cells at designed pressures and temperatures, and the pressure decline was recorded during the dissolution of CO<sub>2</sub> in liquids at different p-T conditions.

A cubic EOS was used for the phase equilibrium calculation of CO<sub>2</sub>-brine system, and the binary interaction parameter was adjusted to match the experimental data. Thus a correlation equation was generated as a function of pressure, temperature and salinity for determination of the binary interaction parameter. But more experiments need to be done at a wider p-T region to testify the applicability of the correlation equation.

The equilibrium diffusion model by Civan et. al. is applied for determination of the gas-diffusion of CO<sub>2</sub> from pressure decline by dissolution of CO<sub>2</sub> in liquids. The obtained diffusion coefficients from experimental data are average values for a certain concentration range at a given temperature.

However, several errors of our experimental method can not be eliminated.

First of all, the time for gas/liquid phase reaching equilibrium is much longer than expected. The true value of the gas pressure at the equilibrium  $p^*$  has not been measured in our test, the final pressure we used for our evaluation are very close to the equilibrium pressure, because the pressure decline curves were almost stabilized.

Second is that the convection enhanced the mass transfer. The experimental data show that in the early hours of the dissolution process, the pressure decline is much faster than in late stage, and the mass transfer rate is larger than we calculated from Fick's law in which the rate is only driven by diffusion mechanism. The density changes in the fluid were calculated, and the density variation in liquid induced the convection mechanism, this is another driving mechanism for mass transfer which enhanced the dissolution rate of CO<sub>2</sub> in liquid and influenced the dissolution process. This can not be eliminated in our measurements.

But also the accuracy of the present values is limited by the inherent simplified assumptions in Civan's analytic interpretation methods. Besides this,  $k$  in Civan's model defined as mass-transfer Boit number in the analytical solution did not have its mathematical description, which makes Eq 4.12 not very consistent.

Consequently the experimental values of the diffusion coefficients determined by the present methods are somehow higher than the true values.

Therefore, it is suggested to solve the equations of Fick's law numerically using a finite volume approach for better results.

## 6. Future work

For better experimental results, the appropriate observation time of the experiment for determination of diffusion coefficient of CO<sub>2</sub> in our oil sample should be approximately 15 to 50 days; for brine, the observation time should be at least a week or two, and the time increases with the salinity of brine. Even for the short-time approximation, a certain minimum observation time is still needed to build valid data. The observation time plays a very important role for diffusion coefficient estimation. High error can occur for insufficient observation time. For heavier oil, the pressure decrease could last for months until it reaches the equilibrium pressure due to the low diffusion rate.

According to the pressure profiles from our experiments and the phase diagram of CO<sub>2</sub> (Fig. 1), the recommended initial pressure and the temperature of the experiment should not exceed their critical values, otherwise we could have unstable phase of CO<sub>2</sub>, which cause the typical convex-concave shaped pressure decline curves like in Fig. 27 and 28, and the errors will increase with higher temperature and pressure. From the density calculation results, we can see that the density effect is more sensitive to the temperature than to the pressure, which means at higher temperature convection enhances the mass transfer rate more effectively in the dissolution process.

If possible, the measure equipment should have a better pressure resolution for the decline curve at the late stage of the test. This belongs to the errors associated with data measurement and processing techniques.

## Nomenclature

A	=	cross-sectional area of the test cylinder, [cm]
b	=	slope
c	=	concentration of CO <sub>2</sub> in solution, [mol/L] or [mol/cm <sup>3</sup> ]
D <sub>0</sub>	=	pre-exponential factor, [cm <sup>2</sup> /s]
D <sub>CO<sub>2</sub>-water</sub>	=	diffusion coefficient of CO <sub>2</sub> in water
D	=	diffusion coefficient, [cm <sup>2</sup> /s]
F <sub>i</sub>	=	mol fraction of substance i in liquid phase, [%]
H	=	height of the gas column in test cylinder, [cm]
J	=	diffusion flux, [mol/cm <sup>2</sup> .s]
k	=	mass-transfer Boit number, [cm/s]
L	=	height of the liquid column in the test cylinder, [cm]
m	=	mass, [g]
M <sub>i</sub>	=	mol mass of substance i, [g/mol]
n <sub>i</sub>	=	mol number of substance I, [mol]
OD	=	outside diameter of PVT-cell, [mm]
p	=	pressure, [bar]
Q	=	cumulative mass of gas dissolved in the liquid phase per unit cross-sectional area of the gas/liquid interface, [g/cm <sup>2</sup> ]
q	=	diffusion rate, [mol/s]
R	=	universal gas constant, [bar.cm <sup>3</sup> /mol/K]
r	=	particle radius
t	=	time, [s] or [h]
T	=	temperature, [K]
v	=	molar volume [L/mol]
V	=	volume, [cm <sup>3</sup> ]
Z	=	compressibility factor / Z-factor, [/]
a	=	thermal expansion coefficient, [K <sup>-1</sup> ]
b	=	Isothermal compressibility coefficient, [bar <sup>-1</sup> ]
k	=	binary interaction parameter. [/]
ρ	=	density, [kg/m <sup>3</sup> ]
ε	=	activation energy for diffusion, [J/mol] or [eV/mol]
m	=	viscosity, [mPa.s]
I	=	roots of $\tan I = k_D / I$

**Subscripts**

c	=	critical value
D	=	Dimensionless
dis	=	dissolved
exp	=	experimental value
g	=	Gas
L	=	long-time approximation
o	=	initial state
r	=	Reduced
S	=	short-time approximation

**Superscripts**

*	=	equilibrium state
---	---	-------------------

## References

- [1] *Statistical Mechanics of Non-equilibrium Liquids*. D.J.Evans and G.P.Morriss, Academic Press (1990).
- [2] *On the molecular mechanism of thermal-diffusion in liquids*. B.Hafskjold, T. Ikeshoji, S.K. Ratkje, Mol. Phys. (1993).
- [3] *Accurate Measurement of Gas Diffusivity in Oil and Brine under Reservoir Condition*. Faruk Civan. SPE 67319, presented at the 2001 SPE Production and Operations Symposium Oklahoma City, Oklahoma, 24-27 March.
- [4] *Analysis and Interpretation of Gas Diffusion in Quiescent Reservoir, Drilling, and Completion Fluids: Equilibrium vs. Non-equilibrium Models*. Faruk Civan (SPE 840772) presented at the 2003 SPE Annual Technical Conference and Exhibition, Denver, 5-8 October.
- [5] *The Mathematics of Diffusion*, Crank, J. Oxford U. Press, London (1956).
- [6] *Swelling of Oil-Based Drilling Fluids Resulting From Dissolved Gas*. O'Bryan, P.L. and Bourgoyne, A.T. Jr. SPEDE (1990) 5.
- [7] *An Experimental Study of Gas Solubility in Oil-Based Drilling Fluids*. O'Bryan, P.L. and Bourgoyne, A.T. Jr. SPEDE (1998).
- [8] *Chemical Engineering Progress (2003)*. Peress, J.
- [9] *A New Method For Experimental Measurement of Diffusion Coefficients in Reservoir Fluids*. Riazi, M.R. J. Petroleum Science and Engineering (1996).
- [10] *The Diffusion of Methane in Water at Reservoir Conditions, A First Attempt*. Sachs, W. Erdoel Erdgas Kohle (1997)
- [11] *The Diffusional Transport of Methane in Liquid Water: Method and Result of Experimental Investigation at Elevated Pressure*. Sachs, W. J. Petroleum Science and Engineering (1998).
- [12] *Modeling with Differential Equations in Chemical Engineering*. Walas, S.M. Butterworth-Heinemann Series in Chemical Engineering, Boston (1991).
- [13] *Measurement of Gas Diffusion in Heavy Oils*. Zhang, Y.P., Hyndman, C.L., and Maini. J. Petroleum Science and Engineering (2000).
- [14] *Handbook of Physics and Chemistry (76<sup>th</sup> Edition) [Lide, 2004]*
- [15] *Chemical Engineerings' Handbook*, Perry, R.H
- [16] *Properties of Gases and Liquids*, Robert C. Reid

- [17] [http://en.wikipedia.org/wiki/Fick%27s\\_law](http://en.wikipedia.org/wiki/Fick%27s_law) actual data in June 2007
- [18] <http://en.wikipedia.org/wiki/Diffusion> actual data in June 2007
- [19] *Carbon Dioxide Flooding, Basic Mechanisms and Project Design*, Mark A. Klins
- [20] *Compositional Modelling of CO<sub>2</sub> Flooding and the Effect of CO<sub>2</sub> water solubility (SPE 11438)*. J. Mansoori, Research and Development, Phillips Petroleum Company Bartlesville, Oklahoma.
- [21] *Ten Years with the CPA (Cubic-Plus-Association) Equation of State. Part 1. Pure Compounds and Self-Associating Systems*. Georgios M. Kontogeorgis
- [22] *Specs V4.0 Manual*. Eduardo Pretel, 1999, 2000
- [23] <http://www.tu-harburg.de/vt2/pe2000/HomePage.html> actual data in August 2007
- [24] *Improved Measurement of Gas Diffusivity for Miscible Gas flooding Under Non-equilibrium vs. equilibrium conditions (SPE 75135)*. Faruk Civan, Maurice L. Rasmussen, University of Oklahoma.
- [25] *Enhanced Mass Transfer of CO<sub>2</sub> into Water and Oil by natural Convection (SPE 107380)*. R. Farajzadeh, H.A. Delil, P.L.J. Zitha & J. Bruining
- [26] *Determination of Gas Diffusion and Interface-Mass-Transfer Coefficients for Quiescent Reservoir Liquids (SPE 84072)*. Faruk Civan, Maurice L. Rasmussen, The University of Oklahoma.
- [27] *Hydrocarbon Phase Behavior (Volume 7)*. Tarek Ahmed
- [28] *Compositional Model for CO<sub>2</sub> Floods Including CO<sub>2</sub> solubility in Water (SPE 35164)*. Yih-Bor Chang, B.K.Coats, J.S. Nolsen, western Atlas Software.
- [29] *Behavior of the CO<sub>2</sub>-H<sub>2</sub>O system and Preliminary Mineralization Model and Experiments*. S.J.T.Hangx, HPT Laboratory, Department of Earth Sciences Utrecht University
- [30] *Thermodynamic Properties of Mixtures of H<sub>2</sub>O and D<sub>2</sub>O in the Critical Region*, Abdulkadirova, K. S., Wyczalkowska, A. K., Anisimov, M. A. and Sengers. J. Chem. Phys. (2002)
- [31] *Three-Parameter Equation of State, Fluid Phase Equilibrium*. Adachi, Y., Lu, B. C. Y. and Sugie, H. (1983)
- [32] *Equation-of-State Methods for the Modelling of Phase Equilibria, Fluid Phase Equilib.* Anderko, A. (1990)
- [33] *Generalization of Binary Interaction Parameters of Peng-Robinson Equation of State for Systems containing Hydrogen. Fluid Phase Equilibria, (1990)*. Hideo Nishiumi and Hironobu Gotoh.